The strong coupling constant of QCD with four flavors

D I S S E R T A T I O N

zur Erlangung des akademischen Grades

Dr. rer. nat.
im Fach Physik

eingereicht an der
Mathematisch-Wissenschaftlichen Fakultät I
Humboldt-Universität zu Berlin

von
Dipl.-Phys. Fatih Tekin
10.06.1980 Berlin

Präsident der Humboldt-Universität zu Berlin:
Prof. Dr. Dr. h.c. Christoph Markschies

Dekan der Mathematisch-Wissenschaftlichen Fakultät I:
Prof. Dr. Andreas Herrmann

Gutachter:
1. Prof. Dr. Ulrich Wolff
2. Dr. Rainer Sommer
3. Prof. Dr. Kari Rummukainen

eingereicht am: 9. Juli 2010
Tag der mündlichen Prüfung: 1. November 2010

Bu çalışmamı
aileme ithaf ediyorum.

Ich widme meine Dissertation
meiner Familie.

I dedicate my dissertation work
to my family.

Abstract

In this thesis we study the theory of strong interaction **Quantum Chromodynamics** on a space-time lattice (lattice QCD) with four flavors of dynamical fermions by numerical simulations. In the early days of lattice QCD, only pure gauge field simulations were accessible to the computational facilities and the effects of quark polarization were neglected. The so-called fermion determinant in the path integral was set to one (quenched approximation). The reason for this approximation was mainly the limitation of computational power because the inclusion of the fermion determinant required an enormous numerical effort. However, for full QCD simulations the virtual quark loops had to be taken into account and the development of new machines and new algorithmic techniques made the so-called dynamical simulations with at least two flavors possible. In recent years, different collaborations studied lattice QCD with dynamical fermions. In our project we study lattice QCD with four degenerated flavors of $\mathcal{O}(a)$ improved Wilson quarks in the Schrödinger functional scheme and calculate the energy dependence of the strong coupling constant. For this purpose, we determine the $\mathcal{O}(a)$ improvement coefficient c_{sw} with four flavors and use this result to calculate the step scaling function of QCD with four flavors which describes the scale evolution of the running coupling. Using a recursive finite-size technique, the Λ parameter is determined in units of a technical scale L_{max} which is an unambiguously defined length in the hadronic regime. The coupling α_{SF} of QCD in the so-called Schrödinger functional scheme is calculated over a wide range of energies non-perturbatively and compared with 2-loop and 3-loop perturbation theory as well as with the non-perturbative result for only two flavors.

Zusammenfassung

In dieser Arbeit studieren wir durch numerische Simulationen die Theorie der starken Wechselwirkung *Quantenchromodynamik* auf einem Raumzeit-Gitter (Gitter QCD) mit vier dynamischen Quark-Flavors. In den Anfängen der Gitter QCD wurden die Effekte der Quark-Polarisation aufgrund von technischer Begrenzung der Rechenkapazität vernachlässigt und die sogennante "quenched Approximation" angewendet. Dabei setzte man die im Pfadintegral auftretende Fermion-Determinante auf eins und vernachlässigte damit alle Effekte, die durch virtuelle (dynamische) Quark-Antiquark-Schleifen verursacht wurden. Der Grund für die "quenched" Approximation war, dass der numerische Aufwand um die Fermion-Determinante auszuwerten die damaligen technischen Möglichkeiten überstieg. In der Tat ist dies immer noch eine große Herausforderung für die numerische Simulation der QCD aber durch neue technische und algorithmische Entwicklungen kann man heutzutage die Quark-Polarisationseffekte mit mindestens zwei Quark-Flavors berücksichtigen. Seit einigen Jahren werden solche Simulationen in verschiedenen Kollaborationen durchgeführt. In unserem Projekt wird die Gitter-QCD mit vier degenerierten $\mathcal{O}(a)$ verbesserten Wilson Quarks im Schrödinger Funktional Schema untersucht mit dem Ziel, die Energieabhängigkeit der starken Kopplung zu berechnen. Zu diesem Zweck bestimmen wir erst den $\mathcal{O}(a)$ Verbesserungskoeffizienten $c_{\rm sw}$ mit vier Flavors und benutzen dieses Ergebnis um die Step-Scaling Funktion der QCD zu bestimmen, die das Laufen der Kopplung über einen großen Skalenbereich beschreibt. Unter Benutzung eines Finite-Size Verfahrens berechnen wir den Λ Parameter in Einheiten von einer Skala $L_{\rm max}$, die eine eindeutig definierte Länge im hadronischen Bereich darstellt. Die QCD-Kopplung $\alpha_{\rm SF}$ im sogenannten Schrödinger Funktional Schema wird dann über einen weiten Bereich der Energie bestimmt und ein Vergleich mit 2-loop und 3-loop Störungstheorie sowie mit dem nicht-perturbativen Ergebnis für den Fall von zwei Flavors durchgeführt.

Contents

1 Introduction - Continuum QCD

In this chapter, we are going to give a brief overview of some aspects of *quantum chromodynamics* in continuum. For more detailed discussions of the topic the interested reader is referred to [1–5].

1.1 The QCD Lagrangian

The current standard model of particle physics covers three of four known forces in nature which are the electromagnetic force, the weak force, and the strong force. Due to the non-renormalizability of the gravitational force, it is not included yet. In the following, we want to concentrate on the theory of the strong force. The currently accepted theory of the strong interaction (force) is known as *quantum chromodynamics* (QCD) which was developed as an analogous theory to the very successful *quantum electrodynamics* (QED). The fundamental difference between both theories is that QED operates in $U(1)$ and is therefore an abelian gauge theory, while QCD operates in $SU(3)$ and is a non-abelian gauge theory. This makes QCD much more complicated than QED. The QED gauge field, which describes the photon field, turns into a new gauge field A_μ in QCD

$$A_\mu(x) = \sum_{a=1}^{8} A_\mu^a(x)\frac{\lambda^a}{2}, \tag{1.1}$$

which is a linear combination of the eight generators λ^a of $SU(3)$, the so-called Gell-Mann matrices (see appendix A), multiplied by the coefficients A_μ^a. From a physical point of view, these matrices represent the quanta of interaction (so-called *gluons*) of the theory. The field strength tensor $F_{\mu\nu}$ of QED

$$F_{\mu\nu} = \partial_\mu A_\nu - \partial_\nu A_\mu \tag{1.2}$$

changes due to (1.1) into

$$F_{\mu\nu}^a = \partial_\mu A_\nu^a - \partial_\nu A_\mu^a - g f^{abc} A_\mu^b A_\nu^c \tag{1.3}$$

where f^{abc} are structure constants of $SU(3)$ and are listed in the appendix A (see equation (3)). Their determination can be done by explicit calculation of the commutator

$$\left[\frac{\lambda^a}{2}, \frac{\lambda^b}{2}\right] = i\sum_{c=1}^{8} f^{abc}\frac{\lambda^c}{2}. \tag{1.4}$$

The parameter g which appears in (1.3) is the strong coupling constant and will be discussed later. The gluonic part of the QCD Lagrangian could now be constructed analogously to its counterpart in QED. It can be taken to

$$\mathscr{L}_{\text{gluon}} = -\frac{1}{2} tr\{F_{\mu\nu}F^{\mu\nu}\} \tag{1.5}$$

where $F_{\mu\nu}$ is the QCD version (1.3) of the field strength tensor. Due to the trace, the gauge-invariance is obviously preserved. With (1.1) and the property

$$\text{tr}\,(\lambda^a\lambda^b) = 2\delta_{ab} \tag{1.6}$$

of the Gell-Mann matrices, we can write down the gluonic part of the Lagrangian

$$\mathscr{L}_{\text{gluon}} = -\frac{1}{4}\sum_{a=1}^{8} F^a_{\mu\nu}F^{a\mu\nu}. \tag{1.7}$$

The fermionic part is in principle the same expression as in the QED Lagrangian but only in the covariant derivative the gauge field A_μ is replaced by the gauge field of QCD

$$\mathscr{L}_{\text{fermion}} = \sum_{f=1}^{6} \overline{\Psi}_f(i\gamma^\mu D_\mu - m_f)\Psi_f \tag{1.8}$$

with the covariant derivative

$$D_\mu = \partial_\mu - igA^a_\mu\frac{\lambda^a}{2}. \tag{1.9}$$

The parameter m_f denotes the different masses of the quarks and Ψ and $\overline{\Psi}$ represent the quark and anti-quark fields, respectively. The complete Lagrangian of the theory of strong interaction is now given only by the following equation

$$\mathscr{L}_{QCD} = \sum_{f=1}^{6} \overline{\Psi}_f(i\gamma^\mu D_\mu - m_f)\Psi_f - \frac{1}{4}\sum_{a=1}^{8} F^a_{\mu\nu}F^{a\mu\nu}. \tag{1.10}$$

So the theory is now well-defined and we can enter into the world of quarks and gluons.

1.2 Quarks and Gluons

As mentioned previously, the fundamental particles of QCD are the *quarks* and the interaction between them is mediated through the *gluons*. In Table 1.1 some properties of them are itemized. The *antiquarks* have the same mass as the quarks but the opposite charge and they are denoted by a bar over the abbreviated form (e.g. $u \leftrightarrow \bar{u}$). The current state of knowledge about quarks is that they can be arranged into three families (generations) with one up-type and one down-type quark in each of them. They obey the Fermi-Dirac statistics and are spin-$\frac{1}{2}$ particles (fermions). The fractional electric

generation	flavor	abbrev.	electric charge	mass
I.	Up	u	2/3	$1.5 - 3.3$ MeV
	Down	d	-1/3	$3.5 - 6.0$ MeV
II.	Charmed	c	2/3	$1.27\ ^{+0.07}_{-0.11}$ GeV
	Strange	s	-1/3	$104\ ^{+26}_{-34}$ MeV
III.	Top	t	2/3	171.2 ± 2.1 GeV
	Bottom	b	-1/3	$4.20\ ^{+0.17}_{-0.07}$ GeV
gauge boson	eight gluons	g	0	0

Table 1.1: Properties of quarks and gluons [6]. The masses are given in $\overline{\text{MS}}$ scheme.

charge follows from the fact that the baryons are composed of three quarks; for example, the proton is made of two up and one down quark but the complete charge of the proton is $+1e$. Due to this, the quarks which build the proton have to have fractional electric charges. This quark model was first proposed by *M. Gell-Mann* and *G. Zweig* in 1963 and consisted of three flavors. A short time later the particle physicists realized that this model provided a baryon called Δ^{++} which was experimentally proven and therefore seemed to cause a spin-statistics problem. Its quark content of three up-quarks with parallel spins would violate the *Pauli exclusion* principle because all of them had to be in the same quantum mechanical state. In 1965, *M.-Y. Han* with *Y. Nambu* and *O.W. Greenberg* proposed an idea of a new quantum number *color* to solve this spin-statistics problem. According to this idea, every quark flavor carries a color charge of red, green, or blue. In other words, they supposed a new $SU(3)$ color symmetry, which was later confirmed by experimental measurements. In some textbooks of particle physics, the width of the low-energy process $\pi^0 \to \gamma\gamma$ is quoted as a quantity which is explicitly dependent on the number of colors (N_c) and hence it is argued that this width can be used for fixing N_c from experiment. However, *Bär et al.* showed in [7] that this argumentation is misleading because the N_c dependence of the aforementioned width appears only if one assumes that the quark charges are fixed to $Q_u = 2/3$ and $Q_d = -1/3$ by varying N_c. But varying N_c without adjusting the quark charges is inconsistent and a more general treatment of the process $\pi^0 \to \gamma\gamma$ where quark charges are not fixed beforehand and are functions of N_c shows that the width of the π^0 decay is not N_c dependent. The authors calculated that the decay $\eta \to \pi^+\pi^-\gamma$ has indeed an explicit N_c dependence. They suggested that this process should be used to illustrate that experimental results are only consistent with the choice $N_c = 3$. In the high energy regime, the authors of [7] quote that the Drell ratio R is still a good quantity to fix the number of colors from experiment if one takes the quark charges as function of N_c without fixing them to the known values

$$R = \frac{\sigma(e^+e^- \to \text{hadrons})}{\sigma(e^+e^- \to \mu^+\mu^-)} \propto N_c(Q_u^2 + 2Q_d^2) = \frac{3}{4}\left(N_c + \frac{1}{N_c} - \frac{2}{3}\right). \tag{1.11}$$

The idea that the proton could not be a fundamental particle arose from results of deep inelastic scattering experiments at SLAC in 1969 where a proton beam collided with an electron beam. The result was that the structure function F_2 of the proton depended only on a scale q^2/ν (*Bjorken scaling*), where q^2 is the momentum transfer and ν is the energy transfer, and not only on q^2, i.e. for a fixed value of q^2/ν, $F_2(q^2)$ was constant within the errors of the measurements. Such a behavior was expected for scattering at point-like particles [8]. Subsequent experiments revealed that the baryons like protons and neutrons are made of three quarks and mesons like pions etc. are made of pairs of quark-antiquark.

1.3 Symmetries of the Lagrangian

The QCD Lagrangian (1.10) possesses some crucial symmetries which we are going to discuss here very briefly. One of the exact symmetries is the local gauge invariance, i.e. the quark fields could be transformed at every space point independently without changing the physics. This symmetry is very important because it is responsible for the renormalizability of QCD. Furthermore, the Lagrangian is invariant under the discrete symmetry of *parity*, *charge conjugation* and *time reversal*. These symmetries were tested in experiments determining the properties of the strong interaction and are in good agreement with the findings [6]. In addition, some approximate symmetries are also present. If we first look on the lightest quarks in Table 1.1, we will find that the masses of an up- and down-quark are small (and approximately the same) compared to the quarks of II. or III. generation. This implies to put the u-quark and the d-quark together

$$\Psi = \begin{pmatrix} u \\ d \end{pmatrix} \tag{1.12}$$

and write the fermionic part of the Lagrangian as

$$\mathscr{L}_{\text{fermion}} = \overline{\Psi}(i\gamma^\mu D_\mu - M)\Psi \tag{1.13}$$

where M is the *mass matrix*

$$M = \begin{pmatrix} m_u & 0 \\ 0 & m_d \end{pmatrix}. \tag{1.14}$$

If we now assume that m_u and m_d are small than the hadronic scale which is typically considered in QCD, we can write the *mass matrix* as a multiple of an unit matrix, i.e. $m = m_u = m_d$. In this way a further approximate symmetry of the Lagrangian, namely the invariance under a 2×2 unitary transformation of the quark fields, occurs. This approximate symmetry $U(2)_V$ can be written as the product $U(1)_V \otimes SU(2)_V$ where $U(1)_V$ is the quark number (conservation) symmetry and $SU(2)_V$ is the *isospin* symmetry. For degenerated u- and d-quarks, this approximate isospin symmetry turns

into an exact symmetry of the Lagrangian. The $SU(2)_V$ symmetry can be extended into $SU(3)_V$ if the *strange* quarks is included into (1.12). Its mass is not so small anymore compared to the quarks in the first generation but it is still small compared to the scale of hadrons masses, for example, the proton mass ($m_\mathrm{P} \approx 1$ GeV). This extension of the flavor symmetry gives the grouping of the baryons and mesons into flavor octets and decuplets. The symmetry increases further if we consider the case of vanishing mass of up and down quark. With the use of the projection operator (see appendix A for definition), the quark fields can be decomposed into left-handed and right-handed components $\Psi_L = P_-\Psi$, $\Psi_R = P_+\Psi$. Due to this decomposition the fields become decoupled in the fermionic part of the Lagrangian

$$\mathscr{L}_\mathrm{fermion} = \overline{\Psi}_L i\gamma^\mu D_\mu \Psi_L + \overline{\Psi}_R i\gamma^\mu D_\mu \Psi_R. \tag{1.15}$$

Between left-handed and right-handed fields, there is no mixing term anymore. Therefore we can perform rotations on both fields independently $U(2)_L \otimes U(2)_R$. Such a symmetry is called *chiral symmetry*. In our case, where we considered only the up and down quark, it is a chiral $SU(2)$ symmetry. It can be extended to chiral $SU(3)$ through adding the strange quark as mentioned before. In the spectrum of QCD, chiral symmetry does not appear. It is *spontaneously broken*, i.e. the ground state does not share the same symmetry as the Lagrangian. The *quark condensate* has a non-vanishing vacuum expectation value

$$\langle\overline{\Psi}\Psi\rangle = \langle 0|\overline{\Psi}_L\Psi_R + \overline{\Psi}_R\Psi_L|0\rangle \neq 0. \tag{1.16}$$

If chiral symmetry exists in QCD this expectation value, where the left-handed and right-handed fields mix, would vanish. According to the *Goldstone theorem* [9] spontaneously broken exact symmetries generate massless spin-zero particles called *Goldstone bosons*. The number of such particles is given by the number of spontaneously broken symmetry generators. Indeed, the experiment shows that this particles exist, not massless but very light compared to other hadrons. In the case of chiral $SU(2)$ the number of broken generators is three which are identified with the pions π^0, $\pi^\pm$. For chiral $SU(3)$ the eight broken generators produce an octet of mesons π^0, $\pi^\pm$, K^0, $\bar{K}^0$, $K^\pm$, and η. In reality, the quarks are not massless as shown in Table 1.1. Therefore chiral symmetry of the Lagrangian is not exact which is also reflected in the fact that the pions etc. have a finite mass as shown in Table 1.2. Nevertheless the masses of the pions are much lower

particle	anti-partic.	mass in MeV	(mean) lifetime in seconds
π^0	self	134.9766 ± 0.0006	$(8.4 \pm 0.6) \times 10^{-17}$
π^+	π^-	139.57018 ± 0.00035	$(2.6033 \pm 0.0005) \times 10^{-8}$
K^+	K^-	439.677 ± 0.016	$(1.2380 \pm 0.0021) \times 10^{-8}$
K^0	$\bar{K}^0$	497.614 ± 0.024	-
η	self	547.853 ± 0.024	$(5.1 \pm 0.3) \times 10^{-19}$

Table 1.2: Properties of mesons [6]

than the kaons and the η meson. This points out that the chiral $SU(3)$ symmetry is less reliable compared to the chiral $SU(2)$ symmetry as we would expect it when we consider the mass differences of an up/down and a strange quark. The non-zero small masses of u and d (and s) quarks can be treated as a perturbation. In the low energy regime of QCD where the standard perturbation theory breaks down due to the large value of the strong coupling, the *chiral perturbation theory* [10] which bases on the chiral symmetry is a powerful tool and gives a exceptionally consistent picture of the strong interaction below the hadronic scale of 1 GeV. For chiral $SU(N)$ symmetry with $N > 3$ the quarks (mainly charm and bottom; top has a tiny lifetime and it is not expected to build bound states) become so heavy that the chiral perturbation theory is not applicable anymore. For the heavy quark sector, we can consider another approximate symmetry of the Lagrangian, namely the *heavy quark symmetry*. A quark is considered to be heavy when its *Compton wavelength* is much smaller than the typical extension of a hadron, say, proton (about 1 fm). This means that the quark has to be much heavier than 200 MeV. Such bound states are, for example, the B and D mesons where one quark is a (anti-) bottom and (anti-) charm, respectively, and the other one is (anti-) up, (anti-) down or (anti-) strange to build a quark-antiquark pair. The heavy quark serves as a static source of color charge and the effective theory which describes such bounds states is invariant under flavor and spin changes (for more details see [11, 12]).

1.4 Confinement and asymptotic freedom

In 1973, as *H. D. Politzer* [13] and *D. J. Gross* and *F. Wilczek* [14–16] pointed out that non-abelian gauge theories like QCD have a peculiar property which they called *asymptotic freedom*. In that context, it is important to discuss the concept of *running coupling* what we will do next in few words (for detailed discussions, see [3, 5]). At the beginning of this chapter, we introduced QCD as an analogous theory to QED and discussed the main differences between both theories. For the discussion of running coupling, we want to start from the QED case and bridge to the non-abelian case. If we consider an electron in "vacuum", we know from quantum electrodynamics that the electron is covered by a cloud of virtual electron-positron pairs (due to *the uncertainty principle*) which screens off the "bare" charge of the electron. But if we go to higher energy scales and try to penetrate more and more through this cloud of virtual particles, we will measure an increasing value of the electron charge and respectively of the coupling constant ($\alpha_{\mathrm{EM}} \propto e^2$). This is the so-called *running of the coupling with the energy scale*. The situation is completely different in the case of QCD. A quark in QCD "vacuum" is covered by a cloud of gluons and quark-antiquark pairs. The color charge of the quark is then reduced by the virtual quark-antiquark pairs, but the virtual gluons which carry also color charge in contrast to photons can thus increase the color charge of the original quark due to the self-coupling effect (see below), i.e. if we penetrate through this cloud of virtual particles, the coupling will decrease more and more. In the lowest

order perturbation theory, the effective strong coupling constant behaves as follows

$$\alpha_S(\mu^2) \propto \frac{1}{\ln(\mu^2/\Lambda^2)}. \tag{1.17}$$

This property appears in all orders of perturbation theory. Here, μ is the energy scale and Λ is a constant about 200 MeV [17] which has to be determined experimentally. Equation (1.17) implies that α_S decrease with increasing energy. This prediction was also proven through the experiment. Figure 1.1 shows a summary plot of the strong

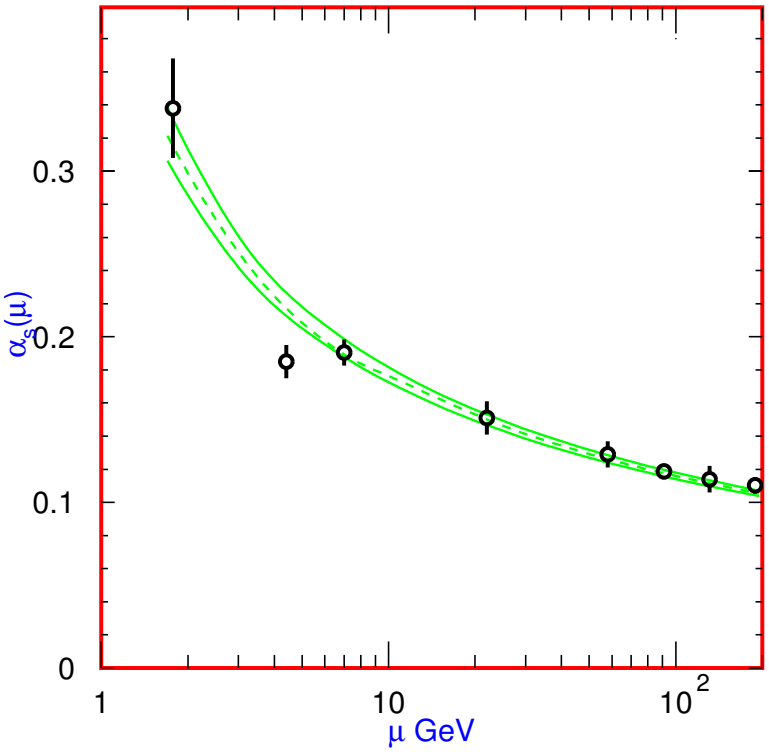

Figure 1.1: The running of the strong coupling constant α_S. It is taken from [6]

coupling constant $\alpha_S(\mu)$ measured experimentally at different scales μ. The dashed line and the solid lines are the world average and the $\pm 1\sigma$ limits, respectively. The decreasing behavior of α_S is clearly shown by this plot (for more details, see [6, 18–20]). At short distances (high energy scales), the strong coupling becomes so small that the gluons and quarks behave like free particles (asymptotically free) and their interaction can be treated in perturbation theory, but in the low-energy regime, when the energy scale goes toward Λ, the coupling becomes stronger (and even diverges at $\mu = \Lambda$ and the perturbation theory breaks down), a new phenomenon called *confinement* sets in and quarks and gluons are confined in hadrons. It means that this particles cannot appear as free particles. This big difference to QED stems originally from the fact that gluons carry also a color charge. As mentioned before, they can interact with themselves.

The additional self-interaction vertices, which have no counterparts in QED, are given pictorially in Figure 1.2. These diagrams cause the additional term "$gf^{abc}A^b_\mu A^c_\nu$" in the

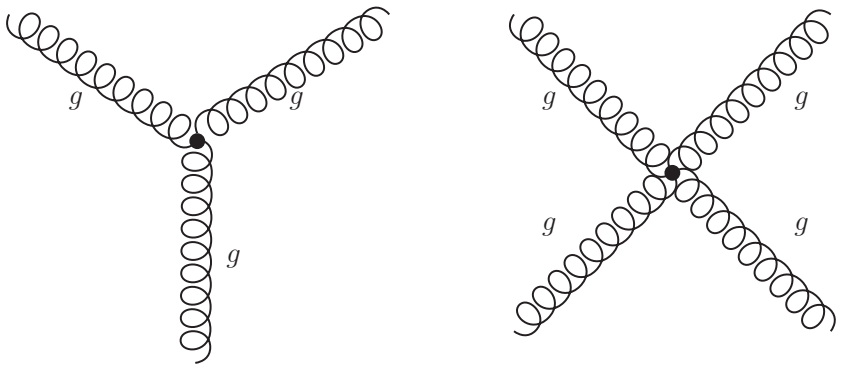

Figure 1.2: Three and four gluon interactions

field strength tensor (1.3) of QCD. The remainder of the work is organized as follows. In the next chapter, we want to give a brief introduction to lattice QCD and describe how one can formulate QCD on lattice. After discussing different formulations of fermions, we will explain the $\mathcal{O}(a)$ improved Wilson quarks which we will use in our simulations. In the third chapter, we will discuss the working horse of lattice QCD the so-called Hybrid Monte Carlo (HMC) algorithm. The evaluation of the path integral with dynamical fermions is a demanding task and since the first suggestion of HMC a lot of efforts have been made to improve the performance of the algorithm to make lattice QCD calculations accessible on current computational facilities. We will give a summary of those tricks and some popular variants of HMC. Then, we will give some theoretical foundations of the running parameters of QCD and introduce our model the Schrödinger functional scheme and discuss how a coupling can be defined in this scheme. In the subsequent chapter, we will explain the two flavor ALPHA code and how we intend to extend it to arbitrary even numbers of flavors. Finally, we want to discuss our results in detail and show the energy dependence of the QCD coupling with four flavors of $\mathcal{O}(a)$ improved Wilson quarks in Schrödinger functional scheme. Then, we will give a summary.

2 Lattice QCD

In this chapter, we want to discuss how to find a suitable formulation of a quantum field theory, especially quantum chromodynamics, for numerical treatments. The crucial idea of *K. Wilson* putting QCD on a space-time lattice, which he proposed in [21], and further developments will be discussed. We are going to give an overview about this subject. For detailed discussions, we refer the interested reader to the following textbooks [22–26] and to the following papers [27–32].

2.1 Path integral

The path integral formulation of quantum mechanics, which was introduced by *Feynman* [33] in 1948, is an equivalent way, beside *Schrödinger's wave mechanics* and *Heisenberg's matrix mechanics*, to describe quantum effects and calculate matrix elements. The idea is based on *the principle of least action of classical mechanics*. Instead of considering a single trajectory of, e.g., a moving particle, one regards all possible paths, weights them with a Feynman factor (the counterpart in statistical mechanics is the Boltzmann factor) and sums over all paths to compute quantum amplitudes. The path with the smallest action will dominate. This concept can be generalized from quantum mechanics to quantum field theories (QFTs). It is also possible to use a Hamiltonian formulation of QFTs with non-commuting operators, but for the purpose of numerical evaluation, a formulation of the theory with ordinary commuting numbers is more suitable.
The starting point for the path integral formulation is the partition function

$$Z = \int \mathscr{D}A_\mu \mathscr{D}\Psi \mathscr{D}\overline{\Psi} \exp\{iS_{\mathrm{QCD}}[A_\mu, \Psi, \overline{\Psi}]\} \tag{2.1}$$

where the operator $\mathscr{D}$ denotes $\mathscr{D}\square \mathrel{\widehat{=}} \prod_{x,\alpha} d\square_\alpha(x)$. The action of QCD is given in term of the Lagrangian by

$$S_{\mathrm{QCD}}[A_\mu, \Psi, \overline{\Psi}] = \int dx^4 \underbrace{\mathscr{L}_{\mathrm{QCD}}}_{\mathrm{from}(1.10)} . \tag{2.2}$$

The paths in (2.1) are weighted with an oscillating function. Therefore it makes sense to transform the path integral by a Wick rotation from Minkowski space to Euclidian space to circumvent the oscillating integral kernel in numerical simulations. The real time of (2.1) is then turned into an imaginary time

$$x_0 = ix_4. \tag{2.3}$$

As a consequence of this, the commutation relation of the Dirac γ-matrices changes slightly (here, γ^E denotes the γ matrices in Euclidean space)

$$\{\gamma_\mu, \gamma_\nu\} = 2g_{\mu\nu}1_{4\times4} \Rightarrow \{\gamma_\mu^E, \gamma_\nu^E\} = 2\delta_{\mu\nu}1_{4\times4} \tag{2.4}$$

with

$$\gamma_4^E = \gamma^0, \quad \gamma_j^E = -i\gamma^j. \tag{2.5}$$

Details about the γ matrices and the metric can be found in appendix A. The partition function (2.1) becomes

$$Z = \int \mathscr{D}A_\mu \mathscr{D}\Psi \mathscr{D}\overline{\Psi} \exp\{-S_{\mathrm{QCD}}^E[A_\mu, \Psi, \overline{\Psi}]\}. \tag{2.6}$$

In the following, we are going to stay in the Euclidean space and therefore drop the index E. The expectation value of a physical observable $\mathscr{O}$ is then given by

$$\langle \mathscr{O} \rangle = \frac{1}{Z} \int \mathscr{D}A_\mu \mathscr{D}\Psi \mathscr{D}\overline{\Psi}\ \mathscr{O}[A_\mu, \Psi, \overline{\Psi}] \exp\{-S_{\mathrm{QCD}}[A_\mu, \Psi, \overline{\Psi}]\} \tag{2.7}$$

where the normalization factor Z was defined in (2.6). The integral in (2.7) is infinite-dimensional and is therefore mathematically ill-defined, but the lattice regularization, which we are going to introduce next, will make it finite and thus mathematically well-defined.

2.2 Lattice discretization

As mentioned in the previous chapter, in the low-energy regime of QCD, the coupling constant is of order one. Due to this large coupling constant, the perturbation theory which works excellently in the high-energy regime, breaks down and one needs a new approach. In 1974, *K. Wilson* proposed in his famous paper *"Confinement of quarks"* [21] the idea of a discrete hypercubic space-time lattice where the quarks are defined at the lattice sites and the gluons on the links. The advantage of Wilson's idea is the non-perturbative approach to QCD. On the lattice, one does not have to worry about the breaking down of the perturbation expansion because the only expansion is the one around the lattice spacing a which is usually a small parameter. Originally, this technique was used to show numerically that QCD provides confinement.

2.2.1 Lattice set-up

The discretization of the space-time can be performed in different ways, but the simplest strategy is to choose an isotropic lattice with only one lattice spacing a in temporal and spatial extension. But an anisotropic lattice with different lattice spacings for temporal and spatial extensions is also conceivable [34]. In our case, we take an isotropic lattice.

So, the integrals and derivatives in continuum have to be discretized on the lattice

$$\int d^4x \to a^4 \sum \tag{2.8}$$

$$\partial_\mu \Psi \to \begin{cases} \Delta^f_\mu \Psi(x) = \frac{1}{a}[\Psi(x + a\hat{\mu}) - \Psi(x)] \\ \Delta^b_\mu \Psi(x) = \frac{1}{a}[\Psi(x) - \Psi(x - a\hat{\mu})] \end{cases} \tag{2.9}$$

where $x = (x_1, x_2, x_3, x_4)$ is the lattice site where the derivative is to be taken and $\hat{\mu}$ denotes the unit vector in μ direction and the superscripts f and b denote the forward and backward derivatives respectively. For the boundaries we choose periodic boundary conditions in spatial direction and Dirichlet boundary condition for the temporal direction. With these boundary conditions, the case where a point $x \pm a\mu$ in the above derivatives could fall outside the lattice is well-defined.
On the lattice the Poincaré invariance of the continuum theory is reduced to a discrete group. The hypercubic lattice is only invariant under a rotation by $\pi/2$ and a translation by at least one lattice spacing a.

2.2.2 Link variables

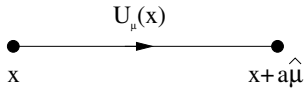

Figure 2.1: Link variable

In the continuum, a fermion which moves from x to y collects a phase factor, due to the presence of a gauge field, that is given by the path ordered product

$$\Psi(y) = \mathcal{P} \exp\left\{ ig \int_x^y dx^\mu A_\mu(x) \right\} \Psi(x). \tag{2.10}$$

This equation indicates that the gauge fields on the lattice should be associated with the links which connect lattice site x with lattice site y. So, Wilson proposed a discrete version of the path ordered product and defined a link variable (Figure 2.1) from x to the neighboring site $x + a\hat{\mu}$ to

$$U(x, x + a\hat{\mu}) = U_\mu(x) = \exp\left\{ igaA_\mu\left(x + \frac{a\hat{\mu}}{2}\right)\right\}. \tag{2.11}$$

Since the lattice spacing a is a small parameter, the integral in (2.10) is approximated by

$$\int_x^{x+a\hat{\mu}} dy^\mu A_\mu(y) \approx a \cdot A_\mu\left(x + \frac{a\hat{\mu}}{2}\right), \tag{2.12}$$

and replaced in (2.11). The link variable in the other direction (from x to $x - a\hat{\mu}$) is

then given by

$$U(x, x - a\hat{\mu}) = U_{-\mu}(x) = \exp\left\{-igaA_\mu\left(x - \frac{a\hat{\mu}}{2}\right)\right\} = U^\dagger(x - a\hat{\mu}, x). \tag{2.13}$$

With these link variables, we can construct two types of objects on the lattice which are gauge invariant. The first one is a string, which we can build as a path-ordered product of link variables $U_\mu(x)$, connecting a fermion and an anti-fermion, i.e.

$$\text{“string”} = \text{tr}\left(\overline{\Psi}(x)U_\mu(x)U_\nu(x+\hat{\mu})\ldots U_\omega(y-\hat{\omega})\Psi(y)\right), \tag{2.14}$$

and the second one is a closed Wilson loop (in Figure 2.2, 1×1 Wilson loop is shown which is also called a plaquette)

$$W_{\mu\nu}^{1\times1} = Re\left\{tr\left[U_\mu(x)U_\nu(x+\hat{\mu})U_\mu^\dagger(x+\hat{\nu})U_\nu^\dagger(x)\right]\right\}. \tag{2.15}$$

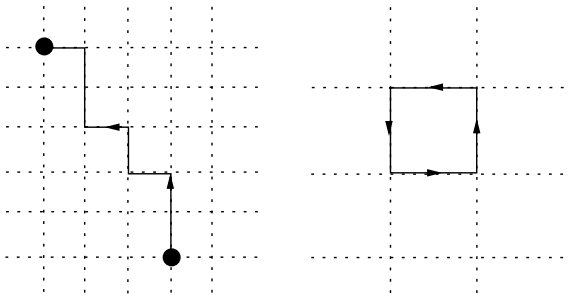

Figure 2.2: Gauge invariant object on the lattice; left: string, right: closed 1×1 Wilson loop

2.3 Gauge action

The invariant action on the lattice has to be built out of strings and loops which we introduced above. But the important point is that the lattice action has to result in the continuum action if one takes the limit $a \to 0$. First we should have a look at the gauge part of the action. The plaquette which is shown in Figure 2.3 can be written in terms of the $U_\mu(x)$ as follows

$$U_{\mu\nu} = U_\mu(x)U_\nu(x+\hat{\mu})U_\mu^\dagger(x+\hat{\nu})U_\nu^\dagger(x). \tag{2.16}$$

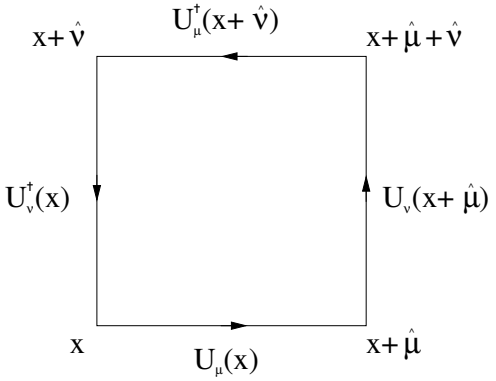

Figure 2.3: The plaquette

Replacing the link variables $U_\mu(x), U_\nu(x+\hat{\mu}), \ldots$ with (2.11) gives (for the sake of convenience, $a\hat{\mu} \to \hat{\mu}$ and $a\hat{\nu} \to \hat{\nu}$ in the following)

$$U_{\mu\nu} = \exp\left\{iagA_\mu\left(x+\frac{\hat{\mu}}{2}\right)\right\}\cdot\exp\left\{iagA_\nu\left(x+\hat{\mu}+\frac{\hat{\nu}}{2}\right)\right\}\cdot \exp\left\{-iagA_\mu\left(x+\hat{\nu}+\frac{\hat{\mu}}{2}\right)\right\}\cdot\exp\left\{-iagA_\nu\left(x+\frac{\hat{\nu}}{2}\right)\right\}. \quad (2.17)$$

For merging the exponential functions, we need the Campbell-Baker-Hausdorff formula because the A_μs are non-commuting $SU(3)$-matrices

$$\begin{aligned}\exp\{gA\}\exp\{gB\} &= \exp\left\{g(A+B)+\frac{g^2}{2}[A,B]+\ldots\right\}\\ &= \exp\{CBH(A_\mu,A_\nu)\}\end{aligned}$$

where $CBH(A_\mu, A_\nu)$ in our case is given by

$$\begin{aligned}CBH(A_\mu,A_\nu) = iag\Bigg\{&A_\mu\left(x+\frac{\hat{\mu}}{2}\right)+A_\nu\left(x+\hat{\mu}+\frac{\hat{\nu}}{2}\right)+\\ &\frac{iag}{2}\left[A_\mu\left(x+\frac{\hat{\mu}}{2}\right),A_\nu\left(x+\hat{\mu}+\frac{\hat{\nu}}{2}\right)\right]-A_\mu\left(x+\hat{\nu}+\frac{\hat{\mu}}{2}\right)-A_\nu\left(x+\frac{\hat{\nu}}{2}\right)+\\ &\frac{iag}{2}\left[A_\mu\left(x+\hat{\nu}+\frac{\hat{\mu}}{2}\right),A_\nu\left(x+\frac{\hat{\nu}}{2}\right)\right]\Bigg\}-\\ &\frac{a^2g^2}{2}\left(\left\{A_\mu\left(x+\frac{\hat{\mu}}{2}\right),-A_\nu\left(x+\frac{\hat{\nu}}{2}\right)\right\}+\ldots\right).\end{aligned}$$

Expanding the $A_{\mu/\nu}$s about the midpoint $x + \frac{\hat{\mu}+\hat{\nu}}{2}$ of the plaquette gives the following approximation

$$\begin{aligned}
A_\mu\left(x+\frac{\hat{\mu}}{2}\right) &= A_\mu\left(x+\frac{\hat{\mu}+\hat{\nu}}{2}\right) - \frac{a}{2}\partial_\nu A_\mu\left(x+\frac{\hat{\mu}+\hat{\nu}}{2}\right)+\dots \\
A_\mu\left(x+\hat{\nu}+\frac{\hat{\mu}}{2}\right) &= A_\mu\left(x+\frac{\hat{\mu}+\hat{\nu}}{2}\right) + \frac{a}{2}\partial_\nu A_\mu\left(x+\frac{\hat{\mu}+\hat{\nu}}{2}\right)+\dots \\
A_\nu\left(x+\hat{\mu}+\frac{\hat{\nu}}{2}\right) &= A_\nu\left(x+\frac{\hat{\mu}+\hat{\nu}}{2}\right) + \frac{a}{2}\partial_\mu A_\nu\left(x+\frac{\hat{\mu}+\hat{\nu}}{2}\right)+\dots \\
A_\nu\left(x+\frac{\hat{\nu}}{2}\right) &= A_\nu\left(x+\frac{\hat{\mu}+\hat{\nu}}{2}\right) - \frac{a}{2}\partial_\mu A_\nu\left(x+\frac{\hat{\mu}+\hat{\nu}}{2}\right)+\dots
\end{aligned}$$

Considering only the leading order contributions, we obtain

$$\begin{aligned}
CBH\left(A_\mu, A_\nu\right) &\approx iag\left\{a(\partial_\mu A_\nu - \partial_\nu A_\mu) + iag\left[A_\mu, A_\nu\right]\right\} && (2.18)\\
&\approx ia^2 g\left\{\partial_\mu A_\nu - \partial_\nu A_\mu + ig\left[A_\mu, A_\nu\right]\right\}, && (2.19)
\end{aligned}$$

where we can identify the field strength tensor $F_{\mu\nu}$ of QCD

$$CBH\left(A_\mu, A_\nu\right) \approx iga^2 F_{\mu\nu}. \tag{2.20}$$

Let us now expand the exponential function $\exp\{CBH(A_\mu, A_\nu)\}$

$$U_{\mu\nu} = \exp\{CBH(A_\mu, A_\nu)\} \approx 1 + ia^2 g F_{\mu\nu} - \frac{a^4 g^2}{2} F_{\mu\nu}F^{\mu\nu} + \mathcal{O}(a^6), \tag{2.21}$$

and consider the real part of the trace:

$$Re\ \ \mathrm{tr}\left(1 - U_{\mu\nu}\right) = \frac{a^4 g^2}{2} tr\left[F_{\mu\nu}F^{\mu\nu}\right] + \mathcal{O}(a^6). \tag{2.22}$$

In (2.22), we have to sum over all plaquettes with one orientation ($\mu < \nu$). Because of double counting, we have to take care of a factor $1/2$. If we consider

$$\begin{aligned}
\frac{1}{2g^2}\sum_x \sum_{\mu<\nu} Re\ tr\left[1 - U_{\mu\nu}(x)\right] &\to \frac{a^4}{4}\sum_x \sum_{\mu<\nu}\left\{tr\left[F_{\mu\nu}F^{\mu\nu}\right] + \mathcal{O}(a^2)\right\} \\
&\to \frac{1}{4}\int d^4x\ \ tr\left[F_{\mu\nu}F^{\mu\nu}\right], && (2.23)
\end{aligned}$$

we see that the gauge action, which is composed of the plaquette, leads to the continuum gauge action. The simplest formulation, the so-called *Wilson gauge action* [21], uses the 1×1 Wilson loop

$$S_\mathrm{G} = \beta \sum_x \sum_{\mu<\nu}\left(1 - \frac{1}{N_c} Re\ tr[U_{\mu\nu}]\right) \tag{2.24}$$

where $\beta = 2N_c/g^2$ and N_c is the number of colors (for $SU(3)$: $N_c = 3$). Above we discussed only the simplest gauge action where the leading order lattice artifacts are $\mathcal{O}(a^2)$. According to *Symanzik's improvement* [35–37], *Lüscher* and *Weisz* worked out in [38] how to improve the gauge action through a linear combination of 1×1 and 1×2 Wilson loops with coefficients chosen appropriately such that the resulting action has only $\mathcal{O}(a^4)$ leading order corrections. In our simulations, we will use the Wilson plaquette action (2.24).

2.4 Fermions on the lattice

The formulation of fermions on the lattice produces some problems. For example, the naive discretization of the fermion action, where the continuum derivatives are replaced by the discrete versions, contains additional fermions to the physical one; these are called *doublers*. For removing all of these unphysical fermions, Wilson proposed an additional term in the fermion action, the so-called *Wilson term*, which solved the doubling problem but caused another one: It broke chiral symmetry explicitly, even for $m = 0$. For dealing with all these difficulties many approaches have been developed. In 1981, *Nielsen* and *Ninomiya* [39] proved a no-go theorem in which they showed the constraints of formulating fermions on the lattice. According to this theorem, the lattice Dirac operator D of a type of action

$$S = \sum_{x,y} \overline{\Psi}(x)(D + m)\Psi(y) \tag{2.25}$$

cannot have all of the following properties simultaneously (we denote by $\tilde{D}(p)$ the Fourier space representation of the Dirac operator D):

1. $\tilde{D}(p)$ is periodic in momentum space with period $2\pi/a$ (translation invariance).
2. $\tilde{D}(p)$ is continuous in momentum space (locality of interaction).
3. For small p_μ and $a \to 0$, $\tilde{D}(p) \to i\gamma_\mu p_\mu$
4. No doublers.
5. For the massless case ($m = 0$), chiral symmetry is preserved:

$$\gamma_5 D + D\gamma_5 = 0$$

The present formulation of fermions on the lattice could be roughly classified in two categories. The first type of approach gives up fully or partly the preservation of chiral symmetry and obtains a simple discretization which has numerical advantages (numerically cheap). The second type keeps the chiral symmetry on the lattice as much as possible which has the drawback of being very computer time intensive. The different formulations are compared in Table 2.1 [40]. A natural starting point of finding a

formulation	doubler	locality	chiral sym.	discret. effects
naive	16	yes	yes	$\mathcal{O}(a^2)$
staggered	4	yes	some	$\mathcal{O}(a^2)$
rooted staggered	1	no	some	$\mathcal{O}(a^2)$
Wilson	1	yes	no	$\mathcal{O}(a)$
improved Wilson	1	yes	no	$\mathcal{O}(a^2)$
twisted mass Wilson	1	yes	discrete	$\mathcal{O}(a^2)$
Ginsparg-Wilson	1	num. ok	lattice version.	$\mathcal{O}(a^2)$
Domain-Wall	1	num. ok	approx.	$\approx \mathcal{O}(a^2)$

Table 2.1: Summary of fermion formulations on the lattice

formulation for lattice fermions is the the continuum free fermion action

$$S_{\mathrm{F}}^{\mathrm{cont}} = \int d^4x \{\overline{\Psi}(x)\gamma_\mu \partial_\mu \Psi(x) + m\overline{\Psi}(x)\Psi(x)\}. \tag{2.26}$$

In equation (2.9) the continuum derivative was discretized without gauge fields. In oder to preserve the gauge symmetry on the lattice, we have to introduce the covariant derivatives in analogy to (2.9)

$$\nabla_\mu^f \Psi(x) = \frac{1}{a}[U_\mu(x)\Psi(x + a\hat{\mu}) - \Psi(x)] \tag{2.27}$$

$$\nabla_\mu^b \Psi(x) = \frac{1}{a}[\Psi(x) - U_\mu^\dagger(x - a\hat{\mu})\Psi(x - a\hat{\mu})]. \tag{2.28}$$

Generally, the symmetric combination of the covariant forward and backward derivatives is used

$$\tilde{\nabla}_\mu \Psi(x) = \frac{1}{2}\left[\nabla_\mu^f + \nabla_\mu^b\right]\Psi(x). \tag{2.29}$$

The reason for this is the leading order of the discretization error. In the case of the simple covariant forward and backward derivatives, the leading order is $\mathcal{O}(a)$, whereas the symmetric covariant derivative improves this to $\mathcal{O}(a^2)$. The naive lattice fermion action now becomes

$$S_{\mathrm{F}}^{\mathrm{naive}} = a^4 \sum_x [\overline{\Psi}(x)\gamma_\mu \tilde{\nabla}_\mu \Psi(x) + m\overline{\Psi}(x)\Psi(x)]. \tag{2.30}$$

This action is local and has the right continuum behavior. Chiral symmetry is preserved but (2.30) now contains doublers. If we consider the Fourier transform of the lattice Dirac operator for free fermions,

$$\tilde{D}(p) = m + \frac{i}{a}\sum_\mu \gamma_\mu \sin(p_\mu a), \tag{2.31}$$

in the chiral limit $m \to 0$, we can easily see, that beside the physical fermion at $p_\mu = (0,0,0,0)$, it provides 15 additional unphysical fermions at the corners of the Brillouin zone:

$$p_\mu = \begin{cases} (\pi/a, 0, 0, 0) & \times 4 \\ (\pi/a, \pi/a, 0, 0) & \times 6 \\ (\pi/a, \pi/a, \pi/a, 0) & \times 4 \\ (\pi/a, \pi/a, \pi/a, \pi/a) & \times 1 \end{cases} \tag{2.32}$$

This is the well-known *doubling problem*. Wilson introduced an irrelevant operator to the naive discretized action to avoid such a doubling problem. The effect of this term is that the 15 unphysical fermions decouple and become infinitely heavy in the continuum limit and only the physical fermion remains. The modified Dirac operator D_w is then given by

$$\overline{\Psi}(x) D_\mathrm{w} \Psi(x) = \overline{\Psi}(x) \gamma_\mu \tilde{\nabla}_\mu \Psi(x) - \frac{ar}{2} \overline{\Psi}(x) \nabla^b_\mu \nabla^f_\mu \Psi(x), \tag{2.33}$$

where r is the Wilson parameter ($r \in]0,1]$). The disadvantage of the Wilson action is that it explicitly breaks chiral symmetry for $m \to 0$ due to the Wilson term. In 1975 and 1977, *Kogut* and *Susskind* [41, 42] proposed a different way to tackle the doubling problem. The so-called *staggered fermions* reduce the 16 doublers of the naive lattice fermions to 4 by a spin diagonalization. In this formulation, the fermion fields Ψ and $\overline{\Psi}$ are changed to

$$\Psi(x) = \Gamma_x \chi(x), \tag{2.34}$$

$$\overline{\Psi}(x) = \bar{\chi}(x) \Gamma^\dagger_x, \tag{2.35}$$

where

$$\Gamma_x = \gamma_0^{x_0} \gamma_1^{x_1} \gamma_2^{x_2} \gamma_3^{x_3}. \tag{2.36}$$

The naive action (2.30) then becomes

$$S_\mathrm{stag} = a^4 \sum_x \left[\bar{\chi}(x) \Gamma^\dagger_x \gamma^\mu \Gamma_{x+a\hat{\mu}} \tilde{\nabla}_\mu \chi(x) + m \bar{\chi}(x) \chi(x) \right]. \tag{2.37}$$

Using the relation

$$\alpha_\mu(x) = \Gamma^\dagger_x \gamma^\mu \Gamma_{x+a\hat{\mu}} = (-1)^{x_0 + x_1 + \cdots + x_{\mu-1}} 1_{4\times 4}, \tag{2.38}$$

the action (2.37) can be rewritten in the following way:

$$S_\mathrm{stag} = a^4 \sum_x \left[\alpha_\mu(x) \bar{\chi}(x) \tilde{\nabla}_\mu \chi(x) + m \bar{\chi}(x) \chi(x) \right]. \tag{2.39}$$

The Dirac γ_μ matrices have disappeared due to the above transformation and the action is now diagonal in spinor space. The fields χ and $\bar{\chi}$ also have four Dirac components like Ψ and $\overline{\Psi}$, but all of them are decoupled because the phase factor $\alpha_\mu(x)$ is diagonal. So, taking only the first component and neglecting the rest, reduces the 16 flavors to 4 so-called tastes. In contrast to the Wilson fermions, the staggered fermions have remnant chiral symmetry but do not ultimately solve the doubling problem. In connection with staggered fermions, a "fourth-root" trick has been much discussed in the literature: In 1981 *Marinari et al.* [43] suggested a "rooting" trick to reduce the degeneracy of staggered fermions in a massive Schwinger model in QED. This trick was adopted in QCD and is used up to now. For describing a single flavor, the fourth root of the fermion determinant is taken in the path integral

$$\int \mathscr{D}U e^{-S_\mathrm{G}} \det(D_\mathrm{stag} + m) \Rightarrow \int \mathscr{D}U e^{-S_\mathrm{G}} \det(D_\mathrm{stag} + m)^{1/4}. \tag{2.40}$$

Now, if one wants to reconstruct the action of the rooted staggered fermions from the right-hand side of (2.40), one would fail because the corresponding Dirac operator D_action of the rooted determinant, which appears in the action, is not known

$$\det(D_\mathrm{stag} + m)^{1/4} \stackrel{?}{=} \det(\underbrace{D_\mathrm{action}}_{\text{not known}} + m). \tag{2.41}$$

As shown in Table 2.1, the locality requirement of the *rooted staggered fermions* is violated [44], and hence universality is threatened, i.e. if universality is not maintained, the continuum limit would give wrong results and the *rooted staggered fermions* would not describe physics. Despite these problems, the underlying motivation of using rooted staggered fermions comes from the numerical point of view. They are numerically cheaper than the Wilson fermions because of the reduction of the four Dirac components per site to one and they are automatically $\mathcal{O}(a)$ improved, which is a priori not given in the Wilson formulation (but in the improved Wilson fermions, see next section). Nevertheless, the hope is that the effect of non-locality disappears in the continuum limit and does not influence the universality.

The next lattice fermion formulation that we want to mention here is the *twisted mass (tm) Wilson fermion.* As its name implies, this formulation is based on Wilson fermions but with a fundamental difference. In 1999, *Frezotti et al.* [45, 46] suggested a way of improving Wilson fermions by adding a chirally rotated mass term to the lattice Dirac operator for a two flavor QCD. The Dirac-Wilson operator D_w in (2.33) is modified slightly to

$$D_\mathrm{tm} = D_\mathrm{w} + m + i\mu\gamma_5\tau_3, \tag{2.42}$$

where the parameter μ is the so-called twisted mass parameter and τ_3 is the isospin generator which acts in flavor space. For any finite μ, the fermion determinant for two

flavors

$$\det\{D_{\mathrm{tm}} D_{\mathrm{tm}}^{\dagger}\} = \det\left\{(D_{\mathrm{w}} + m)(D_{\mathrm{w}} + m)^{\dagger} + \mu^2\right\} > 0 \tag{2.43}$$

is manifestly positive. In other words, the Dirac operator of the tm QCD is protected against zero modes. Therefore, the so-called exceptional configurations, those configurations where the determinant would vanish, are excluded. At the expense of flavor symmetry, chiral symmetry is partly preserved. At maximal twist $\mu = \pi/2$, the fermions automatically become $\mathcal{O}(a)$ improved and there is no need to tune improvement coefficients (see e.g. improved Wilson fermions). Up to cutoff effects, the twisted mass QCD is equivalent to standard QCD [45].

Until now, we have described lattice fermions which violate the chiral symmetry fully or partly. But it has been discussed in literature that chiral symmetry could hold exactly on the lattice with a slight modification of the last requirement of the Nielsen-Ninomiya theorem. In 1982, *Ginsparg* and *Wilson* [47] proposed a modified definition of chiral symmetry adapted to the lattice discretization

$$\gamma_5 D + D\gamma_5 - aD\gamma_5 D = 0. \tag{2.44}$$

The additional term on the left-hand side could be understood as a result of the lattice version of the infinitesimal continuum chiral rotation, i.e.

$$\begin{array}{ccc} \text{continuum} & & \text{lattice} \\ \delta\Psi = i\epsilon\gamma_5\Psi & \Rightarrow & \delta\Psi = i\epsilon\gamma_5(1 - \frac{a}{2}D)\Psi \\ \delta\overline{\Psi} = i\epsilon\overline{\Psi}\gamma_5 & \Rightarrow & \delta\overline{\Psi} = i\epsilon\overline{\Psi}(1 - \frac{a}{2}D)\gamma_5 \end{array}$$

where a is the lattice spacing. Calculating

$$\delta\mathscr{L} = (\delta\overline{\Psi})D\Psi + \overline{\Psi}D\delta\Psi = 0 \tag{2.45}$$

then gives the above mentioned famous Ginsparg-Wilson (GW) relation (2.44). An action which is built out of a Dirac operator D fulfilling this relation is invariant under the continuous chiral symmetry. Indeed, the Ginsparg-Wilson relation achieves the continuum chiral symmetry requirement, when the lattice spacing goes to zero

$$\{\gamma_5, D\} = aD\gamma_5 D \xrightarrow{a\to 0} \{\gamma_5, D\} = 0. \tag{2.46}$$

Since the publication of the GW relation, different approaches have been proposed to satisfy it. The first proposal was made by *Kaplan* [48] and involved actions with five dimensional fermions (so-called domain wall fermions), followed by *Hasenfratz* [49] with the *fixed point action* and *Neuberger's overlap* approach [50]. As mentioned before, simulations with fermions which preserve chiral symmetry are numerically expensive and they are still a big challenge for algorithms and computer resources. Nevertheless, chiral symmetry is an important property of QCD and should be preserved as much as possible on the lattice.

In this work, we will use the $\mathcal{O}(a)$ improved Wilson fermions and discuss them in some detail in the following section. For further details, we refer the reader to [25].

2.5 Improved Wilson fermions

In the previous section, we already introduced Wilson fermions which broke chiral symmetry due to the Wilson term. The discretization error went with the lattice spacing a ($\propto \mathcal{O}(a)$) which is a drawback compared to other formulations (see Table 2.1). In 1985, *Sheikholeslami* and *Wohlert* worked out in [51] that the $\mathcal{O}(a)$ lattice artifacts of the Wilson action could be removed according to the Symanzik improvement program by adding a dimension-five operator. The resulting improved action is then given by

$$S_{\text{impr}} = S_{\text{Wilson}} + \frac{ia^5 c_{\text{sw}}}{4} \sum_x \overline{\Psi}(x)\sigma_{\mu\nu}\mathcal{F}_{\mu\nu}(x)\Psi(x) \tag{2.47}$$

where $\mathcal{F}_{\mu\nu}$ is the lattice representation of the gluon field tensor and $\sigma_{\mu\nu} = \frac{i}{2}[\gamma_\mu, \gamma_\nu]$. The action (2.47) now includes the Wilson term, which cancels the doublers, and the Sheikholeslami Wohlert term, which causes an $\mathcal{O}(a)$ improvement of the Wilson action. Generally, (2.47) is called the *Sheikholeslami Wohlert (SW) action* or *clover action*. The latter name originally comes from the pictorial representation of $\mathcal{F}_{\mu\nu}$ (Figure 2.4). Actually, the clover term is a sum of four oriented plaquettes and we can easily read off

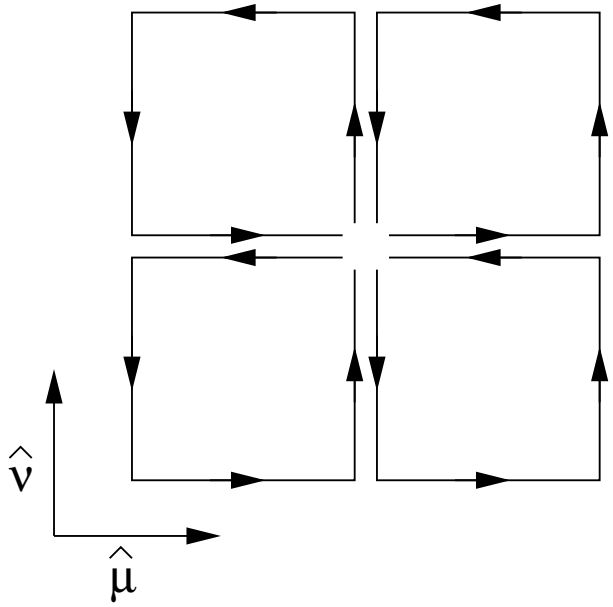

Figure 2.4: Sheikholeslami Wohlert (clover) term

the following expression in terms of the gauge links $U(x)$ for the lattice version of the

field strength tensor from Figure 2.4

$$\begin{aligned}\mathcal{F}_{\mu\nu}(x) = \frac{1}{8a^2}\Big[\Big\{&U_\mu(x)U_\nu(x+\hat{\mu})U_\mu^\dagger(x+\hat{\nu})U_\nu^\dagger(x)\\ &+U_\nu(x)U_\mu^\dagger(x+\hat{\nu}-\hat{\mu})U_\nu(x-\hat{\mu})U_\mu^\dagger(x-\hat{\mu})\\ &+U_\mu^\dagger(x-\hat{\mu})U_\nu^\dagger(x-\hat{\mu}-\hat{\nu})U_\mu(x-\hat{\mu}-\hat{\nu})U_\nu(x-\hat{\nu})\\ &+U_\nu^\dagger(x-\hat{\nu})U_\mu(x-\hat{\nu})U_\nu(x-\hat{\nu}+\hat{\mu})U_\mu^\dagger(x)\Big\}\\ &-\text{hermitian conjugate}\Big]. \end{aligned} \tag{2.48}$$

The parameter c_{sw} in (2.47) is a function of the bare coupling g_0 and has to be tuned such that the $\mathcal{O}(a)$ effects cancel out. A first estimate for the appropriate value of c_{sw} was given by *Sheikholeslami* and *Wohlert* from perturbation theory at tree level [51],

$$c_{\text{sw}} = 1. \tag{2.49}$$

Later, Wohlert acquired the one loop formula [52]

$$c_{\text{sw}} = 1 + 0.26590(7) \cdot g_0^2 + \mathcal{O}(g_0^4). \tag{2.50}$$

With increasing availability of computational power, the non-perturbative determination of c_{sw} became feasible and of interest. In 1996, a first method was proposed by *Lüscher et al.* [53, 54] in the framework of the Schrödinger functional scheme. The ALPHA collaboration and CP-PACS and JLQCD collaborations have investigated the functional dependence of c_{sw} of the Sheikholeslami-Wohlert fermion action with the plaquette gauge action for different numbers of flavors. The results are summarized in Table 2.2. A graphical comparison of c_{sw} for various N_{f} shows (see Figure 2.5) that c_{sw} for

$c_{\text{sw}}^{N_{\text{f}}=0} = \frac{1-0.656g_0^2-0.152g_0^4-0.054g_0^6}{1-0.922g_0^2}$,	$0 \le g_0^2 \le 1$	[54]
$c_{\text{sw}}^{N_{\text{f}}=2} = \frac{1-0.454g_0^2-0.175g_0^4+0.012g_0^6+0.045g_0^8}{1-0.720g_0^2}$,	$0 \le g_0^2 \le 6/5.4$	[55]
$c_{\text{sw}}^{N_{\text{f}}=3} = \frac{1-0.19478g_0^2-0.110781g_0^4-0.0230239g_0^6+0.137401g_0^8}{1-0.460685g_0^2}$,	$0 \le g_0^2 \le 6/5.2$	[56]

Table 2.2: c_{sw} for different N_{f}

two dynamical fermions is significantly different than from the quenched case. But for two and three flavors, the graphs are very close to each other. An interesting question is now to investigate if c_{sw} for four flavors behaves like c_{sw} for three flavors or if there is an significant deviation? Indeed, the first part of this work is dedicated to this topic. In later chapters, we will discuss the method, which was introduced by Lüscher, and a slight modification of it for our purposes in detail.

In general, the Wilson and the improved Wilson fermion action is usually expressed in terms of the *hopping parameter* $\kappa = (2am + 8r)^{-1}$ and the rescaled fields $\Psi \to$

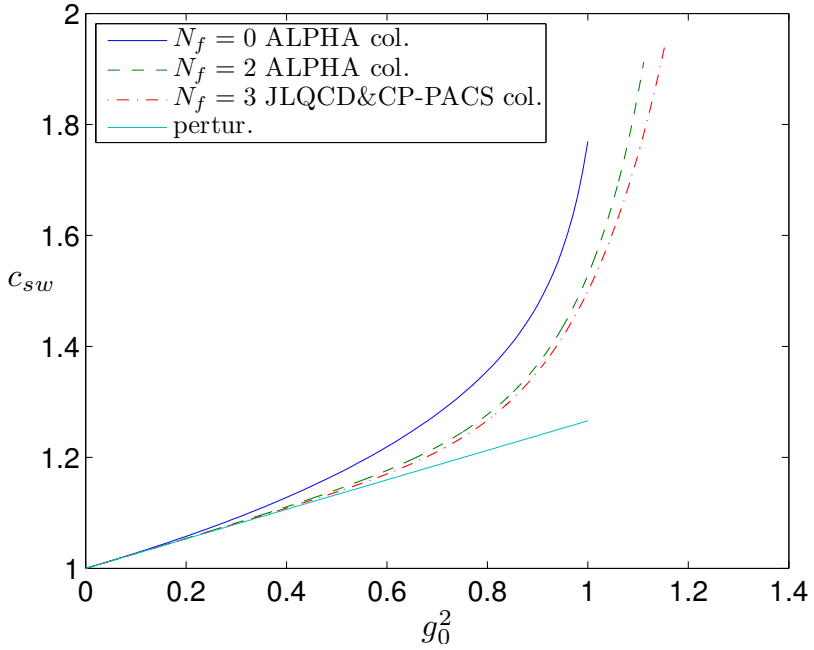

Figure 2.5: Comparison of c_{sw} for various N_{f} and the 1-loop formula (2.50) (lowest line)

$\sqrt{2\kappa}a^{-3/2}\Psi$, where the Wilson parameter r is usually set to one. The complete action of interacting improved Wilson fermions is then given by

$$\begin{aligned} S_{\mathrm{impr}} = & \sum_x \overline{\Psi}(x)\Psi(x) \\ & - \kappa \sum_x \Big[\overline{\Psi}(x)(1-\gamma_\mu)U_\mu(x)\Psi(x+\hat{\mu}) + \overline{\Psi}(x)(1-\gamma_\mu)U^\dagger(x-\hat{\mu})\Psi(x-\hat{\mu})\Big] \\ & - \frac{ia^5\kappa c_{\mathrm{sw}}}{2}\sum_x \overline{\Psi}(x)\sigma_{\mu\nu}\mathcal{F}_{\mu\nu}(x)\Psi(x) \end{aligned} \tag{2.51}$$

2.6 Symanzik improvement

The beautiful idea of introducing a space-time lattice into QCD and thus giving the path integral (2.6) a mathematical well-defined meaning has some drawbacks. The lattice spacing a which had to be introduced due to the discretization and the space-time box in which the simulation has to be carried out are finite. In order to extract physics from simulation data, one has to calculate the observable of interest for various lattice spacings a and has to take the continuum limit $a \to 0$ (continuum extrapolation). Therefore, simulations with small lattice spacings and large space-time boxes are needed, but in practice, they are difficult to perform nowadays. The currently used algorithms, mainly variants of *Hybrid Monte Carlo*, in lattice QCD, which we will discuss later, have

the drawback of critical slowing down if the lattice spacing a becomes smaller and smaller ($a \to 0$). Overcoming this problem demands developing new algorithms and strategies. But, presently, the best available method is the above-mentioned *Hybrid Monte Carlo*. On the other hand, an improvement of the action and local fields of the lattice theory would lead to a reduction of discretization errors and would make the extrapolation to the physical point more accurate. In the previous sections, we discussed the leading order effects of different lattice fermion formulations and focused on the Wilson fermions and its drawback of being an $\mathcal{O}(a)$ action. We then discussed how Sheikholeslami and Wohlert improved the Wilson fermion action by adding a dimension-five term to the action. The origin of this Sheikholeslami-Wohlert term lies in a systematic way of improving action and operators. This so-called *Symanzik improvement program [35–37]* considers the lattice theory as the main object of interest and constructs an effective continuum theory with an explicit cutoff dependence which describes the lattice theory asymptotically. In other words, the lattice action corresponds to the following effective continuum action

$$S_{\text{eff}} = \int d^4x \left\{ \mathscr{L}_0(x) + a\mathscr{L}_1(x) + a^2\mathscr{L}_2(x) + \dots \right\}. \tag{2.52}$$

with the effective lattice fields

$$\phi_{\text{eff}} = \phi_0 + a\phi_1 + a^2\phi_2 + \dots. \tag{2.53}$$

$\mathscr{L}_0(x)$ is the known continuum QCD Lagrangian and $\mathscr{L}_1(x), \mathscr{L}_2(x), \dots, \mathscr{L}_k(x)$ consist of linear combinations of local operators of dimension $4+k$. The restriction to these terms is that they have to have the appropriate dimension and respect the lattice symmetries. For the effective Lagrangian $\mathscr{L}_1$ of the Wilson fermion action, only the following fields are possible (dimension-five fields)

$$\begin{aligned} &\mathcal{O}_1 = \overline{\Psi} i\sigma_{\mu\nu} F^{\mu\nu} \Psi, \quad \mathcal{O}_2 = \overline{\Psi} D_\mu D^\mu \Psi + \overline{\Psi} \overleftarrow{D}_\mu \overleftarrow{D}^\mu \Psi, \qquad \mathcal{O}_3 = m\, tr(F_{\mu\nu} F^{\mu\nu}), \\ &\qquad\qquad\quad \mathcal{O}_4 = m(\overline{\Psi}\gamma_\mu D^\mu \Psi - \overline{\Psi} \overleftarrow{D}_\mu \gamma^\mu \Psi) \text{ and} \quad \mathcal{O}_5 = m^2 \overline{\Psi}\Psi. \end{aligned}$$

This list of fields can be reduced by using the field equations. One can eliminate $\mathcal{O}_2$ and $\mathcal{O}_4$ in favor of $\mathcal{O}_1$, $\mathcal{O}_3$ and $\mathcal{O}_5$. By a redefinition of the coupling constant and the quark mass, $\mathcal{O}_3$ and $\mathcal{O}_5$ can be absorbed in the corresponding terms in $\mathscr{L}_0$ [57]. The only remaining term for the $\mathcal{O}(a)$ improvement in the effective action is then proportional to $\mathcal{O}_1$.

Symanzik's improvement program is a very general procedure for improving lattice theories systematically order by order in the lattice spacing. We discussed above the case of the Wilson action and gave a list of required fields for $\mathscr{L}_1$. In a more general picture, the improvement in a lattice theory can be achieved by modifying the lattice action such that $\mathscr{L}_k$ in the effective continuum theory disappear up to a given order k. If we assume, for example, that $\mathscr{L}_1$ is a linear combination of operators $\mathcal{O}_i$, then an $\mathcal{O}(a)$ improvement requires that this term has to be canceled. In other words, one adds an irrelevant operator $\sum c_i \hat{\mathcal{O}}_i$ to the lattice action and chooses the improvement coefficient c_i such that $\mathscr{L}_1$ vanishes on the lattice ($\hat{\mathcal{O}}_i$ is the lattice version of $\mathcal{O}_i$). The physics

is, of course, not affected by these additional irrelevant operators because in the limit $a \to 0$ all $\mathscr{L}_k, k > 0$ disappear.

2.7 Critical behavior and continuum limit

The extraction of physical information from lattice data is a demanding task and it is, a priori, not obvious why any lattice formulation should give continuum QCD results in the limit of vanishing lattice spacing. We intend to discuss this topic shortly in the following. As mentioned before, the simplest lattice action, namely the Wilson action, gives the continuum QCD action for $a \to 0$. But in fact, the Wilson action is not the only choice and there exist an infinite number of other actions that give the same naive continuum limit. However, in order to make physical predictions, the chosen lattice theory must be in the same universality class as continuum QCD, and therefore it has to have a critical region in parameter space where the correlation length diverges. In this case, the underlying lattice structure would disappear. If a lattice theory has no critical behavior, it cannot describe any continuum field theory, more specifically continuum QCD. Thus, criticality is a crucial requirement.
As mentioned before, the Feynman path integral formulation of quantum mechanics has deep connections to statistical mechanics and a generalization of this concept leads to a correspondence between statistical mechanics and field theories. A partition function of a field theory resembles a partition function of a statistical mechanical system. In this statistical analogy, the mass spectrum, for example, can be extracted from the exponential decay of appropriate correlation functions on the lattice, and, generally, the mass in lattice units is related to the inverse of the correlation length. Therefore, the largest correlation length in the system is dictated by the smallest mass. If this system now has a continuum limit with a finite physical mass, the mass in lattice units has to vanish in the limit $a \to 0$ and, consequently, the correlation length in lattice units has to diverge. Thus a continuum field theory can only be realized at the critical point of a statistical mechanical system with a corresponding partition function.
The continuum limit of lattice QCD demands to send the lattice spacing a to zero or equivalently the bare coupling g_0 to zero. The evolution of the bare coupling with the lattice spacing is described by the *Callan-Symanzik β-function*

$$\beta(g_0) = -a\frac{\partial g_0}{\partial a}. \tag{2.54}$$

For $g_0 \to 0$, the β-function can be approximated in perturbation theory and the resulting equation for $a(g_0)$ shows exponentially decreasing behavior for the lattice spacing (*asymptotic scaling*). In other words, the decrease of a for a fixed number of lattice sites causes a reduction of the physical volume. Therefore one has to increase the number of lattice sites with the decrease of a such that the physical volume of the space-time box is constant. This in turn drives up the computational time of simulations. In practice, one calculates the observables of interest only for three or four values of lattice spacing a on the lattice and performs then the continuum extrapolation to $a = 0$.

3 Monte Carlo Methods

In the previous chapter, we described how the continuum QCD theory can be discretized in an appropriate manner and discussed different aspects of a discretized theory. Now, the evaluation of the path integral (2.6) on a four-dimensional hypercubic lattice is a demanding task and it is not obvious how it is supposed to be performed. If we consider, e.g., a small lattice of 4^4 lattice sites and a simple integration method like Simpson with a mesh of 10 points per integral, the total number of terms which has to be evaluated amounts to $\approx 10^{8200}$. This huge number grows fast with the lattice size. Hence, standard numerical integration methods are not suitable for lattice gauge theories because the numerical computational costs grow with increasing dimension of the integral. For such high dimensional integrals, *Monte Carlo* methods are usually the only choice. In the following, we are going to sketch how a Monte Carlo method can be applied to lattice gauge theories. For further details, we refer the reader to standard textbooks on lattice gauge theories and to the following introductory papers [28, 31, 32, 58].

3.1 Basic idea

The Monte Carlo calculation of an integral is based on the idea of statistical evaluation. In other words, the calculation of the integral has to be performed many times and averaged over all results. Indeed, there exists better techniques for performing integrals numerically but, as explained above, they become very expensive with increasing dimensions.
In a quantum field theory, the quantity in which one is interested in is the *vacuum expectation value* of an observable $\mathscr{O}$ which is given by

$$\langle \mathscr{O} \rangle = \frac{\int \mathscr{D}U \mathscr{O}[U] e^{-S[U]}}{\int \mathscr{D}U e^{-S[U]}}. \tag{3.1}$$

$S[U]$ is a real-valued functional which depends on the link variables U. The weight factor $e^{-S[U]}$ has the same meaning as the Boltzmann factor in statistical mechanics. It weights the different contributions of $\mathscr{O}$ in such a way that $\mathscr{O}[U]$ with the smallest action $S[U]$ contributes mostly (*the principle of least action*). This technique is also known as *important sampling* and accelerates the convergence of the Monte Carlo evaluation enormously. The expression in the denominator of (3.1) guarantees that the normalization condition $\langle 1 \rangle = 1$ holds.
The general strategy of evaluating equation (3.1) with the Monte Carlo method is to average the observable $\mathscr{O}$ evaluated on N gauge field configurations $\{U\}_i$ which are

generated with the probability distribution $e^{-S[\{U\}_i]}$

$$\langle \mathscr{O} \rangle \approx \frac{1}{N} \sum_{i=1}^{N} \mathscr{O}(\{U\}_i). \tag{3.2}$$

The sequence of gauge configuration are usually obtained by a so-called *Markov chain*

$$\{U\}_1 \to \{U\}_2 \to \ldots \{U\}_i \to \ldots \{U\}_N. \tag{3.3}$$

As a starting gauge configuration any gauge configuration can be used. One can set all link variables to the unite matrix (*cold start*) or to some random matrices (*hot start*). Also a mixture of both is conceivable. After starting from an initial configuration, one has to update the configuration (change the configuration) many times according to an algorithm, which we will discuss, such that one obtains eventually configurations (3.3) with the desired distribution. Hence the configuration needs some update steps to become *thermalized*. Actually, there is no general rule for the number of this thermalization updates but one can compare e.g. how a set of observables change with the number of updates (*Monte Carlo histories*) from simulations which started from a hot and a cold configuration for example. As soon as both Monte Carlo history curves reach each other, one can assume that the configuration is thermalized. In general, this is an expensive method because every Monte Carlo simulation has to be carried out, at least, twice. Therefore, usually one looks at the Monte Carlo histories of a set of observables and cut off the measurements until the values of the observabels fluctuate around a mean value. If the thermalized configurations could be considered as statistically independent, the approximation (3.1) would have an error of order $1/\sqrt{N}$. However, in the sequence of configurations, $\{U\}_i$ is generated from $\{U\}_{i-1}$ and therefore they are not completely statistically independent. In this context, the autocorrelation time is an important quantity which has to be included in the error estimation [59] (section 3.6).

3.2 Markov chains

As explained in the last section, we need a sequence of configurations for measuring the expectation value (3.1). For this purpose we number every field configuration in the sequence with a discrete index $n = 1, 2, 3, \ldots$ as in (3.3). A *Markov process*, which is an ergodic stochastical generation process, produces then configuration i' from configuration i with the transition probability $P(i \to i')$ which obeys the following requirements

$$\forall i, i' : \; P(i \to i') \geq 0 \tag{3.4}$$

$$\forall i' : \; \sum_{i'} P(i \to i') = 1. \tag{3.5}$$

Stochastical means that the choice of the next configuration from the present one is randomly with the probability $P(i \to i')$. Ergodicity ensures that the probability of going from one configuration to any other one in finite number of steps N is greater

than zero

$$\forall i, i' : \; P^N(i \to i') > 0. \tag{3.6}$$

The Markov process has to have the following property (*balance equation*)

$$\sum_i P(i \to i') \exp\{-S(i)\} \stackrel{!}{=} \sum_i P(i' \to i) \exp\{-S(i')\}. \tag{3.7}$$

Here $S(i)$ means $S(\{U\}_i)$. The balance equation expresses that the total probability to end up in configuration i' starting from all possible starting configurations i weighted by $\exp\{-S(i)\}$ is equal to the probability finding the system in configuration i' multiplied by the sum over all transition probabilities $P(i' \to i)$ over all possible final state i. Using (3.5), equation (3.7) results in

$$\sum_i P(i \to i') \exp\{-S(i)\} = \exp\{-S(i')\}. \tag{3.8}$$

This equation expresses the fact that the equilibrium distribution $\exp\{-S(i)\}$ is a fixed point of the Markov process. One can start from an arbitrary initial configuration and will end up in the equilibrium (thermalized) state applying the Markov process iteratively. A stronger requirement as the balance equation is that the equality (3.7) holds for every term

$$\exp\{-S(i)\}P(i \to i') = \exp\{-S(i')\}P(i' \to i). \tag{3.9}$$

This sufficient condition for a solution of the balance equation is known as *detailed balance*. Algorithm which satisfies the detailed balance condition lead to the equilibrium distribution started from any configuration. If we now have such a chain of configurations where configuration i is independent of all configurations except for $i-1$, such a chain is called Markov chain.

3.3 Metropolis versus heat bath

The realization of such an algorithm with the above requirements was first proposed by *Metropolis et al.* in 1953 [60]. The key idea is to change a single variable at a time and to check after every proposal $(i \to i')$ if the action is lowered. The new configuration i' is always accepted if the new action $S(i')$ is lowered. Otherwise a random number is taken which is uniformly distributed on $[0, 1]$ and compared to $\exp\{-[S(i') - S(i)]\}$. If the exponential is equal or greater then the random number, the proposed new configuration will be accepted otherwise the old configuration will be kept. This procedure is known as "accept/reject" step which will be a crucial ingredient of the *Hybrid Monte Carlo* algorithm. For a fast update of the variables, an algorithm which updates globally would be desirable but such a procedure would involve a large change in the action generally and this would cause a poor acceptance rate. Hence the configuration would

not move or would move very slowly in the configuration space.

The heat bath algorithm which was first proposed by *Creutz* [61] for $SU(2)$ in 1980 and extended by *Cabibbo et al.* [62] to $SU(N)$ and improved by *Kennedy et al.* [63] goes through all lattice links (a sweep) and thermalizes the current link with its vicinity while keeping the rest fixed. The idea is originally adopted from statistical mechanics. The next neighbors of the current link represent a "heat bath" and through updating, this link becomes equilibrated with the "heat bath". The transition probability of the heat bath algorithm is independent of previous configuration i

$$P_{\mathrm{HB}}(i \to i') \propto \exp\{-S(i')\}. \tag{3.10}$$

Due to accelerate the decorrelation of the subsequent configurations, these algorithms can be combined with an *overrelaxation* update step. This step changes the configuration without changing the action. The overrelaxation step moves the configuration to the diagramatically opposite side of the minimum of the action. The proposed new configuration will be accepted with the probability one in the case of the Metropolis "accept/reject" step. The overrelaxation algorithm is not ergodic because it samples configuration on a subspace of constant action. Therefore the overrelaxation algorithm has to be combined with *Metropolis* or *heat bath* algorithms.

Both *Metropolis* and *heat bath* algorithms are efficient for local actions (pure gauge simulations) but become very inefficient for dynamical simulations of QCD because the so-called fermion determinant, which appears in the path integral and represents the fermionic part of the action, is non-local. Hence a new algorithm is needed which can handle with the fermion determinant.

3.4 Hybrid algorithm

For the subsequent discussion of the *Hybrid algorithm* and *Hybrid Monte Carlo algorithm*, we follow standard textbooks of lattice field theory (for example [23–25]).

The Hybrid algorithm was first proposed by *Duane* [64] in 1985. The basic idea of this algorithm is that one defines conjugate momenta $\{\pi_i\}$ to $\{\phi_i\}$ (for the sake of simplicity we consider a scalar field ϕ_i) with the probability distribution

$$P(\{\pi_i\}) = \left(\prod_i \frac{1}{\sqrt{2\pi}}\right) \exp\left\{-\sum_i \frac{1}{2}\pi_i^2\right\} \tag{3.11}$$

and builds a Hamiltonian

$$H[\phi, \pi] = \sum_i \frac{1}{2}\pi_i^2 + S[\phi]. \tag{3.12}$$

It does not affect our expectation value (3.1) if we replace $S[\phi]$ with $H[\phi, \pi]$ because the

observable is independent of the conjugate momenta π_i. Therefore we can write

$$\langle \mathscr{O} \rangle = \frac{1}{Z} \int \prod_i d\pi_i \, d\phi_i \;\; \exp\{-H[\phi_i, \pi_i]\} \mathscr{O}(\phi_i) \tag{3.13}$$

where

$$Z = \int \prod_i d\pi_i \, d\phi_i \;\; \exp\{-H[\phi_i, \pi_i]\}. \tag{3.14}$$

As aformentioned, the equivalence of an euclidean path integral in quantum field theory and a classical canonincal ensemble in statistical mechanics allows to use the same techniques as in statistical mechanics. Especially, if the number of degrees of freedom tends to go to infinity, the canonical ensemble average can be replaced by the microcanonical average evaluated at a constant energy which is given by the parameters of the system. Once the Hamiltonian is well defined, the classical Hamilton equation of motion can be used for the evolution of the initial configuration (*molecular dynamics*) with constant energy

$$\dot{\phi} = +\frac{\partial H[\phi, \pi]}{\partial \pi_i} \tag{3.15}$$

$$\dot{\pi} = -\frac{\partial H[\phi, \pi]}{\partial \phi_i}. \tag{3.16}$$

These equations of motion define an area-preserving reversible mapping on the phase space $\{\phi, \pi\}$. For numerical purposes, we have to discretize the equation of motion and therefore first we will expand ϕ and π in a Taylor series

$$\phi_i(\tau + \epsilon) = \phi_i(\tau) + \epsilon \dot{\phi}_i(\tau) + \frac{\epsilon^2}{2} \ddot{\phi}_i(\tau) + \mathcal{O}(\epsilon^3) \tag{3.17}$$

$$\pi_i(\tau + \epsilon) = \pi_i(\tau) + \epsilon \dot{\pi}_i(\tau) + \frac{\epsilon^2}{2} \ddot{\pi}_i(\tau) + \mathcal{O}(\epsilon^3). \tag{3.18}$$

Applying (3.15) and (3.16) on (3.12), we derive the equations of motion for the molecular dynamics

$$\dot{\phi}_i(\tau) = \pi_i(\tau) \tag{3.19}$$

and

$$\ddot{\phi}_i(\tau) = \dot{\pi}_i(\tau) = -\frac{\partial S}{\partial \phi_i(\tau)}. \tag{3.20}$$

As quoted in [23], the pure molecular dynamics (MD) algorithm for full QCD has problems with the fulfillment of the ergodicity requirment. However, the problem can be solved by refreshing the conjugate momenta from time to time (after a fixed MD time) in the evolution and, thus, give the configuration a random chosen direction in the config-

uration space instead of generating once at the begining of MD algorithm. This strategy is also known from the *Langevin algorithm* and based on the method of *stochastic quantization* (for details [65]). Back to MD equations of motion, the second derivative can be approximated as follows

$$\dot{\pi}_i(\tau+\epsilon) = \dot{\pi}_i(\tau) + \epsilon\ddot{\pi}_i(\tau) + \mathcal{O}(\epsilon^2) \tag{3.21}$$

$$\Rightarrow \quad \ddot{\pi}_i(\tau) = \frac{\dot{\pi}_i(\tau+\epsilon) - \dot{\pi}_i(\tau)}{\epsilon} + \mathcal{O}(\epsilon) \tag{3.22}$$

using (3.20) for the right-hand side, we obtain

$$\ddot{\pi}_i = -\frac{1}{\epsilon}\left(\frac{\partial S}{\partial\phi_i(\tau+\epsilon)} - \frac{\partial S}{\partial\phi_i(\tau)}\right) + \mathcal{O}(\epsilon). \tag{3.23}$$

Replacing $\dot{\pi}_i$ and $\ddot{\pi}_i$ in (3.17) and (3.18) by (3.20) and by (3.23), respectively and rearranging, we derive

$$\phi_i(\tau+\epsilon) = \phi_i(\tau) + \epsilon\left(\pi_i(\tau) - \frac{\epsilon}{2}\frac{\partial S}{\partial\phi_i(\tau)}\right) + \mathcal{O}(\epsilon^3) \tag{3.24}$$

$$\left(\pi_i(\tau+\epsilon) - \frac{\epsilon}{2}\frac{\partial S}{\partial\phi_i(\tau+\epsilon)}\right) = \left(\pi_i(\tau) - \frac{\epsilon}{2}\frac{\partial S}{\partial\phi_i(\tau)}\right) - \epsilon\frac{\partial S}{\partial\phi_i(\tau+\epsilon)} + \mathcal{O}(\epsilon^3). \tag{3.25}$$

The expressions within the brackets are the first two terms of the Taylor expansion of $\pi_i(\tau+\epsilon/2)$. Therefore (3.24) and (3.25) are equivalent to the following equations up to $\mathcal{O}(\epsilon^3)$ corrections

$$\phi_i(\tau+\epsilon) = \phi_i(\tau) + \epsilon\pi_i(\tau+\epsilon/2) \tag{3.26}$$

$$\pi_i(\tau+3\epsilon/2) = \pi_i(\tau+\epsilon/2) - \epsilon\frac{\partial S}{\partial\phi_i(\tau+\epsilon)}. \tag{3.27}$$

Iterating these both equations means integrating the Hamilton equations of motion. This scheme is also known as the *leapfrog* integration scheme which is a member of the class of *symplectic integrators*. The crucial properties of such integrators are area-preserving, which means that the integration measure in phase space is unchanged, and reversible. It is possible to derive a quantity which can be measured easily in numerical simulation to proof area preserving of the used integration scheme. By assuming the invariance of the integration measure, we can obtain the following relationship [66]

$$\langle e^{-\Delta H}\rangle = 1 \tag{3.28}$$

where ΔH is the difference of the Hamiltoninan between the old and the new configuration. The violation of this condition is a good indicator that the numerical integrator of equations of motion does not preserve the integration measure.
So, at the beginning of the leapfrog integration, we have to know the half step $\pi_i(\tau+\epsilon/2)$.

To perform this, we expand it up to order ϵ

$$\pi_i(\tau + \epsilon/2) = \pi_i(\tau) - \frac{\epsilon}{2}\frac{\partial S[\phi]}{\partial \phi_i(\tau)} + \mathcal{O}(\epsilon^2) \tag{3.29}$$

and replace it in (3.26) and (3.27). The numerical procedure now consists of five steps

1. Generate the coordinates $\{\phi_i\}$.
2. Generate the Gaussian distributed conjugate momenta $\{\pi_i\}$.
3. Compute the half step (3.29).
4. Put this result in (3.26) and (3.27) and iterate these equations for several time steps and store the generated configurations.
5. Repeat the steps 2,3, and 4.

In 1986, *Duane* and *Kogut* [67] showed that this algorithm generates configurations with the desired distribution $\exp\{-S[\phi]\}$ in the equilibrium (for $\epsilon \to 0$) but due to the finiteness of the time step, the algorithm introduces systematic errors which should be considered carefully.

3.5 Hybrid Monte Carlo

The Hybrid Monte Carlo method goes back to a proposal of *Duane*, *Kennedy*, *Pendelton*, and *Roweth* 1987 [68]. It is a combination of the two algorithms discussed above (Metropolis and Hybrid algorithms). The problem with the Hybrid algorithm is that one has to take care of the systematic errors which are induced by the finite time step. On the other hand the Metropolis algorithm is exact but this algorithm becomes very slow when updating configurations the action of which is non-local. The Hybrid Monte Carlo algorithm combines the advantages of both to one exact algorithm. The update step is performed globally and the "accept/reject" step of Metropolis algorithm makes it exact. In contrast to the Hybrid algorithm, the conjugate momenta are refreshed at the beginning of every trajectory. The procedure for generating configurations which was given above is now changed a little bit.

1. Generate the coordinates $\{\phi_i\}$.
2. Generate the Gaussian distributed conjugate momenta $\{\pi_i\}$.
3. Compute the half step (3.29).
4. Put this result in (3.26) and (3.27) and iterate these equations for several time steps.

5. Accept the last configuration $\{\phi_i', \pi_i'\}$ in the molecular dynamics chain as the new configuration with the probability

$$p = \min\left\{1, \frac{\exp\{-H[\phi', \pi']\}}{\exp\{-H[\phi, \pi]\}}\right\}. \tag{3.30}$$

6. If the new configuration is accepted, use the new coordinates $\{\phi_i'\}$ for starting from step 2 otherwise keep the old configuration and start from step 2.

It can be shown easily that this algorithm fulfills the requirement of detailed balance. The proof starts with the choice of the momenta according to the following probability distribution:

$$P_{\mathrm{G}}(\pi) = N \exp\left\{-\frac{1}{2}\sum_i \pi_i^2\right\} \tag{3.31}$$

where the subscript G denotes that P_{G} is the generation probability distribution and N is a normalization constant such that $\int \mathscr{D}\pi P_{\mathrm{G}}(\pi) = 1$. We now consider an initial configuration $\{\phi, \pi\}$ which evolves in time by (3.26) and (3.27) $\{\phi, \pi\} \to \{\phi^{(N)}, \pi^{(N)}\}$. The demand of reversibility implies that the motion from initial state to the final state ($\phi \to \phi^{(N)}$) can be reversed by changing the sign of all momenta. The probability for going forwards and backwards is the same

$$P_{\mathrm{M}}(\{\phi, \pi\} \to \{\phi', \pi'\}) = P_{\mathrm{M}}(\{\phi', -\pi'\} \to \{\phi, -\pi\}) \tag{3.32}$$

where the subscript M stands for molecular dynamics evolution. In the Metropolis "accept/reject" test (subscript A in (3.33)), the generated configuration $\{\phi', \pi'\}$ is accepted with probability

$$P_{\mathrm{A}}(\{\phi, \pi\} \to \{\phi', \pi'\}) = \min\left\{1, \frac{\exp\{-H[\phi', \pi']\}}{\exp\{-H[\phi, \pi]\}}\right\}. \tag{3.33}$$

Integrating over the momenta of the product of P_G, P_M, and P_A gives the complete probability of the transition

$$P(\{\phi, \pi\} \to \{\phi', \pi'\}) = \int \mathscr{D}\pi \mathscr{D}\pi' P_{\mathrm{G}}(\pi) P_{\mathrm{M}}(\{\phi, \pi\} \to \{\phi', \pi'\}) P_{\mathrm{A}}(\{\phi, \pi\} \to \{\phi', \pi'\}). \tag{3.34}$$

Multiplying (3.34) by $\exp\{-S[\phi]\}$ and replacing the resulting expression

$$\exp\{-H[\phi, \pi]\} P_{\mathrm{A}}(\{\phi, \pi\} \to \{\phi', \pi'\})$$

by

$$\exp\{-H[\phi', \pi']\} P_{\mathrm{A}}(\{\phi', \pi'\} \to \{\phi, \pi\})$$

and $P_{\mathrm{M}}(\{\phi,\pi\} \to \{\phi',\pi'\})$ with the right-hand side of (3.32) in (3.34) and making use of the fact that $H[\phi,\pi] = H[\phi,-\pi]$, we find

$$\exp\{-S[\phi]\}P(\phi \to \phi') = \exp\{-S[\phi']\} \int \mathscr{D}\pi\mathscr{D}\pi' P_{\mathrm{G}}(\pi')P_{\mathrm{M}}(\{\phi',\pi'\} \to \{\phi,\pi\})P_{\mathrm{A}}(\{\phi',\pi'\} \to \{\phi,\pi\}) = \exp\{-S[\phi']\}P(\phi' \to \phi). \quad (3.35)$$

Consequently, the Hybrid Monte Carlo algorithm fulfills the detailed balance condition (3.9) and is therefore an exact algorithm.

3.6 Error estimation

As we explained, the configurations are produced one after another in a so-called Markov chain according to the Hybrid Monte Carlo algorithm. That means the configurations are unavoidable correlated to each other. In an ideal world, the configuration i should only know from its predecessor but in real Hybrid Monte Carlo simulations strong correlations can appear. Eventually the correlation of configurations is then reproduced in the correlation of measured quantities. This gives rise to the question how one can find a reliable error estimation of the data?
As discussed in [59], since the popular binning methods (jackknife analysis) for error analysis of Monte Carlo data handles the effect of autocorrelation implicitly, the error estimation is not optimal. The basic idea of such a jackknife analysis is that the average over bins in which the data are divided into are considered as uncorrelated and a naive error analysis is made. For a more accurate error estimation, an explicit consideration of the autocorrelation time is needed. The key quantity here is the autocorrelation function Γ_A

$$\Gamma_A(i-j) = \langle (a_i - A)(a_j - A) \rangle \quad (3.36)$$

where a_k is the k'th measurement of the primary observable $\mathscr{A}$ (for *primary* and *derived* quantities see [59]) on the k'th configuration C_k

$$a_k = \mathscr{A}(C_k), \quad k = 1,\ldots,N, \quad A = \langle \mathscr{A}(C) \rangle. \quad (3.37)$$

Equation (3.36) implies that Γ_A is only a function of the separation $i-j$ and does not depend on the separation from the beginning of the series. With increasing separation ($\to \infty$), the autocorrelation function Γ_A decrease exponentially

$$\Gamma_A(t) \overset{t\to\infty}{\propto} \exp\{-t/\tau\}. \quad (3.38)$$

The finite scale τ which characterizes the asymptotic exponential decay of $\Gamma_A(t)$ can take several update steps.

The decisive factor for the error estimation is now the integrated form of the autocor-

relation function Γ_A which is called *integrated autocorrelation time* τ_{int}

$$\tau_{\text{int}} := \frac{1}{2} \sum_{t=-\infty}^{\infty} \frac{\Gamma_A(t)}{\Gamma_A(0)}. \tag{3.39}$$

The appearing quantity $\Gamma_A(0)$ is also known as the variance of the observable A. For high statistics, that means $N \gg \tau$, equation (3.39) can be approximated by

$$2N\tau_{\text{int}} = N \sum_{t=-\infty}^{\infty} \frac{\Gamma_A(t)}{\Gamma_A(0)} \approx \sum_{i=1}^{N} \sum_{j=1}^{N} \frac{\Gamma_A(i-j)}{\Gamma_A(0)}. \tag{3.40}$$

For the purposes of evaluation one needs an estimator for $\Gamma_A(t)$ which is accessible numerically

$$\Gamma_A(t) \simeq \frac{1}{N-t} \sum_{i=1}^{N-t} \left(a_i - \frac{1}{N} \sum_{j=1}^{N} a_j \right) \left(a_{i+t} - \frac{1}{N} \sum_{k=1}^{N} a_k \right). \tag{3.41}$$

This estimation has also an error which has to be considered carefully. The calculation of τ_{int} as described above needs to sum up $\Gamma_A(t)$ until its value is sufficiently close to zero. Otherwise one would obtain an incorrect estimation for τ_{int}. For this purpose, a graphical examination of $\Gamma_A(t)$ is advisable. So, the standard deviation σ is then given by

$$\sigma^2(N, A) = \frac{\text{var}(A)}{N/(2\tau_{\text{int}})}. \tag{3.42}$$

Here, $\text{var}(A)$ denotes the variance of the quantity which one wants to consider. τ_{int} is also a good measure for the quality of the algorithm which produces the configurations in the Markov chain. A detailed description of this method of error analysis is given in [59] and the author provides also an inplementation (`UWerr.m`) in MATLAB® which we will use for our data analysis.

4 Algorithmic improvements

The numerical realization of the HMC algorithm as we discussed in the last section becomes a demanding task when dynamical fermions are included. Special techniques are needed for a fast evaluation of the fermion determinant to make numerical simulations accessible on current computer resources. In this chapter, we want to discuss the commonly used algorithmic techniques.

4.1 Fermion determinant and pseudo-fermion fields

As currently believed, the matter fields in nature can be divided into two fundamental different types of particles. Bosons, which carry integer spins, obey the Bose-Einstein statistics while the fermions with half-integer spins obey the Fermi-Dirac statistics. In contrast to the bosons, fermions have to respect the *Pauli exclusion principle* and hence the existence of two fermions in the same quantum state simultaneously is impossible. In other words, the elements of the algebra, which should describe the fermionic fields, have to anticommute. A convenient way is to use the so-called *Graßmann algebra*. In the following sections, we will give a brief reminder about certain properties of the Graßmann variables and discuss how the fermionic part of the action can be integrated out analytically (for details, see in standard textbooks of lattice field theory). Generally, the *Graßmann algebra* of n dimensions is an algebra $\mathcal{A}$ over the field $\mathcal{K}$, which is generated by n anticommuting elements η_i

$$\forall i, j : \{\eta_i, \eta_j\} = 0. \tag{4.1}$$

Especially, the square of a Graßmann variable vanishes

$$\eta_i^2 = 0. \tag{4.2}$$

Due to the property of anticommuting, integration over the Graßmann variables is slightly modified

$$\int d\eta_i 1 = 0, \quad \int d\eta_i \eta_j = \delta_{ij} \qquad (\textit{Berezin's convention}). \tag{4.3}$$

By calculating multiple integrals, it has to be taken into account that the integration measure anticommutes also

$$\forall i, j : \{d\eta_i, d\eta_j\} = \{d\eta_i, \eta_j\} = 0. \tag{4.4}$$

Due to (4.2) the Taylor series of the exponential function of Graßmann variables reduces from a infinite sum to

$$\exp\{\eta_i \eta_j\} = 1 + \eta_i \eta_j. \tag{4.5}$$

It can be shown that the n-dimensional integration measure

$$d^n \eta = d\eta_n d\eta_{n-1} \dots d\eta_1 \tag{4.6}$$

transforms under a linear change of variables which is given by

$$\eta_i' = \sum_{j=1}^{n} M_{ij} \eta_j \tag{4.7}$$

where M is a complex $n \times n$ matrix as follows [69]

$$d^n \eta = \det\{M\} d^n \eta'. \tag{4.8}$$

So, the so-called *Matthews-Salam formula* can be proven now

$$I = \int d\eta_n \, d\bar{\eta}_n \dots d\eta_1 \, d\bar{\eta}_1 \, \exp\left\{ \sum_{i,j=1}^{n} \bar{\eta}_i M_{ij} \eta_j \right\} \stackrel{!}{=} \det\{M\}. \tag{4.9}$$

As mentioned above M denotes here an complex $n \times n$ matrix. Applying a linear transformation as given in (4.7) to the integral I in (4.9) and using

$$d\eta_n d\bar{\eta}_n \dots d\eta_1 d\bar{\eta}_1 = \det\{M\} d\eta_n' d\bar{\eta}_n \dots d\eta_1' d\bar{\eta}_1 \tag{4.10}$$

which is derived from (4.8) results in

$$I = \det\{M\} \int \left(\prod_{i=1}^{n} d\eta_i' d\bar{\eta}_i \right) \exp\left\{ \sum_{j=1}^{n} \bar{\eta}_j \eta_j' \right\} \tag{4.11}$$

$$= \det\{M\} \prod_{i=1}^{n} \int d\eta_i' d\bar{\eta}_i \exp\{\bar{\eta}_j \eta_i'\}. \tag{4.12}$$

In (4.12), we made use of the fact that pairs of Graßmann variables like $\eta_i' \bar{\eta}_i$ and $d\eta_j' d\bar{\eta}_j$ commute with other pairs. With the expansion (4.5) of the exponential function we obtain

$$I = \det\{M\} \prod_{i=1}^{n} \int d\eta_i' d\bar{\eta}_i (1 + \bar{\eta}_j \eta_i'). \tag{4.13}$$

According to the properties in (4.3) the result for the product of integrals in the above equation is one

$$I = \det\{M\}. \tag{4.14}$$

The integral I in (4.9) describes exactly the fermionic part of the path integral

$$Z_f = \int \mathscr{D}\Psi\mathscr{D}\overline{\Psi}\exp\{-\overline{\Psi}(D+m)\Psi\} \tag{4.15}$$

when we set $M = -(D+m)$. In other words, the exact solution of (4.15) is the determinant of M. The numerical calculation of this so-called *fermion determinant* $\det\{M\}$ is very time consuming. In the early days of lattice simulations when the computational power was very limited, this determinant had been set to one and the simulations had been performed in pure gauge (*quenched approximation*). However, neglecting the fermion determinant means that the effect of the *sea quarks* is ignored. The quenched approximation in the non-perturbative approach corresponds to a tree level calculation (ignoring the loop contributions) in the perturbative regime of QCD. Nevertheless the quark polarization effects are important and should be considered. In Figure 4.1, the effect of the *sea quarks* on the results for meson masses can be seen clearly.

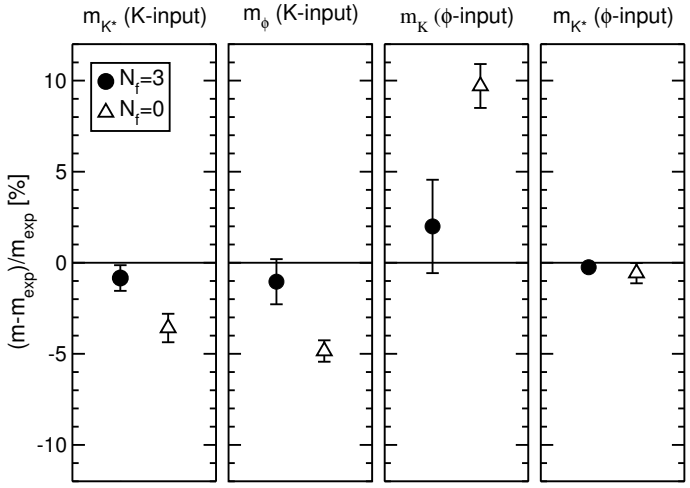

Figure 4.1: Comparison of quenched and dynamical simulations. The deviation of the lattice results from the experimental value is shown. The picture is taken from [70].

In recent years dynamical simulations (full QCD simulations) with at least two quarks became feasible and have been performed by many collaborations. But, the direct calculation of the determinant is still a demanding task and almost impossible because it would be very time consuming and numerically instable. Instead of the direct calculation, a more convenient way that can be used is calculating the determinant through a path integral over pseudo-fermionic fields.

A closer look on matrix M reveals the different indices of it: Dirac, color and flavor. If we split off the flavor index explicitly and build the determinant then, it turns out that the flavor number appears in the exponent of the determinant [24]

$$\det M = \left(\det \hat{M}\right)^{N_\mathrm{f}}. \tag{4.16}$$

The matrix $\hat{M}$ is now independent of the flavor index and is real ($\det \hat{M} = \det \hat{M}^\dagger$) but not necessarily positive definite. The calculation of the determinant with the pseudo-fermion fields requires positivity. Otherwise the exponential function in (4.18) cannot be interpreted as a probability measure. This lack can be fixed easily by considering the matrix product K

$$K = \hat{M}^\dagger \hat{M}. \tag{4.17}$$

In this combination, K is positive and hermitian, and represents the Dirac matrix of two degenerated quarks. Since K is positive definite, the determinant can be rewritten in terms of the pseudo-fermion fields ϕ [71]

$$\det K = \int \mathscr{D}\phi^\dagger \mathscr{D}\phi \exp\{-\phi^\dagger K^{-1} \phi\}. \tag{4.18}$$

According to this description of the determinant, the partition function becomes a path integral over ordinary c-numbers

$$Z = \int \mathscr{D}U \mathscr{D}\phi^\dagger \mathscr{D}\phi \exp\left\{-S_\mathrm{G}[U] - \sum_{i,j} \phi_i^\dagger (K^{-1})_{ij}[U] \phi_j\right\}. \tag{4.19}$$

As can be seen in equation (4.18), the inverse of K is needed. Therefore the efficiency of the pseudo-fermion method will depend on the performance of the algorithms for the inversion of the matrix K.

4.2 Inverting the Dirac matrix

As discussed in the section 4.1, the inversion of the Dirac matrix is essential and standard methods like *Gauß-Jordan* and *LU decomposition* cannot be used due to the certain properties of the Dirac matrix (size, sparseness). The cost of the aforementioned methods is proportional to N^3 [72] (for an $N \times N$ matrix) and are therefore very inefficient for the inversion of large sparse matrices. For solving such a large sparse system of linear equations

$$A \ \vec{x} = \vec{b}, \tag{4.20}$$

Hestenes and *Stiefel* [73] proposed the conjugate gradient (CG) method which provides an efficient tool for this task [74]. For a positive definite and symmetric (hermitian for

complex matrices) matrix A, the conjugate gradient algorithm minimizes the function

$$f(\vec{x}) = \frac{1}{2}\ \vec{x}^T\ \ A\ \ \vec{x} - \vec{b}^T\ \ \vec{x}. \tag{4.21}$$

by solving

$$\nabla f(\vec{x}) = A\ \ \vec{x} - \vec{b}^T \stackrel{!}{=} \vec{0}. \tag{4.22}$$

In principle, the initial vector $\vec{x}_0$ for the minimizer can be chosen arbitrarily. The CG algorithm improves this minimizer iteratively so that in the $(k+1)$'th step, $\vec{x}_{k+1}$ is calculated from the predecessor

$$\vec{x}_{k+1} = \vec{x}_k + \alpha_k \vec{p}_k \tag{4.23}$$

where $\vec{p}_k$ is the direction of search and α_k is the coefficient which minimizes $f(\vec{x}_k + \alpha_k \vec{p}_k)$. The $\vec{x}_k$ and $\vec{p}_k$ are also constructed in such a way that (4.23) minimizes f over the vector space of directions which is already taken $\{\vec{p}_0, \vec{p}_1, \ldots,\ \ \vec{p}_k\}$. After N iterations the minimizer $\vec{x}_N$, which solves the equation (4.20), is obtained [72, 73]. In numerical realizations, one has to deal with rounding errors. Hence, the algorithm will stop after a finite number of iterations when an appropriate error criterion is met.
The name "conjugate" should not be mixed with the notion of complex conjugate. Conjugate means in this context that two vectors are conjugate to each other with respect to a matrix A: $u^\dagger A v = 0$. After each iteration, the new direction is chosen in such a way that it is conjugate to the preceding directions. Since the convergence of CG algorithm is guaranteed, the rate is slow. An accelerated and generalized version to non-symmetric matrices is the stabilized biconjugate gradient method *BiCGstab* which was proposed by *van der Vorst* [75]. In contrast to the CG algorithm, its convergence is not always given. This is due to the way of calculation of the residue in each iteration step in the BiCGstab algorithm. For saving a matrix multiplication, the residue of the current iteration step is calculated from the preceding one and the accumulation of numerical rounding errors could cause a difference between the iterated residue and the real residue r

$$r = \frac{||\vec{b} - A\ \ \vec{x}||^2}{||\vec{b}||^2} \tag{4.24}$$

and could therefore suggest a wrong solution for (4.20). This can happen for ill-conditioned matrices like the Dirac matrix. The condition number of a matrix A, for example, in (4.20) is a measure for the accessibility of the problem on a computer. If a small change in $\vec{b}$ or a small change in A causes a large change of the solution vector $\vec{x}$, then the matrix is called ill-conditioned otherwise it is well-conditioned. For a *normal* matrix A (here, *normal* in the sense of being diagonalizable), the condition number

cond(A) is simply defined as the ratio of the largest and smallest eigenvalue

$$\mathrm{cond}(A) = \left| \frac{\lambda_{\max}(A)}{\lambda_{\min}(A)} \right|. \tag{4.25}$$

In practice, a combination of both algorithms makes a fast calculation of the solution vector $\vec{x}$ possible. For example, one can start with the BiCGstab and let it run until a given precision or a maximum number of iterations is reached and uses this result as initial solution vector for a CG call and run it until the required (real) residue (4.24) is obtained [76]. The advantage of such a combination is that the following CG call will need only a couple of iterations to reach the desired precision in contrast to a pure CG call (in worst case, it would need the same number of iterations).

4.3 Even-odd preconditioning

The technique of preconditioning is a powerful tool for improving the efficiency and robustness of, for example, iterative Krylov subspace methods like CG and BiCGstab. In textbooks, different strategies for preconditioning of an ill-conditioned matrix are discussed [74]. In this section we want to restrict our discussion to the most popular *even-odd preconditioning* of the Dirac matrix in lattice QCD.
From now on, we will set the lattice spacing a to one and write a explicitly in formulas when we want to point out the dependence.
The key idea of the even-odd preconditioning [77, 78] is to divide the lattice sites into even and odd sites according to the sum over the coordinates $\sum_{\mu=0}^{3} x_\mu$. If this sum is *even* for the lattice site x, the site is called *even* otherwise it is called *odd*. Following this strategy, the Dirac matrix M (we call $\hat{M}$ again M for the sake of simplicity) decompose into the following block form

$$M = \begin{pmatrix} M_{ee} & M_{eo} \\ M_{oe} & M_{oo} \end{pmatrix}, \tag{4.26}$$

where the components are given by [79]

$$\begin{aligned} M_{x,x'} = {} & (1 + T_{x,x})\delta_{x,x'} \\ & - \kappa \sum_{\mu} \left[(1 - \gamma_\mu) U_\mu(x) \delta_{x+\hat{\mu},x'} + (1 + \gamma_\mu) U_\mu^\dagger(x - \hat{\mu}) \delta_{x-\hat{\mu},x'} \right]. \end{aligned} \tag{4.27}$$

The matrix $T_{x,x}$

$$T_{x,x} = \frac{i}{2} c_{\mathrm{sw}} \kappa \sigma_{\mu\nu} \mathcal{F}_{\mu\nu}(x) \tag{4.28}$$

vanishes if the improvement coefficient c_{sw} is set to zero and the submatrices M_{ee} and M_{oo} become equal to the unit matrix. However, in our case, we consider the $\mathcal{O}(a)$ improved Sheikoleslami-Wohlert action where the coefficient c_{sw} is determined non-perturbatively

in $N_\mathrm{f} = 4$. Furthermore the submatrices of M possess the following properties

$$\begin{array}{rclcrcl} M_{ee}^\dagger &=& M_{ee} & & M_{oo}^\dagger &=& M_{oo} \\ M_{eo}^\dagger &=& \gamma_5 M_{oe} \gamma_5 & & M_{oe}^\dagger &=& \gamma_5 M_{eo} \gamma_5. \end{array} \tag{4.29}$$

The origin of the algorithmic acceleration of even-odd preconditioning lies in the factorization of the determinant which we want to show subsequently. In this context, two possibilities appear. First, we can factorize only M_{ee} or M_{oo} (*asymmetric*), or second, we can factorize both (*symmetric*). The derivations of both versions are very similar. The key idea is based on the calculation of the determinant of a matrices like (4.26) using its *Schur complement*. For a general matrix which consist of submatrices, the determinant can be calculated in the following way [58]

$$\det \begin{pmatrix} A & B \\ C & D \end{pmatrix} = \det\{AD - ACA^{-1}B\}. \tag{4.30}$$

In our case, the determinant of $Q = \gamma_5 M$[a] leads to

$$\det Q = \det\{M_{ee}\} \det\{\hat{Q}_A\} \tag{4.31}$$

for the asymmetric version (factorization of only M_{oo} is analogous) and

$$\det Q = \det\{M_{ee}\} \det\{M_{oo}\} \det\{\hat{Q}_S\} \tag{4.32}$$

for the symmetric one, where

$$\hat{Q}_A = \gamma_5 (M_{oo} - M_{oe} M_{ee}^{-1} M_{eo}) \tag{4.33}$$

$$\hat{Q}_S = \gamma_5 (1 - M_{oo}^{-1} M_{oe} M_{ee}^{-1} M_{eo}). \tag{4.34}$$

The asymmetric even-odd preconditioned Dirac matrix $\hat{Q}_A$ is hermitian while the Dirac matrix $\hat{Q}_S$, in the case of symmetric preconditioning, is non-hermitian

$$\hat{Q}_A^\dagger = \hat{Q}_A \tag{4.35}$$

$$\hat{Q}_S^\dagger = M_{oo} \hat{Q}_S M_{oo}^{-1}. \tag{4.36}$$

After simple matrix algebra and using of $[\gamma_5, M_{ee}] = [\gamma_5, M_{oo}] = 0$, we find the subsequent relations between the symmetric and the asymmetric preconditioned Dirac matrices

$$\begin{array}{rclcrcl} \hat{Q}_S &=& M_{oo}^{-1} \hat{Q}_A & & \hat{Q}_S^\dagger &=& \hat{Q}_A M_{oo}^{-1} \\ \hat{Q}_A &=& M_{oo} \hat{Q}_S = \hat{Q}_S^\dagger M_{oo}. & & & & \end{array} \tag{4.37}$$

In our numerical implementation, we only use the *symmetric even-odd preconditioning* but there is no fundamental problem to implement the *asymmetric even-odd precondi-*

[a] Usually Q is defined as $Q = c_0 \gamma_5 M$ where c_0 is a normalization constant (see [79] for details). Since it is irrelevant for our discussion, we set it to one.

tioned version. However, it should be kept in mind that the authors of [80] found that the performance of HMC with symmetric even-odd preconditioning is almost 30% higher than the HMC algorithm with asymmetric even-odd preconditioning. They showed that the total gain of preconditioning is almost a factor two compared to the unpreconditioned HMC.
So, the advantage of even-odd preconditioning is that only the half length of the vectors is needed. A simple way to see this is to decompose the matrix Q as follows

$$Q = \gamma_5 \begin{pmatrix} M_{ee} & M_{eo} \\ M_{oe} & M_{oo} \end{pmatrix} \tag{4.38}$$

$$= \begin{pmatrix} \gamma_5 M_{ee} & 0 \\ \gamma_5 M_{oe} & 1 \end{pmatrix} \begin{pmatrix} 1 & M_{eo}\gamma_5 \\ 0 & \gamma_5 M_{oo}\gamma_5 \end{pmatrix} \times \tag{4.39}$$

$$\begin{pmatrix} 1 & (M_{ee}^{-1} - 1 + M_{eo}M_{oo}^{-1}M_{oe}M_{ee}^{-1})M_{eo} \\ 0 & \gamma_5(1 - M_{oo}^{-1}M_{oe}M_{ee}^{-1}M_{eo}) \end{pmatrix}. \tag{4.40}$$

As we will discuss later, the matrices in (4.39) contribute to the determinant part of the action. However, the computational challenge is to calculate the determinant of (4.40). This will be performed with the pseudo-fermion method as discussed in section 4.1. The matrix in (4.40) which we abbreviate with Ω has the following structure

$$\Omega = \begin{pmatrix} 1 & \Delta_1 \\ 0 & \Delta_2 \end{pmatrix} \tag{4.41}$$

where Δ_1 and Δ_2 can be read off from equation (4.40). The problem of solving the system of linear equations

$$\Omega\vec{\psi} = \vec{\phi} \Rightarrow \begin{pmatrix} 1 & \Delta_1 \\ 0 & \Delta_2 \end{pmatrix} \begin{pmatrix} \vec{\psi}_e \\ \vec{\psi}_o \end{pmatrix} = \begin{pmatrix} \vec{\phi}_e \\ \vec{\phi}_o \end{pmatrix} \tag{4.42}$$

where the subscript e and o refers to the even and odd components respectively turns out to be reduced with the preconditioned Dirac matrix. It is sufficient to solve the equation for the odd components

$$\vec{\psi}_o = \Delta_2^{-1}\vec{\phi}_o \tag{4.43}$$

and calculate the even components of $\vec{\psi}$ using this solution

$$\vec{\psi}_e = \vec{\phi}_e - \Delta_1\vec{\psi}_o. \tag{4.44}$$

Finally, we can express the partition function with the symmetric preconditioned Dirac matrix for two flavors $QQ^\dagger$ as

$$Z = \int \mathscr{D}U \mathscr{D}\phi_o^\dagger \mathscr{D}\phi_o \exp\left\{-S_{\mathrm{G}}[U] - S_{\mathrm{det}}[U] - S_{\mathrm{pf}}[U, \phi_o^\dagger, \phi_o]\right\} \tag{4.45}$$

with the gauge part $S_{\mathrm{G}}[U]$ which was defined in (2.24) and

$$S_{\mathrm{det}}[U] = 2 \cdot (\ln \det\{M_{ee}[U]\} + \ln \det\{M_{oo}[U]\}) \tag{4.46}$$

$$S_{\mathrm{pf}}[U, \phi_o^\dagger, \phi_o] = \phi_o^\dagger (\hat{Q}_S[U] \hat{Q}_S^\dagger[U])^{-1} \phi_o. \tag{4.47}$$

4.4 Hasenbusch preconditioning

As we discussed, the expense of inversion of the Dirac matrix is very sensitive to the condition number. Hence, any reduction in the condition number would accelerate the inversion algorithms. In this context, a well-known algorithmic trick is the so-called *Hasenbusch preconditioning* [81, 82]. This technique is based on the simple fact that an arbitrary $n \times n$ matrix A can be rewritten in the following way

$$A = B \cdot (B^{-1} A). \tag{4.48}$$

The preconditioner B – an arbitrary invertible $n \times n$ matrix – is chosen in such a way that the condition numbers of B and $(B^{-1}A)$ are smaller than their product. In the case of the Dirac matrix this simple trick would accelerate the calculation of the determinant with the pseudo-fermion method due to the lowered condition numbers of the matrices on the r.h.s. of (4.48). In a first proposal, the authors of [81] suggested to precondition the Dirac matrix

$$M = 1 - \kappa H \tag{4.49}$$

where κ is the hopping parameter with

$$\tilde{M} = 1 - \tilde{\kappa} H, \quad 0 \leq \tilde{\kappa} \leq \kappa. \tag{4.50}$$

The author implemented this proposal on top of even-odd preconditioning in a two dimensional Schwinger model with two flavors of Wilson fermions and found a factor two of gain in performance. For QCD the authors of [81, 82] proposed and tested for an asymmetric even-odd preconditioned Dirac matrix with clover term (equation (4.26) and (4.31)) a preconditioner W which was inspired by the twisted mass QCD [46]. The choice for preconditioner W was made by

$$W = \hat{Q} + i\rho 1 \tag{4.51}$$

where $\hat{Q}$ is given by (4.33). The preconditioner W can also be used for a symmetric even-odd preconditioned Dirac matrix. The transcription of the determinant with pseudo-fermion fields is then given by

$$\begin{aligned} \det(\hat{Q}^2) = \det(WW^\dagger) \det([W^{-1}\hat{Q}][W^{-1}\hat{Q}]^\dagger) \propto \int \mathscr{D}\phi_1^\dagger \mathscr{D}\phi_1 \mathscr{D}\phi_2^\dagger \mathscr{D}\phi_2 \\ \exp\left\{-\phi_1^\dagger (WW^\dagger)^{-1} \phi_1\right\} \exp\left\{-\phi_2^\dagger ([W^{-1}\hat{Q}][W^{-1}\hat{Q}]^\dagger)^{-1} \phi_2\right\}. \end{aligned} \tag{4.52}$$

The authors quoted an optimal choice for the parameter ρ

$$\rho^2 = \sqrt{\lambda_{\min}\lambda_{\max}}. \tag{4.53}$$

The explicit application of such a modification of the Dirac matrix in HMC revealed a gain of factor two [83]. Above, we discussed the Hasenbusch preconditioning with two pseudo-fermion fields but, in principle, it is also possible to apply the Hasenbusch preconditioning with more than two pseudo-fermion fields.

4.5 Schwarz-preconditioning

A further improvement of the preconditioning the Dirac matrix is discussed by *Lüscher* in [84, 85]. This variant of preconditioning starts with dividing the lattice into a set of domains Λ such that the domains can be chessboard-colored (black-white). The set of black blocks is denoted by Ω and the set of white blocks by Ω^*. Then the Dirac matrix decomposes into the following block form

$$M = \begin{pmatrix} M_\Omega & M_{\partial\Omega} \\ M_{\partial\Omega^*} & M_{\Omega^*} \end{pmatrix} \tag{4.54}$$

where the submatrix M_Ω corresponds to the Dirac operator on the set of black blocks Ω with Dirichlet boundary conditions and $M_{\partial\Omega}$ is the sum of all hopping terms which connect the boundary $\partial\Omega$ of Ω to the boundary $\partial\Omega^*$ of Ω^*. The calculation of the quark determinant with (4.30) results in

$$\det M = \det\{M_\Omega\}\det\{M_{\Omega^*}\}\det\{1 - M_{\Omega^*}^{-1}M_{\partial\Omega^*}M_\Omega^{-1}M_{\partial\Omega}\}. \tag{4.55}$$

The first two determinants on the right-hand side of (4.55) describe the fermion dynamics within the subsets Ω and Ω^* (cheap part of the determinant) and the third determinant involves the coupling between them and is therefore numerically expensive. The molecular dynamics evolution is now restricted to those links (*active links*) of which the both endpoints are within the domain Λ while those links (*boundary links*) of which the one endpoint is in the neighboring domain are kept fixed. The update of the boundary links is realized by a shift of all gauge links by a random vector v after each update cycle

$$\forall x, \mu : U_\mu(x) \to U_\mu(x + v). \tag{4.56}$$

For the cheap and expensive part of the determinant, separate pseudo-fermion fields are introduced. The use of a split time scale integrator like *Sexton-Weingarten method*, as we will discuss next, makes the choice of a coarser step size possible for the expensive part compared to the step size of the cheaper part. The performance depends on the choice of the block size Λ. The algorithm becomes inefficient if the block size consist of only a few lattice spacings. The reason is that only a small fraction of the links, namely the active links, become updated in each cycle. However, the block size should not be larger than 1 fm because the Dirichlet boundary conditions then would not provide a safe

infrared cutoff on the spectrum of the block Dirac operators M_Λ. The choice should be as large as possible but smaller than 1 fm [85]. In context with Schwarz-preconditioning, *Lüscher* discussed in recent years a further algorithmic improvement which goes under the name *low-mode deflation* technique. An application of the Schwarz-preconditioning and the low-mode deflation technique and using a *generalized conjugate residual* [74] solver in HMC accelerates QCD simulations very impressively [86, 87].

4.6 Sexton-Weingarten scheme

The simplest formulation of the leap frog integrator contains only one time scale for the gauge part and fermion part of the action. However, as discussed in [88], the numerical expense for the gauge part is much smaller than for the fermion part. An improvement of the standard leap frog algorithm can be achieved then by introducing different time scales for both parts. The equations of motion for the molecular dynamics evolution (3.19) and (3.20) expressed in terms of the link variable U and the conjugate momenta Π are

$$\dot{U} = \Pi, \quad \dot{\Pi} = -\delta\{S\} \tag{4.57}$$

where $S = S_\mathrm{G} + S_\mathrm{pf}$ and $\delta\{\dots\}$ is the variation of the action with respect to group elements. In the standard leap frog integration scheme with one time scale and hence one step size $\Delta\tau$, the update can be defined as follows [89]

$$T_\mathrm{U}(\Delta\tau) : U \to U' = \exp\{i\Delta\tau\Pi\}U \tag{4.58}$$

$$T_\mathrm{S}(\Delta\tau) : \Pi \to \Pi' = \Pi - i\Delta\tau\delta\{S\}. \tag{4.59}$$

$\delta\{S\}$ denotes the most expensive part of the HMC algorithm due to the inversion of the Dirac matrix. One basic time step of the standard leap frog algorithm for the above equation of motion can be written down as

$$T = T_\mathrm{S}(\Delta\tau/2)T_\mathrm{U}(\Delta\tau)T_\mathrm{S}(\Delta\tau/2) \tag{4.60}$$

where a complete trajectory is obtained after $N_\mathrm{MD} = \tau/\Delta\tau$ times application of the transformation T (τ is the length of the trajectory). The global error which is made by the approximation (4.60) of the time evolution operator is $\mathcal{O}(\tau \cdot \Delta\tau^2)$. A reduction of the discretization error can be obtained by the following modified sequence [88]

$$T = T_\mathrm{S}(\Delta\tau/6)T_\mathrm{U}(\Delta\tau/2)T_\mathrm{S}(2\Delta\tau/3)T_\mathrm{U}(\Delta\tau/2)T_\mathrm{S}(\Delta\tau/6). \tag{4.61}$$

For the *Sexton Weingarten scheme*, we need to decompose the Hamiltonian in the following way

$$H = \frac{1}{2}\sum_{x,\mu}\Pi_{x,\mu}^2 + S_\mathrm{G}[U] + S_\mathrm{pf}[U, \phi^\dagger, \phi]. \tag{4.62}$$

The improved standard leap frog scheme (4.61) with one time scale can be easily extended to a multiple time scale scheme. The time evolution operator $T_{\mathrm{SW_G}}$ for the gauge part of (4.62) is

$$T_{\mathrm{SW_G}} = T_{S_\mathrm{G}}(\Delta\tau_\mathrm{G}/6)T_\mathrm{U}(\Delta\tau_\mathrm{G}/2)T_{S_\mathrm{G}}(2\Delta\tau_\mathrm{G}/3)T_\mathrm{U}(\Delta\tau_\mathrm{G}/2)T_{S_\mathrm{G}}(\Delta\tau_\mathrm{G}/6). \tag{4.63}$$

The so-called *Sexton-Weingarten (SW) integration scheme* is now given by

$$T_{\mathrm{SW_{pf}}} = T_{S_\mathrm{pf}}(\Delta\tau_\mathrm{pf}/6)[T_{\mathrm{SW_G}}]^{N_\mathrm{G}}T_{S_\mathrm{pf}}(2\Delta\tau_\mathrm{pf}/3)[T_{\mathrm{SW_G}}]^{N_\mathrm{G}}T_{S_\mathrm{pf}}(\Delta\tau_\mathrm{pf}/6) \tag{4.64}$$

where T_{S_pf} and T_{S_G} are the transformation (4.59) with S replaced by the appropriate action. As can be seen in (4.63) and (4.64), both the gauge part and the pseudo-fermion part have different time scales $\Delta\tau_\mathrm{G}$ and $\Delta\tau_\mathrm{pf}$ respectively. This now allows to choose larger step size for the expensive part (pseudo-fermion part) of the action than for the gauge part. Nevertheless the length of trajectory τ has to be kept fixed.
The authors of [88] quote that they tested the leap frog scheme with multiple time scales in HMC with two flavors of Wilson quarks on a 4^4 lattice and gained 30% to 40% in performance. A generalization to more than one pseudo-fermion action in (4.62) was suggested by *Urbach et al.* [89]. The authors tested this idea in combination with Hasenbusch preconditioning and could find a comparable gain of performance as in the HMC variant which was suggested by *Lüscher* in [85].

4.7 n^{th} Root Trick

The so-called n^{th} *root trick* concerns a special factorization of the quark determinant and is discussed by *Kennedy* in [58]. The proposed factorization is

$$\det\{MM^\dagger\} = \left(\det\{MM^\dagger\}^{\frac{1}{n}}\right)^n. \tag{4.65}$$

The motivation is based on the property of the condition number cond of hermitian matrices like the Dirac matrix $MM^\dagger$ for two flavors

$$\mathrm{cond}(\{MM^\dagger\}^{\frac{1}{n}}) = \sqrt[n]{\mathrm{cond}(MM^\dagger)}. \tag{4.66}$$

For each factor of the determinant on the right-hand side of (4.65), a separate pseudo-fermion field is introduced

$$\det\{MM^\dagger\} = \left(\det\{MM^\dagger\}^{\frac{1}{n}}\right)^n \propto \prod_{i=1}^{n}\int \mathscr{D}\phi_i^\dagger\mathscr{D}\phi_i \exp\left\{-\phi_i^\dagger(MM^\dagger)^{-\frac{1}{n}}\phi_i\right\} \tag{4.67}$$

and the matrix which appears in the above exponent has reduced condition number according to (4.66). The author argues that under certain conditions, the maximal force which can appear is reduced by a factor of $n \cdot \mathrm{cond}(MM^\dagger)^{\frac{1}{n}-1}$ and hence the step size can be increased by the reciprocal of this factor. Furthermore the choice of the number of pseudo-fermions n is important and an estimate for the optimal value is obtained by

minimizing the costs

$$n_{\text{opt}} \approx \ln(\text{cond}(MM^\dagger)). \tag{4.68}$$

The advantage of this factorization is that all Dirac matrices have the same condition number. There is no need for a special treatment for different pseudo-fermions. On the other hand, this method needs the approximation of $MM^{-\frac{1}{n}}$ and the benefits of a split time integration scheme like the Sexton Weingarten scheme cannot be applied.

4.8 Multiboson method

The multiboson method [90] is based on the idea that a lattice theory with dynamical fermions can be mapped to a local bosonic theory by using an appropriate chosen fermion matrix inversion algorithm in the functional integral. In this way, familiar simulation algorithms from pure gauge theory and from Higgs models can be applied. In the multiboson method, the inverse of the Dirac matrix which is needed in the calculation of the fermion determinant (4.18) is approximated by a polynomial. For the subsequent discussion, we consider Wilson fermions. The quark matrix $Q = c_0\gamma_5 M$ is normalized by c_0 such that the eigenvalues of Q are between -1 and 1. Due to γ_5-hermiticity of the Dirac matrix, the operator Q has a complete set of eigenvectors with real eigenvalues. As discussed before, positive definiteness of the fermion matrix is crucial and therefore we consider two flavors of degenerated Wilson quarks. The key idea of the multiboson method is now to approximate Q^{-2} with a polynomial $P_n(Q^2)$ of order n such that

$$\det\{Q^2\} = \lim_{n\to\infty} \Big(\det\{P_n(Q^2)\}\Big)^{-1}. \tag{4.69}$$

In numerical simulations n cannot be taken to infinity but a rapid convergence to this limit can be achieved by a smart choice of the polynomial $P_n(Q^2)$. A first suggestion of *Lüscher* [90] is (n even)

$$P_n(Q^2) = \prod_{k=1}^{n} \left[(Q-\mu_k)^2 + \nu_k^2\right] \tag{4.70}$$

where μ_k and ν_k are given by

$$\mu_k + i\nu_k = \sqrt{z_k}, \quad \nu_k > 0, \quad z_k = 1 - \exp\left\{i\frac{2\pi k}{n+1}\right\}. \tag{4.71}$$

$P_n(Q^2)$ is positive definite and the eigenvalues are bounded between 0 and 1 due to the proper normalization of Q. To solve the linear system $Q^2\psi = \phi$, it suffices to calculate the product $P_n(Q^2)\phi$. The fermion determinant can then be calculated by a multiple

integration over bosonic fields ϕ_k

$$\det Q^2 = \lim_{n\to\infty} \int \mathscr{D}\phi^\dagger \mathscr{D}\phi \exp\left\{ -\sum_{k=1}^{n} \phi_k^\dagger \left[(Q-\mu_k)^2 + \nu_k^2 \right] \phi_k \right\} \tag{4.72}$$

without any inversion of the Dirac matrix. But a disadvantage is that the bosonic formulation of the theory involves a huge number of complex fields which couple to the gauge fields. The limit $n \to \infty$ in (4.72) cannot be taken in numerical simulations. Therefore the finiteness of n introduces also systematic errors. Since the eigenvalues are bounded between 0 and 1, *Lüscher* proposes in the same publication [90] to use a more sophisticated choice, namely the modified Chebyshev polynomials, due to the convergence properties.

4.9 Variants of HMC

In the preceding sections of this chapter, we summarized a selection of different techniques which are used in current lattice QCD codes. Indeed, the list is not intended to be exhaustive (see [23–25]). Since the first suggestion of the HMC algorithm, some variants of it have been arisen which make use of different algorithmic techniques to overcome numerical problems and/or to gain performance. The **P**olynomial **H**ybrid **M**onte **C**arlo (**PHMC**) which was proposed by *Frezotti* and *Jansen* [91, 92] combines the multiboson technique with the HMC algorithm. The inverse of the fermion matrix is approximated by a polynomial written in powers of the fermion matrix. In the case of two degenerated Wilson quarks (Q is defined as in section 4.8), the partition function

$$Z = \int \mathscr{D}U \, \mathscr{D}\phi^\dagger \, \mathscr{D}\phi \, \mathscr{D}\eta^\dagger \, \mathscr{D}\eta \, W \exp\left\{ -S_\mathrm{G} - S_\mathrm{P} - S_\eta \right\} \tag{4.73}$$

where S_G is Wilson's gauge action and

$$S_\mathrm{P} = \phi^\dagger P_{n,\epsilon}(Q^2)\phi, \tag{4.74}$$

$$S_\eta = \eta^\dagger \eta \tag{4.75}$$

contains a correction factor W which is given by

$$W = \exp\left\{ \eta^\dagger \left(1 - \left[Q^2 P_{n,\epsilon}(Q^2) \right]^{-1} \right) \eta \right\}. \tag{4.76}$$

The description (4.73) of the partition function with (4.74),(4.75) and (4.76) is still exact due to the trivial identity

$$\det(Q^2) = \det(Q^2 P_{n,\epsilon}(Q^2)) \det(P_{n,\epsilon}(Q^2)^{-1})$$

which was used above. The polynomial $P_{n,\epsilon}(Q^2)$ approximates the inverse $(Q^2)^{-1}$ for all eigenvalues λ of Q^2 with $\lambda = [\epsilon, 1]$. Quantities measured on configurations sampled

by the exponential in (4.73) have to be reweighted with $\langle W\rangle_{\mathrm{P}}^{-1}$ to obtain the correct average.

$$\langle\mathcal{O}\rangle = \langle W\rangle_{\mathrm{P}}^{-1}\langle W\mathcal{O}\rangle_{\mathrm{P}}. \tag{4.77}$$

$\langle\dots\rangle_{\mathrm{P}}$ denotes the average evaluated with the action $S_{\mathrm{G}} + S_{\mathrm{P}} + S_\eta$. As the authors quote, the above description of the partition function allows to split up the eigenvalue spectrum of Q^2 smoothly by choosing a suitable polynomial $P_{n,\epsilon}(Q^2)$ in a part which is included in the update procedure and a second part which is handled with the correction factor. The parameter ϵ in $P_{n,\epsilon}(Q^2)$ serves as an infrared cutoff and controls the very low-lying eigenvalues of Q^2. Since the minimal eigenvalue of Q^2 is dictated by ϵ, it is expected that the expense of simulation decreases. Due to the infrared cutoff, the sampling in configuration space is different than with the conventional HMC algorithm. The modes lower than ϵ do not "occur". Therefore extra care has to be taken for observables which receive large contributions from low-lying modes ($\lambda(Q^2) < \epsilon$) [91]. A comparable performance of PHMC to HMC can be achieved easily by choosing n and ϵ according to some estimation which are given in [92], but for a gain of performance, special tunings of n and ϵ are needed. The authors tested the performance of PHMC in comparison to HMC on a 16×8^3 lattice with two flavors of $\mathcal{O}(a)$ improved Wilson quarks with Schrödinger functional boundary conditions, even-/odd- preconditioning and the Chebyschev polynomials as an approximation for $(Q^2)^{-1}$ as suggested by *Lüscher* [90]. They could show a gain of a factor of around two in performance with some extra tuning of n and ϵ and quoted that this gain increases if one simulates on larger volumes. A further advantage of PHMC is that simulations with odd numbers of flavors are possible [80]. Furthermore a non-Hermitian Polynomial Hybrid Monte Carlo (NPHMC) has been studied [93] in which the inverse of the non-Hermitian-Wilson-Dirac operator was approximated by Chebyshev polynomials. Numerical tests showed that the performance of the NPHMC algorithm is comparable with conventional HMC algorithm but under certain conditions a slight gain was achieved.

Instead of approximating the fermion determinant by a polynomial, *Clark* and *Kennedy* proposed a rational approximation (**RHMC**) [94, 95]

$$\det(M^\dagger M)^\alpha = \int \mathscr{D}\phi^\dagger\,\mathscr{D}\phi\,\exp\left\{-\phi^\dagger (M^\dagger M)^{-\alpha}\phi\right\} \tag{4.78}$$

$$\approx \int \mathscr{D}\phi^\dagger\,\mathscr{D}\phi\,\exp\left\{-\phi^\dagger r^2(M^\dagger M)\phi\right\} \tag{4.79}$$

where $r(x) = x^{-\alpha/2}$. Equation (4.78) implies that one can define a theory with arbitrary numbers of flavors N_{f} if one allows non-integer values for the parameter α. The conventional HMC algorithm would fail in this case because there is no method to evaluate the action for fractional α. This is different in the case of RHMC. $r(x)$ is usually written as a partial fraction $r(x) = \sum_{k=1}^{m} \frac{\alpha_k}{x+\beta_k}$ which can be evaluated very efficiently using a multi-shift solver [96]. For the cases of interest $|\alpha| < 1$, all poles and roots of the rational approximation are positive and real, and the coefficients α_k of the partial fractions appear as positive. This leads to a numerically stable algorithm. The reason

for the positivity of the poles, roots and the coefficients α_k is still not understood (and called therefore as miracles in [58]). The force calculation with the pseudo-fermion action in (4.79) would need a double inversion due to the square of $r(x)$. To avoid this problem, a second rational approximation is used in the molecular dynamics [95]. The costs of RHMC as described above is comparable with HMC but RHMC permits the easy introduction of a single quark flavor [95] and is therefore suitable for simulations with odd numbers of flavors. An increasing of the step size, and thus a speedup, can be achieved by using the n^{th} root trick in RHMC. However, as discussed before in section 4.7, the timescale for all pseudo-fermions in the n^{th} root trick is the same due to the same magnitude of pseudo-fermion forces and therefore one cannot derive benefit from the multiple timescale integration. A comparison of the performance of HMC with Hasenbusch preconditioning and RHMC with multiple pseudo-fermion fields (n^{th} root trick) revealed no significant difference between them. But it is reported [97] that the use of higher order integrator in n^{th} root trick leads to an improved volume scaling. As discussed in [95], the rational approximation has much better convergence properties than the polynomial approximation.

The last variant of HMC which we want to mention here is the **DD-HMC** provided by *Lüscher*. DD-HMC stands for **D**omain **D**ecomposed **H**ybrid **M**onte **C**arlo and is a combination of domain decomposition methods [74] and the conventional HMC algorithm [68]. *Lüscher* discusses in [84, 85, 98] the applicability of domain decomposition methods to lattice QCD algorithms and describes the implementation of the Schwarz-alternating procedure as a preconditioner for HMC. Main features of Schwarz-preconditioning have already been discussed in section 4.5. In [87], he demonstrates very impressively how the DD-HMC code can be accelerated by applying *deflation techniques*.

5 Theoretical foundations

In this chapter, we are going to introduce some key concepts which will be used in following chapters and give a brief overview about perturbative and non-perturbative renormalization and the running of quark masses and the coupling. Then we will introduce the step scaling function of QCD and explain our finite-volume scheme (*Schrödinger functional*) and give a definition of a coupling in this scheme. Finally, we want to introduce the PCAC mass.

5.1 Perturbative renormalization

The first need for renormalization arose as the quantum field theory of electrodynamics (QED) was formulated by *Richard Feynman*, *Freeman Dyson*, *Julian Schwinger*, and *Sin-Itiro Tomonaga* in the 1940s. All quantities calculated with the help of perturbation theory (Feynman diagrams) in QED contained a divergent part that made the meaningful interpretation of the results impossible. But the development of renormalization as a tool turned out to be a powerful technique to cope with the infinities arising in QED results. Moreover, this shed light on the fundamental difference between bare parameters of the Lagrangian and the renormalized quantities that can be measured in experiments. Over the years, the theory of renormalization became well-established and an indispensable part of all quantum field theories with physical relevance like QED, QCD etc. Nowadays, one of the standard ways to perform the renormalization in perturbation theory is to construct the Lagrangian $\mathscr{L}$ of the theory in the following way

$$\mathscr{L} = \mathscr{L}_{\mathrm{R}} + \delta\mathscr{L}. \tag{5.1}$$

$\mathscr{L}_{\mathrm{R}}$ is the bare Lagrangian written in terms of the physical quantities and $\delta\mathscr{L}$ consists of so-called counterterms which have absorbed the unobservable infinite shifts between the bare and renormalized parameters. Perturbation theory which is based on such a Lagrangian is known as *renormalized perturbation theory*. It has some technical advantages compared to the bare perturbation theory in multiloop diagrams [3]. $\delta\mathscr{L}$ usually contains coefficients which have to be adjusted ("renormalized") so that the result is finite and independent of the regulator which regulates the divergences. Over the years, different methods as regulator have been suggested like *Pauli-Villars* [99], *dimensional regularization* [100, 101], *momentum cut-off*, *Zeta-function regularization*, *point-splitting regularization* etc. The dimensional regularization turned out to be very useful for gauge theories especially. The basic idea is to continue the dimension of the loop integrals analytically to $D = 4 - 2\epsilon$ and carry them out. The aforementioned coefficients in $\delta\mathscr{L}$ can now be used for canceling the poles. The choice of the coefficients is not unambiguous

and therefore different so-called *renormalization schemes* do exist. In the *minimal subtraction* (MS) scheme, for example, only the poles are subtracted [101]. Whereas in the *modified minimal subtraction* ($\overline{\text{MS}}$) scheme, additional to the poles, some constant terms are subtracted [102]. Both schemes belong to the class of mass independent schemes. In this class of schemes, the renormalization condition is independent of the renormalized mass. As an example, the so-called *momentum-space subtraction* (MOM) scheme [103] is mass dependent.

In principle, a Lagrangian of a field theory could contain all possible types of interactions. However, the renormalization theory eliminates all except for a few interaction terms. Since a non-renormalizable theory would need an infinite number of counterterms to remove the divergences in perturbative loop calculations and had therefore little predictive power, only renormalizable theories seem to be realistic theories which are able to describe nature. The decision whether a theory is renormalizable or not can be made by counting the mass dimension of the coupling constants in the Lagrangian. A negative mass dimension of a coupling constant means that the theory is not renormalizable. A popular example of a non-renormalizable theory is Fermi's theory of weak interaction with a four fermion contact term [104, 105]. Originally this theory was developed to study the decay of a neutron $n \to p + e^- + \bar{\nu}_e$. The details of this process were not known at that time and Fermi assumed that the interaction is pointlike and the interaction Hamiltonian consists of a product of operators representing the involved fermions $(n, p, e^-, \bar{\nu}_e)$ multiplied by a coupling constant G_F. An analysis of the mass dimension turns out that G_F has mass dimension -2. In other words, Fermi's theory of weak interaction is non-renormalizable. Nevertheless it can still serve as low-energy effective theories because in the low-energy regime $q^2 \ll M^2_{\text{W}^\pm}, M^2_{\text{Z}}$, there is not enough energy to create a physical $W^\pm$ or Z boson, so a four fermion contact term describes the above process in that regime well.

5.2 Non-perturbative renormalization

In the low-energy regime where the lattice regularization is the only method that can be applied due to the strength of the coupling constant in QCD, the renormalization has to be performed non-perturbatively. The elimination of the bare parameters in favor of the renormalized counterparts can be carried out, for example, by considering the hadron spectrum (proton, π-, K-, D-, B-mesons) on the lattice. After computing the masses of hadrons in units of the lattice spacing a through suitable correlation functions, the physical value of the lattice spacing can be extracted. This can be done for instance, through setting the proton mass am_{P} in lattice units to the experimental value $m_{\text{P}}^{\text{exp}}$ [106]

$$a = \frac{am_{\text{P}}}{m_{\text{P}}^{\text{exp}}}. \tag{5.2}$$

So, the bare quark masses $am_{0,i}$, where the index i denotes the different quark flavors, can now be fixed by demanding the lattice masses of mesons (π, K, D, B) to be equal

to the experimental values. In principle, the theory is renormalized and predictions can be made. A second technique for setting the scale is to use the so-called hadronic length scale (*Sommer scale*) r_0 [107]. It is defined through the force $F_{q\bar{q}}(r)$ between two static quarks at distance r. The choice of r is based on phenomenological quark potential models which describe accurately the $b\bar{b}$ and $c\bar{c}$ spectra by an effective potential in a range of $r \approx [0.2, 1]$ fm. Thus, the most reliable information about the force between two static quarks is believed to be at an intermediate distance of around $r_0 \approx 0.5$ fm. In a more mathematical way, r_0 is chosen such that the following equation is valid

$$r_0^2 F_{q\bar{q}}(r_0) = 1.65. \tag{5.3}$$

However, converting lattice results with r_0 into corresponding physical results introduces large systematic errors because the physical value of r_0 contains uncertainties. However, the Sommer scale provides a well-defined way to compare lattice results between different simulations with different actions and lattice spacings. Both techniques allow to compare theoretical results with experimental measurements.

However, the fundamental parameters of QCD, i.e. the coupling constant (chapter 1) and masses of the quarks, are scale dependent and the computation of them from low to high energy regime involves scales with different powers of magnitude. For instance, the coupling constant of QCD which is determined non-perturbatively in the low-energy regime has to be connected to the perturbative regime, say around 10 GeV or higher, for comparing to experiments via jet cross sections etc. Covering such a large energy regime sets strong demands at the lattice simulations which have to be performed. First, the scale μ must be chosen in such a way that the lattice discretization effects are not large hence a continuum extrapolation can be made easily. Second, lattice QCD simulations are always restricted to a system with finite extensions and therefore finite-size effects have to be avoided. In other words, the box size L has to be large compared to the mass of the lightest physical state (π meson $\approx 0.14\,\text{GeV}$) and the confinement scale.

$$L \gg \frac{1}{m_\pi} \approx \frac{1}{0.14\,\text{GeV}} \gg \frac{1}{\mu} \approx \frac{1}{10\,\text{GeV}} \gg a \tag{5.4}$$

These requirements imply lattice simulations with $L/a \gg 70$ which are impossible to perform on current computational facilities. An elegant way to circumvent the difficulties was proposed by *Lüscher et al.* in [108]. The basic idea is to use the disturbing finite-size effects as a physical observable and to identify the energy scale μ with the inverse of the system size L: $\mu = 1/L$. This enables the study of the properties of the system as a function of the box size L. An analogous approach is known from numerical simulations of a statistical system. At the critical point, the correlation length becomes the size of the finite box and the only remaining length scale in the simulation is than the box size L. Through the change of the observables with the box size, the critical exponents which one is usually interested in can be extracted numerically.

Back in QCD, an analogous strategy can be used. In such a finite-volume renormalization scheme for QCD, the evolution of the coupling with the energy scale μ is identified with the running of a coupling with the system size. However, first, the bare

parameters of the theory have to be eliminated in favor of the renormalized counterparts. This is achieved by using the hadron spectrum, for example, as described above in the low-energy regime $\mu = 1/L_{\max}$ ($L_{\max} \approx O(0.5\,\mathrm{fm})$). This hadronic scheme can then be related to some finite-volume scheme in which the scale evolution can be performed recursively up to a certain scale $\mu = 2^n/L_{\max}$ where the perturbation theory applies. After perturbative evolution, the Λ parameter and the renormalization group invariant masses of the quarks can be computed and plugged into perturbative expressions to make predictions for jet cross sections or other high energy observables. The remarkable property of this strategy is that in the final results, there is no reference to the finite-volume quantities which were used in the scale evolution (for details [57]).

5.3 Running coupling and quark masses

As mentioned before, the coupling and the quark masses are renormalization scale dependent and run with the energy scale. Therefore the quoted values of the quark masses (Table 1.1) and the world average of α_s, both in $\overline{\mathrm{MS}}$ scheme, are referred to a particular reference scale in [6]. From the theoretical point of view, the running of the QCD parameters is described by the renormalization group equation. However, a physical observable $\mathscr{O}$ should have no reference to a particular renormalization scale μ. This fact is expressed by the Callan-Symanzik equation

$$\left[\mu\frac{\partial}{\partial\mu} + \beta(\bar{g})\frac{\partial}{\partial\bar{g}} + \tau(\bar{g})\sum_{i=1}^{N_\mathrm{f}}\overline{m}_i\frac{\partial}{\partial\overline{m}_i}\right]\mathscr{O} = 0. \tag{5.5}$$

In words: for any change of μ there are accompanying modifications of $\bar{g}$ and $\overline{m}_i$ such that the physics is unchanged. The implied scale dependence of the coupling is given by $\beta(\bar{g})$ in (5.5)

$$\beta(\bar{g}) = \mu\frac{\partial\bar{g}(\mu)}{\partial\mu}. \tag{5.6}$$

For high energies or for weak couplings, the β-function has the following asymptotic expansion

$$\beta(\bar{g}) \overset{\bar{g}\to 0}{=} -\bar{g}^3\left[b_0 + b_1\bar{g}^2 + b_2\bar{g}^4 + \ldots\right]. \tag{5.7}$$

The first two (1- and 2-loop) coefficients b_0 and b_1 in (5.7) are universal and independent of the regularization scheme while the higher order coefficients are scheme-dependent

$$b_0 = \frac{1}{(4\pi)^2}\left(11 - \frac{2}{3}N_\mathrm{f}\right), \tag{5.8}$$

$$b_1 = \frac{1}{(4\pi)^4}\left(102 - \frac{38}{3}N_\mathrm{f}\right). \tag{5.9}$$

The 3-loop coefficient b_2 in the Schrödinger functional scheme, which we will need later, can be extracted from [109] to

$$b_2 = \frac{1}{(4\pi)^3}\left[0.483(7) - 0.275(5)N_\mathrm{f} + 0.0361(5)N_\mathrm{f}^2 - 0.00175(1)N_\mathrm{f}^3\right]. \tag{5.10}$$

In our discussion, we consider a mass-independent scheme where the renormalization conditions are imposed at vanishing quark masses. Well-known representatives of such a scheme are the $\overline{\mathrm{MS}}$ scheme of the dimensional regularization and the so-called Schrödinger functional scheme used here. For $N_\mathrm{f} \leq 16$, the sign of the β-function (5.7) is negative at weak coupling and the integration of (5.6) results in a coupling which decreases with increasing energy. In other words, the quarks behave like free particles in the high energy regime (asymptotic freedom). But for $N_\mathrm{f} > 16$, there is a sign change and the property of asymptotic freedom is lost.

The running of the quark masses is described in a similar manner as the running of the coupling by the renormalization group function $\tau(\bar{g})$

$$\tau(\bar{g})\overline{m}_i = \mu\frac{\partial\overline{m}_i}{\partial\mu}, \quad i = 1, \ldots, N_\mathrm{f}. \tag{5.11}$$

It can also be expanded asymptotically in perturbation theory like (5.7) with the universal coefficient d_0

$$\tau(\bar{g}) \overset{\bar{g}\to 0}{=} -\bar{g}^2(d_0 + d_1\bar{g}^2 + d_2\bar{g}^4 + \ldots), \quad d_0 = \frac{8}{(4\pi)^2}. \tag{5.12}$$

The higher order coefficients $d_1, d_2, \ldots$ are scheme-dependent. In perturbation theory, both the β- and the τ-function are known up to 4-loop in $\overline{\mathrm{MS}}$ scheme [110, 111]. Of course, it should be emphasized that the β-function [112, 113] as well as the τ-function [114–116] are, in general, non-perturbatively defined functions by (5.6) and (5.11), respectively.

The relation of $\overline{m}_i(\mu)$ and $\bar{g}(\mu)$ to the renormalization group invariant (RGI) quark masses M_i and the Λ parameter, respectively, are given by the following solutions of the Callan-Symanzik equation

$$\Lambda = \mu\left[b_0\bar{g}^2(\mu)\right]^{-\frac{b_1}{2b_0^2}}\exp\left\{-\frac{1}{2b_0\bar{g}^2(\mu)}\right\}\times \exp\left\{-\int_0^{\bar{g}(\mu)} dx\left[\frac{1}{\beta(x)} + \frac{1}{b_0x^3} - \frac{b_1}{b_0^2x}\right]\right\}, \tag{5.13}$$

$$M_i = \overline{m}_i(\mu)\left[2b_0\bar{g}^2(\mu)\right]^{-\frac{d_0}{2b_0}}\exp\left\{-\int_0^{\bar{g}(\mu)} dx\left[\frac{\tau(x)}{\beta(x)} - \frac{d_0}{b_0}\right]\right\} \tag{5.14}$$

where $i = 1, \ldots, N_\mathrm{f}$. If these parameters are known, all running parameters will be

uniquely fixed at all scales. It should be mentioned that Λ is scheme-dependent but the transformation to other schemes can be carried out exactly by an 1-loop relation between the couplings in those schemes. The RGI quark masses M_i have no scheme dependence.

5.4 The step scaling function

The concept of the *step scaling function* which was introduced by *Lüscher et al.* in [108] has proven as a very useful recursive technique to scale the coupling from low to high energies. As we discussed before, in our finite-volume scheme, the energy scale μ is identified with L^{-1}. Hence the renormalization group function β (5.6) describes how the coupling changes if the box size is changed infinitesimally. The step scaling function $\sigma(s,u)$, in comparison, gives then a description how the coupling behaves when the box size L is scaled by a factor s

$$\bar{g}^2(sL) = \sigma(s, \bar{g}^2(L)). \tag{5.15}$$

Instead of $\bar{g}^2(1/L)$ we write $\bar{g}^2(L)$ to keep the notation simple. $\sigma(s,u)$ can be regarded as an integrated form of the renormalization group β-function. With the help of the step scaling function (5.15) the coupling can be traced to scales $2^{-k}L_{\max}$ (small box sizes, high energies) starting with an initial value $L = L_{\max}$ recursively. The choice $s = 2$ is commonly used [108, 113, 117] in the application of $\sigma(s,u)$ and we will also use this convention (from now on $s = 2$ and therefore we will drop the factor 2 in the argument of σ). But other choices are conceivable. The relation between the renormalization group β-function and the step scaling function $\sigma(\bar{g}^2(L))$ is given by

$$-2\ln(2) = \int_u^{\sigma(u)} \frac{dx}{\sqrt{x}\beta(\sqrt{x})}. \tag{5.16}$$

For small values of the coupling u, the step scaling function has the following perturbative expansion

$$\sigma(u) = u + s_0 u^2 + s_1 u^3 + s_2 u^4 + \ldots \tag{5.17}$$

where the coefficients are given by [113]

$$s_0 = 2b_0 \ln(2), \tag{5.18}$$

$$s_1 = [2b_0 \ln(2)]^2 + 2b_1 \ln(2), \tag{5.19}$$

$$s_2 = [2b_0 \ln(2)]^3 + 10 b_0 b_1 [\ln(2)]^2 + 2b_2 \ln(2). \tag{5.20}$$

Both equation (5.16) with the truncated β function as well as equation (5.17) can be used as the perturbative result for the step scaling function. They differ from each other only by higher order terms and the difference can be taken to estimate this part. When we compare our Monte Carlo results with perturbation theory we take the first option.

Nevertheless, it is remarkable to notice that $\sigma(u)$ can be studied by Monte Carlo

simulations. The numerical strategy starts with choosing several lattice sizes L/a and tuning the bare coupling g_0^2 and the hopping parameter κ in such a way that the value of the renormalized coupling $\bar{g}^2(L)$ reaches some chosen value $\bar{g}^2(L) = u$ and the quark mass vanishes since we are in a massless scheme. The next step is now to take $L/a \to 2L/a$ and simulate at the same bare parameters. The obtained coupling $\bar{g}^2(2L)$ from the latter simulations is a lattice approximation $\Sigma(u, a/L)$ of the continuum step scaling function $\sigma(u)$. An extrapolation to the continuum of the data points at the same coupling u but growing L/a then leads to one value of the continuum function $\sigma(u)$. The procedure is repeated until a large range of u is covered. An appropriate functional description of the continuum step scaling function can be given in the end in the form of a suitable fit-function that interpolates the data.

The lattice approximation $\Sigma(u, a/L)$ of the step scaling function contains remnant lattice effects of order a. The reason is that beside our non-perturbative value for $c_{\rm sw}$ there are boundary improvement coefficients for which only perturbative estimates are available. We use those to the known order [109, 112, 118] which ensures that $\mathcal{O}(a)$ cutoff effects in the step scaling function appear only starting at three-loop order.

The details of cutoff effects also depend on how the condition of a massless scheme is exactly implemented at a finite lattice spacing. As in the $N_{\rm f} = 2$ computation, we define the massless point on the smaller of the pair of lattices entering the step scaling function. More precisely, the (unrenormalized) PCAC quark mass,

$$m(x_0) = \frac{\tilde{\partial}_0 f_{\rm A}(x_0) + c_{\rm A} a \partial_0^* \partial_0 f_{\rm P}(x_0)}{2 f_{\rm P}(x_0)} \tag{5.21}$$

at $x_0 = \frac{T}{2}$,

$$m_1 = m\left(\frac{T}{2}\right) , \tag{5.22}$$

is set to zero. The definition of the correlation functions $f_{\rm A}, f_{\rm P}$ and the PCAC mass will be discussed in section 5.7. A discussion of the influence of choosing the massless point in a way which differs from (5.22) at finite lattice spacing is given in [119]. For the improvement coefficient $c_{\rm A}$ in (5.21) we used the 1-loop result [120].

In addition to the various improvement terms in the action and $c_{\rm A}$ in (5.21) we exploit our knowledge of δ_1 and δ_2 from the perturbative calculation of

$$\delta(u, a/L) = \frac{\Sigma(u, a/L) - \sigma(u)}{\sigma(u)} = \delta_1(a/L)u + \delta_2(a/L)u^2 + \ldots , \tag{5.23}$$

$$\delta_1(a/L) = \delta_{10}(a/L) + \delta_{11}(a/L)N_{\rm f} \tag{5.24}$$

$$\delta_2(a/L) = \delta_{20}(a/L) + \delta_{21}(a/L)N_{\rm f} + \delta_{22}(a/L)N_{\rm f}^2 \tag{5.25}$$

with the coefficients taken from Table 5.1 [117]. For $N_\mathrm{f} = 4$ we have

L/a	δ_1	δ_2
4	−0.0102	0.0073
6	−0.0045	0.0013
8	−0.0024	0.00013

Using these data we form the lattice step scaling function [121]

$$\Sigma^{(2)}(u, a/L) = \frac{\Sigma(u, a/L)}{1 + \delta_1(a/L)u + \delta_2(a/L)u^2} \tag{5.26}$$

which we expect to have smaller overall cutoff effects. They still start at order $a \times u^4$ but terms of order $a^m \times u^n$ are removed for all m and for $n \leq 3$ (in fact non-perturbatively in a). As mentioned previously, the order $a \times u^4$ terms are due to the only perturbatively known boundary improvement terms. Their influence was explicitly checked for $N_\mathrm{f} = 2$ and found to be minor [113], such that also here we assume that the step scaling function converges *effectively* at a rate

$$\Sigma^{(2)}(u, a/L) = \sigma(u) + \mathcal{O}(a^2). \tag{5.27}$$

The obvious advantage of using such a finite-size scaling technique is, that the strong

L	δ_{10}	δ_{11}	δ_{20}	δ_{21}	δ_{22}
4	−0.01033	0.00002	−0.00159	−0.00069	0.000724
5	−0.00625	−0.00014	−0.00087	−0.00048	0.000411
6	−0.00394	−0.00014	−0.00055	−0.00033	0.000199
7	−0.00268	−0.00014	−0.00038	−0.00021	0.000102
8	−0.00194	−0.00011	−0.00027	−0.00013	0.000058
9	−0.00148	−0.00009	−0.00020	−0.00010	0.000038
10	−0.00117	−0.00007	−0.00015	−0.00007	0.000026
11	−0.00095	−0.00006	−0.00011	−0.00006	0.000020
12	−0.00079	−0.00005	−0.00009	−0.00005	0.000016

Table 5.1: Table of coefficients $\delta_{10}, \delta_{11}, \delta_{20}, \delta_{21}, \delta_{22}$ with 2-loop value of c_t [117].

demand (5.4) to lattice simulations is weakened to $L \gg a$ through identifying $\mu = L^{-1}$.

5.5 The Schrödinger functional scheme

The finite-volume scheme which we want to use for our simulations is the Schrödinger functional scheme. In the following, we will give a brief summary of the main features and properties of this scheme, which are discussed in detail in many papers (for example [109, 118, 122–124]).

For a physical relevance of a quantum field theory, the renormalizability is a crucial property. In the case of ϕ^4 theory with Schrödinger functional boundary conditions, Symanzik showed, that after renormalization of the coupling and mass, the theory becomes finite to all orders in perturbation theory [125] by adding some counter terms to the action. For QCD with Schrödinger functional boundary conditions, the renormalizability is explicitly checked to a 2-loop calculation in $N_\mathrm{f} = 0$ [109] and to an 1-loop calculation for dynamical fermions [124]. Monte Carlo simulation data confirm that this is also valid beyond perturbation theory [106].

The first description of an application of the Schrödinger functional on non-abelian gauge theories has been given by *Lüscher*, *Narayanan*, *Weisz* and *Wolff* in [122]. The motivation was to apply the discussed finite-size scaling technique to gauge theories and compute the running coupling from low to high energy regime. For this purpose a suitable non-perturbative definition of a coupling α_SF (subscript SF stands for Schrödinger Functional) was needed, which is only dependent on L and also accessible numerically with small errors. A 2-loop perturbative calculation of the coupling should also be possible with reasonable efforts. This is important for the conversion of the finite volume coupling to, for example, $\overline{\mathrm{MS}}$ coupling in infinite volume in the high energy regime with small conversion errors

$$\alpha_{\overline{\mathrm{MS}}}(s\mu) = \alpha_\mathrm{SF}(\mu) + c_1(s)\alpha^2_\mathrm{SF}(\mu) + c_2(s)\alpha^3_\mathrm{SF}(\mu) + \dots \tag{5.28}$$

where $c_1(s)$ and $c_2(s)$ are 1-loop and 2-loop coefficients. The estimated systematic errors of conversion of the coupling by using (5.28) is at the level of 1% [109]. These requirements are not easy to fulfill. However the Schrödinger functional which is the Euclidean propagation kernel of a field configuration C at time $x_0 = 0$ to another field configuration C' at time $x_0 = T$ provides a framework where such demands can be satisfied.

So, the theory is set up on a four-dimensional (Euclidean) hypercubic lattice with lattice spacing a. If not explicitly mentioned, the spatial and temporal extensions L and T, respectively, are set to the same value. The SU(3) gauge field lives on the links between neighboring lattice sites, while the quark fields live on the lattice sites. Periodic boundary conditions are imposed for the spatial extension and Dirichlet boundary conditions for the temporal direction. For the purpose of illustration, it can be imagined that the lattice is wrapped up to a cylinder when we put the three spatial dimensions together to one (see Figure 5.1). Special care has to be taken when treating fermionic fields because they obey the periodic boundary conditions up to a phase factor $\exp\{i\theta\}$

$$\Psi(x + L\hat{k}/a) = \exp\{i\theta\}\Psi(x), \quad \overline{\Psi}(x + L\hat{k}/a) = \exp\{-i\theta\}\overline{\Psi}(x), \tag{5.29}$$

where $\hat{k}$ is the unit vector in k'th direction ($k = 1, 2, 3$). The partition function of such a system is given by

$$Z[C', C] = \exp\{-\Gamma\} = \int_\mathrm{V} \mathscr{D}U \mathscr{D}\Psi \mathscr{D}\overline{\Psi} \exp\left\{-S[U, \Psi, \overline{\Psi}]\right\} \tag{5.30}$$

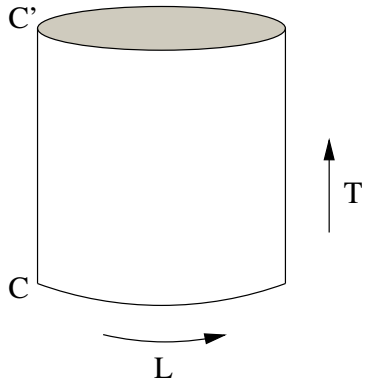

Figure 5.1: Illustration of our lattice with Schrödinger functional boundary conditions. Only one spatial direction is depicted.

where Γ is the so-called effective action. The choice of C_k and C'_k in the boundary gauge fields

$$U(x,k)|_{x_0=0} = \exp\{aC_k\}, \tag{5.31}$$
$$U(x,k)|_{x_0=T} = \exp\{aC'_k\} \tag{5.32}$$

is arbitrarily. Since we are restricted to a finite (small) box and to not arbitrarily small lattice spacings a, lattice artifacts are present. A background field which leads to acceptable small lattice discretization effects would be appreciated. In this context, constant Abelian fields turned out to be appropriate [122]

$$C_k = \frac{i}{L}\begin{pmatrix} \phi_1 & 0 & 0 \\ 0 & \phi_2 & 0 \\ 0 & 0 & \phi_3 \end{pmatrix}, \quad C'_k = \frac{i}{L}\begin{pmatrix} \phi'_1 & 0 & 0 \\ 0 & \phi'_2 & 0 \\ 0 & 0 & \phi'_3 \end{pmatrix}. \tag{5.33}$$

The matrices C_k and C'_k are diagonal and spatially constant and due to SU(3), $\mathrm{tr}\,(C_k)$, $\mathrm{tr}\,(C'_k)$ vanish. We adopt the choice [112]

$$(\phi_1,\phi_2,\phi_3) = \left(\eta - \frac{\pi}{3}, -\frac{\eta}{2} + \eta\nu, -\frac{\eta}{2} + \frac{\pi}{3} - \eta\nu\right) \tag{5.34}$$
$$(\phi'_1,\phi'_2,\phi'_3) = \left(-\eta - \pi, \frac{\eta}{2} + \frac{\pi}{3} + \eta\nu, \frac{\eta}{2} + \frac{2\pi}{3} - \eta\nu\right) \tag{5.35}$$

with parameters η and ν. In [112], it is argued that numerical simulations of the Schrödinger functional showed, that the choice $\nu = 0$ led to a minimum of statistical errors of the coupling. Therefore, we will set ν to zero.

In the partition function (5.30), the contribution where the action S has its minimum will dominate the path integral. As discussed in [112], the corresponding minimal action configuration V, which has to be a solution of the lattice field equations, can be expressed

as follows

$$V_\mu(x) = \exp\{aB_\mu(x)\} \tag{5.36}$$

where

$$B_0 = 0, \quad B_k = \frac{x_0 C'_k + (T - x_0)C_k}{T}, \quad k = 1, 2, 3 \tag{5.37}$$

is the induced background field by C_k and C'_k. The field strength tensor

$$G_{\mu\nu} = \partial_\mu B_\nu - \partial_\nu B_\mu + [B_\mu, B_\nu] \tag{5.38}$$

has non-vanishing components due to (5.37)

$$G_{0k} = -G_{k0} = \partial_0 B_k = \frac{C'_k - C_k}{T}, \quad G_{kl} = 0, \quad l, k = 1, 2, 3. \tag{5.39}$$

Furthermore, the authors proved that V is indeed a configuration with least action, and other configurations which would lead to the same action were gauge equivalent to V.

The insertion of quarks into the Schrödinger functional and the formulation of the Dirichlet boundary conditions for the quark fields was originally discussed and investigated by *Sint* in [123]. The quark fields at the boundary which serve as sources for fermionic correlation functions can be expressed by

$$P_+\Psi(x)|_{x_0=0} = \rho(\mathbf{x}), \quad P_-\Psi(x)|_{x_0=T} = \rho'(\mathbf{x}) \tag{5.40}$$

$$\overline{\Psi}(x)P_-|_{x_0=0} = \bar{\rho}(\mathbf{x}), \quad \overline{\Psi}(x)P_+|_{x_0=T} = \bar{\rho}'(\mathbf{x}), \tag{5.41}$$

where $P_\pm = \frac{1}{2}(1 \pm \gamma_0)$ with $\gamma_0 = \left(\begin{smallmatrix} 1_{2\times 2} & 0 \\ 0 & -1_{2\times 2} \end{smallmatrix}\right)$ is the projection operator. In the fermionic part of the action with Schrödinger functional boundary conditions, additional terms appear

$$\begin{aligned} S_{\mathrm{F}} = &\int d^4x \overline{\Psi}(x)[\gamma_\mu D_\mu + m]\Psi \\ &- \int d^3\mathbf{x}[\overline{\Psi}(x)P_-\Psi(x)]_{x_0=0} - \int d^3\mathbf{x}[\overline{\Psi}(x)P_+\Psi(x)]_{x_0=L}. \end{aligned} \tag{5.42}$$

$[\overline{\Psi}(x)P_-\Psi(x)]_{x_0=0}$ and $[\overline{\Psi}(x)P_+\Psi(x)]_{x_0=L}$ are counter terms which have to be added to the action due to the boundary conditions. This ensures obtaining a finite renormalized functional. So, after renormalization of the coupling and masses in Schrödinger functional, there is no need of additional renormalization for vanishing boundary values $\rho(\mathbf{x})$, $\rho'(\mathbf{x})$, $\bar{\rho}(\mathbf{x})$ and $\bar{\rho}'(\mathbf{x})$.

As discussed before, the performance of simulation algorithms for lattice QCD is very dependent on the condition number of the Dirac matrix. Because of that one has to be careful concerning the smallest eigenvalue. In general, the quark mass introduces a gap into the spectrum of the Dirac operator and serves therefore as a protection from zero-modes. But on the other hand, when one wants to simulate at very light

quark masses, the gap shrinks. This entails that the probability of occurrence of zero-modes increases which makes simulations with very light quark masses more difficult. In simulations with Schrödinger functional boundary conditions, this can also happen in large volumes because the influence of the boundary conditions on the eigenvalues, especially on the smallest eigenvalue, is small. But, as pointed out in [123], in small volumes, the situation is completely different. The effect of the Schrödinger functional boundary conditions becomes important and produces an additional gap in the spectrum of the Dirac operator. This provides hence a smallest non-zero positive eigenvalue which in turn allows to perform simulations at very light quark masses and even with massless quarks. The advantage is now that we can define a mass-independent renormalization scheme. In this scheme the renormalization group equations adopt a simpler form and the renormalization group β function particularly remains mass independent.

Since we want to measure quantities in our Schrödinger functional, a proper definition of the expectation value of any product of fields has to be given

$$\langle \mathscr{O} \rangle = \left[\frac{1}{Z} \int \mathscr{D}U \mathscr{D}\Psi \mathscr{D}\overline{\Psi} \mathscr{O} \exp\{-S[U,\Psi,\overline{\Psi}]\} \right]_{\rho=\rho'=\bar{\rho}=\bar{\rho}'=0} . \tag{5.43}$$

The matter fields ρ, $\bar{\rho}$ (both at $x_0 = 0$) and ρ', $\bar{\rho}'$ (both at $x_0 = T$) at the boundaries are used as sources. They are set to zero after taking the functional derivatives which are involved in $\mathscr{O}$. In our case, the action S consists of the usual Wilson's gauge action. We write it as a sum over all oriented plaquettes p

$$S_{\mathrm{G}}[U] = \frac{1}{g_0^2} \sum_p w(p) \operatorname{tr}\left[1 - U(p)\right] \tag{5.44}$$

and the aforementioned fermion action with the counter terms (5.42). Constructing $\mathscr{O}$ of functional derivatives

$$\zeta(\mathbf{x}) = \frac{\delta}{\delta\bar{\rho}(\mathbf{x})}, \quad \bar{\zeta}(\mathbf{x}) = -\frac{\delta}{\delta\rho(\mathbf{x})}, \tag{5.45}$$

$$\zeta'(\mathbf{x}) = \frac{\delta}{\delta\bar{\rho}'(\mathbf{x})}, \quad \bar{\zeta}'(\mathbf{x}) = -\frac{\delta}{\delta\rho'(\mathbf{x})}, \tag{5.46}$$

which act on the Boltzmann factor in (5.43), produce $\Psi(x)$ and $\overline{\Psi}(x)$ terms in the path integral (5.43). We will need such fermionic correlation function, for example, in the definition of the renormalized mass in the Schrödinger functional scheme.

The weight factor $w(p)$ in (5.44) is needed due to the boundary conditions. It removes the $\mathcal{O}(a)$ effects of the gauge field at the boundary. As mentioned before in section 2.3, the leading order lattice artifacts of Wilson's gauge action are $\mathcal{O}(a^2)$. But if boundaries are involved, a weight factor $w(p)$ has to be introduced in the gauge action. $w(p)$ is only different from one for plaquettes at the boundary that contain the time-direction and

one of the frozen spatial links

$$w(p) = \begin{cases} \frac{1}{2}c_{\mathrm{s}}(g_0) & \text{if } p \text{ is spatial plaquette at } x_0 = 0 \text{ or } x_0 = T, \\ c_{\mathrm{t}}(g_0) & \text{if } p \text{ is a time-like and attached to a boundary.} \end{cases} \tag{5.47}$$

The improvement term which is multiplied by the coefficient c_{s} for the spatial plaquettes vanishes for the special choice of constant Abelian boundary fields (5.33) [118]. Therefore only c_{t} has to be considered. The value for c_{t} is known to 2-loop order in perturbation theory [109]

$$\begin{aligned} c_{\mathrm{t}}(g_0) = 1 &+ [-0.08900(5) + 0.0191410(1)N_{\mathrm{f}}]g_0^2 \\ &+ [-0.0294(3) + 0.002(1)N_{\mathrm{f}} + 0.0000(1)N_{\mathrm{f}}^2]g_0^4 + \mathcal{O}(g_0^6). \end{aligned} \tag{5.48}$$

As explained in section 2.5, the $\mathcal{O}(a)$ improvement of the fermion action requires to add the Sheikoleslami-Wohlert term multiplied by c_{sw} to the Dirac operator. However a further improvement term due to the boundary is needed which is multiplied by $\tilde{c}_{\mathrm{t}}$ [120]. c_{sw} is known non-perturbatively for different flavors of Wilson quarks. A summary can be found in Table 2.2. In contrast the boundary improvement coefficient $\tilde{c}_{\mathrm{t}}$ is only known perturbatively to 1-loop [126]

$$\tilde{c}_{\mathrm{t}}(g_0) = 1 - 0.01795(2)g_0^2 + \mathcal{O}(g_0^4). \tag{5.49}$$

As discussed in [118], the choice of the fermion phase θ is made on the basis of practical considerations. It is observed that the additional gap to the mass in the spectrum of the Dirac operator, which is caused by the Schrödinger functional boundary conditions, can be extended additionally by varying θ. A maximum was obtained by $\theta \approx \pi/5$. In other words, the choice $\theta \approx \pi/5$ led to a significantly smaller condition number of the Dirac matrix. Hence we will adopt this choice for θ, too.

5.6 Coupling constant

The coupling constant can be defined in very different ways as discussed in [108, 122, 127, 128]. But it turns out that a definition of $\bar{g}^2(L)$ through the response of the system to a constant color-electrical background field fulfills the requirements discussed in the last section appropriately. The aforementioned effective action Γ is actually a function of the background field B

$$\Gamma[B] = -\ln Z[C', C]. \tag{5.50}$$

According to (5.37) and (5.33), B is again a function of the parameter η so that varying this parameter would change the background field and thus Γ

$$\Gamma'[B] = \frac{\partial \Gamma[B]}{\partial \eta}. \tag{5.51}$$

$\Gamma'[B]$ is suitable as a renormalized coupling and the Schrödinger functional coupling is indeed defined as follows[112]

$$\left.\frac{\partial\Gamma[B]}{\partial\eta}\right|_{\eta=0} = \frac{k}{\bar{g}^2}, \tag{5.52}$$

where k is the normalization constant. It is chosen in such a way that the perturbative expansion of $\Gamma'[B]$ begins with the bare coupling at tree level [112]

$$k = 12\left(\frac{L}{a}\right)^2[\sin(\vartheta)+\sin(2\vartheta)], \quad \vartheta = \frac{\pi}{3}\left(\frac{a}{L}\right)^2. \tag{5.53}$$

It should be noticed that the only external scale that appears in the definition of the coupling is the box size L. That means recursive finite size techniques can be used for the investigation of the evolution of the coupling with energy scale.

The key quantity $\Gamma'[B]$ in the definition of the coupling is an observable which can be calculated easily through Monte Carlo simulations. Taking the derivative of (5.50) results in

$$\Gamma'[B] = -\frac{\partial}{\partial\eta}\ln\left\{\int \mathscr{D}U\mathscr{D}\Psi\mathscr{D}\overline{\Psi}\exp\{-S[U,\Psi,\overline{\Psi}]\}\right\}, \tag{5.54}$$

$$= \frac{1}{Z}\int \mathscr{D}U\mathscr{D}\Psi\mathscr{D}\overline{\Psi}\left(\frac{\partial S_{\mathrm{G}}}{\partial\eta}+\frac{\partial S_{\mathrm{F}}}{\partial\eta}\right)\exp\{-S[U,\Psi,\overline{\Psi}]\} \tag{5.55}$$

$$= \left\langle\frac{\partial S_{\mathrm{G}}}{\partial\eta}\right\rangle + \left\langle\frac{\partial S_{\mathrm{F}}}{\partial\eta}\right\rangle. \tag{5.56}$$

Explicit expressions for both expectation values in (5.56) can be found in [106, 113]. The calculation of the renormalized coupling $\bar{g}^2$ involves expectation values of a local operator and no correlation functions. Therefore the numerical evaluation on a computer is straight forward once configurations are available.

The relation to the QCD coupling in Schrödinger functional scheme α_{SF} is given by

$$\alpha_{\mathrm{SF}}(\mu) = \frac{\bar{g}^2(L)}{4\pi}, \quad \mu = 1/L. \tag{5.57}$$

5.7 Quark mass

The renormalized quark mass can be defined in different ways. One way is to use the chiral symmetry to obtain an operator identity in which the quark mass is included. The *partially conserved axial current* (PCAC) relation in continuum, for example, (for detailed derivation see [129])

$$\langle\partial_\mu A^a_\mu(x)\mathscr{O}^a\rangle = 2m\langle P^a(x)\mathscr{O}^a\rangle \tag{5.58}$$

is such an operator identity. It provides a possibility to define the quark mass using the isovector axial current

$$A_\mu^a(x) = \overline{\Psi}(x)\gamma_\mu\gamma_5\frac{\tau^a}{2}\Psi(x) \tag{5.59}$$

and the associated pseudo-scalar density

$$P^a(x) = \overline{\Psi}(x)\gamma_5\frac{\tau^a}{2}\Psi(x). \tag{5.60}$$

τ^a $(a = 1, 2, 3)$ are Pauli matrices acting on one pair of degenerated flavors. In our case of $N_\mathrm{f} = 4$, the Pauli matrices act on each pair of flavors. It should be noted that the field $\mathscr{O}^a$ in (5.58) is located in a region that does not contain x. Otherwise, boundary terms would appear due to the integration by parts in the derivation of the PCAC relation[a]. For zero quark mass, the right-hand side of (5.58) vanishes and the remaining equation expresses the conservation of the axial current. As discussed in [130], it was found that the PCAC relation on the lattice has large $\mathcal{O}(a)$ effects. An improvement is achieved by using Symanzik's improvement program and applying on the operators $A_\mu^a(x)$ and $P^a(x)$ to remove the dominant lattice artifacts. It turns out that only the isovector axial current needs an improvement because there is no dimension four operator with the same behavior as $P^a(x)$ under the symmetries of the lattice theory. The $\mathcal{O}(a)$ improvement requires the combination

$$(A_\mathrm{I})_\mu^a(x) = A_\mu^a(x) + a \cdot c_\mathrm{A}\tilde{\partial}_\mu P^a(x), \quad \tilde{\partial}_\mu = \frac{1}{2}(\partial_\mu^* + \partial_\mu). \tag{5.61}$$

∂_μ^* and ∂_μ are the standard forward and backward difference operators on the lattice (equation (2.27) and (2.28) with $U = 1$) and c_A is the improvement coefficient of the axial current which is a function of the bare coupling. It has been determined non-perturbatively as well as in perturbation theory (see Table 5.2). Since c_A for $N_\mathrm{f} = 4$ is

Non-perturbative results	
$N_\mathrm{f} = 0$ [54]	$N_\mathrm{f} = 2$ [131, 132]
$c_\mathrm{A} = -0.00756 g_0^2 \times \frac{1-0.748 g_0^2}{1-0.977 g_0^2}$, $0 \le g_0^2 \le 1$	$c_\mathrm{A} = -0.00756 g_0^2 \times \frac{1-0.4485 g_0^2}{1-0.8098 g_0^2}$, $0.98 \le g_0^2 \le 1.16$
1-loop perturbative result [120] $c_\mathrm{A} = -0.00756(1) g_0^2$	

Table 5.2: Available results for the improvement coefficient c_A.

not available non-perturbatively, we will use the perturbative result in our simulations. The renormalization of the $\mathcal{O}(a)$ improved isospin current and the pseudo-scalar density

[a] The flavor index a at $\mathscr{O}^a$ and the the isovector axial current $A_\mu^a(x)$ should not be mixed with the lattice spacing a and the gluon field in (1.1), respectively.

can be expressed by [130]

$$(A_{\mathrm{R}})^a_\mu(x) = Z_{\mathrm{A}}(1 + b_{\mathrm{A}} a m_{\mathrm{q}})(A_{\mathrm{I}})^a_\mu(x) \tag{5.62}$$

$$(P_{\mathrm{R}})^a_\mu(x) = Z_{\mathrm{P}}(1 + b_{\mathrm{P}} a m_{\mathrm{q}}) P^a(x). \tag{5.63}$$

Since we are in a massless scheme ($m_{\mathrm{q}} = 0$), the expressions above simplifies to

$$(A_{\mathrm{R}})^a_\mu(x) = Z_{\mathrm{A}}(A_{\mathrm{I}})^a_\mu(x) \tag{5.64}$$

$$(P_{\mathrm{R}})^a_\mu(x) = Z_{\mathrm{P}} P^a(x). \tag{5.65}$$

The normalization factors Z_{A} and Z_{P} are functions of the bare coupling where the latter depends also on the scale. Now, a renormalized mass m_{R} on the lattice can be defined through the PCAC relation

$$\langle \tilde{\partial}_\mu (A_{\mathrm{R}})^a_\mu(x) \mathscr{O}^a \rangle = 2 m_{\mathrm{R}} \langle (P_{\mathrm{R}})^a_\mu(x) \mathscr{O}^a \rangle + \mathcal{O}(a^2) \tag{5.66}$$

with an $\mathcal{O}(a)$ improved renormalized field $\mathscr{O}^a$ (or a product of fields) at a non-vanishing distance from x. The leading order lattice effects in (5.66) is very dependent on the choice of the improvement coefficients c_{A} and c_{sw}. If both coefficients are chosen properly, the leading order lattice artifacts would be $\mathcal{O}(a^2)$ as denoted in (5.66). That, in turn, can be used to fix these coefficients non-perturbatively [57]. Moreover, an $\mathcal{O}(a)$ improved bare current quark mass can also be defined by

$$\langle \tilde{\partial}_\mu (A_{\mathrm{I}})^a_\mu(x) \mathscr{O}^a \rangle = 2 m \langle P^a_\mu(x) \mathscr{O}^a \rangle + \mathcal{O}(a^2) \tag{5.67}$$

The relation between the renormalized and unrenormalized mass is given by a ratio of the normalization factors Z_{A} and Z_{P}

$$m_{\mathrm{R}} = \frac{Z_{\mathrm{A}}}{Z_{\mathrm{P}}} m + \mathcal{O}(a^2). \tag{5.68}$$

As mentioned before, the quark and antiquark fields are inserted in the functional integral in (5.43) using the functional derivatives (5.45) and (5.46) in the definition of $\mathscr{O}^a$. The operator

$$\mathscr{O}^a = a^6 \sum_{\mathbf{y},\mathbf{z}} \bar{\zeta}(\mathbf{y}) \gamma_5 \frac{\tau^a}{2} \zeta(\mathbf{z}). \tag{5.69}$$

is one possible choice which creates a quark-antiquark pair at time slice $x_0 = 0$ and spatial coordinates $\mathbf{y}$ and $\mathbf{z}$, respectively, with vanishing spatial momentum. An analog expression could be written for a creation of a quark antiquark pair at $x_0 = T$

$$\mathscr{O}'^a = a^6 \sum_{\mathbf{y},\mathbf{z}} \bar{\zeta}'(\mathbf{y}) \gamma_5 \frac{\tau^a}{2} \zeta'(\mathbf{z}). \tag{5.70}$$

The PCAC relation suggests now to consider the following bare correlation functions

$$f_{\mathrm{A}}(x_0) = -\frac{a^3}{3L^3}\sum_{\mathbf{x}}\langle A_0^a(x)\mathscr{O}^a\rangle \quad f_{\mathrm{P}}(x_0) = -\frac{a^3}{3L^3}\sum_{\mathbf{x}}\langle P^a(x)\mathscr{O}^a\rangle \tag{5.71}$$

and

$$f'_{\mathrm{A}}(T-x_0) = \frac{a^3}{3L^3}\sum_{\mathbf{x}}\langle A_0^a(x)\mathscr{O}'^a\rangle \quad f'_{\mathrm{P}}(T-x_0) = \frac{a^3}{3L^3}\sum_{\mathbf{x}}\langle P^a(x)\mathscr{O}'^a\rangle\,. \tag{5.72}$$

Explicit expressions and detailed derivations of f_{X} and f'_{X} can be found in appendix B of [129]. So, the $\mathcal{O}(a)$ improved PCAC mass in terms of the correlation functions (5.71) and (5.72) is now defined as

$$m(x_0) = \frac{\tilde{\partial}_0 f_{\mathrm{A}}(x_0) + a\cdot c_{\mathrm{A}}\partial_0^*\partial_0 f_{\mathrm{P}}(x_0)}{2f_{\mathrm{P}}(x_0)}. \tag{5.73}$$

Numerical studies revealed that $m(x_0)$ suffers from lattice artifacts near the boundaries. But around $x_0 = T/2$, it forms a plateau. Hence, it seems to be a good choice to define the mass at $x_0 = T/2$

$$m_1 = \begin{cases} m(T/2) & \text{for } T/a \text{ even,} \\ 1/2[m([T-a]/2) + m([T+a]/2)] & \text{for } T/a \text{ odd.} \end{cases} \tag{5.74}$$

6 The ALPHA code and its extension

In this section, we will summarize the source lattice QCD code of the ALPHA collaboration (ALPHA code) with two degenerated flavors of $\mathcal{O}(a)$ improved Wilson quarks [76, 133, 134]. After this brief introduction, we want to discuss our idea to extend the two flavor code of the ALPHA collaboration to a code which can handle with arbitrary (even) numbers of $\mathcal{O}(a)$ improved Wilson quarks.

6.1 The GHMC code

The reference version (CVSv) of the so-called GHMC code (Generalized Hybrid Monte Carlo) on which this work is based is the repository version from 09/26/2007 (DESY Zeuthen). This code which we will refer as the ALPHA code was written in the special high-level programming language TAO suitable for APE (Array Processing Experiment) machines with SIMD (Single Instruction Multiple Data) architecture developed in a joined project of DESY (Germany), INFN (Italy) and University Paris-Sud (France). The first installation of this type of machine APE1 (peak performance of 1 GFlops) started producing physics at DESY Zeuthen in 1987. It was followed by APE100 (peak performance up to 100 GFlops) in 1994, APEmille (peak performance up to 550 GFlops) in 2000 and the last generation apeNEXT (peak performance up to 2.5 TFlops) in 2005 [135–137]. Since 05/2008, only apeNEXT is in operation but our simulations were performed on APEmille as well as on apeNEXT.

The original ALPHA code which was earlier used for $N_{\mathrm{f}} = 2$ studies was an implementation of the HMC algorithm [68] using the symmetric even-odd preconditioning [77, 78, 93] for the Dirac matrix $Q = \gamma_5 M$[a] (see section 4.3)

$$Q = \gamma_5 \begin{pmatrix} M_{ee} & M_{eo} \\ M_{oe} & M_{oo} \end{pmatrix}. \tag{6.1}$$

The determinant is then given by

$$\det\{Q\} = \det\{M_{ee}\} \det\{\hat{Q}_A\} = \det\{M_{ee}\} \det\{M_{oo}\} \det\{\hat{Q}_S\} \tag{6.2}$$

with

$$\hat{Q}_A = \gamma_5 (M_{oo} - M_{oe} M_{ee}^{-1} M_{eo}), \tag{6.3}$$

$$\hat{Q}_S = M_{oo}^{-1} \hat{Q}_A. \tag{6.4}$$

[a] normalization c_0 is set to one

As mentioned before, $\hat{Q}_A$ is hermitian but $\hat{Q}_S$ is not and hence

$$\hat{Q}_S^\dagger = M_{oo}\hat{Q}_S M_{oo}^{-1} \tag{6.5}$$

is valid. The pseudo-fermion representation of the original fermion determinant for two flavors $\phi^\dagger(QQ^\dagger)^{-1}\phi$ (see section 4.1) changes due to the preconditioning to

$$\phi^\dagger(QQ^\dagger)^{-1}\phi \to \phi^\dagger\hat{Q}_A^{-2}\phi - 2\ln\left(\det\{M_{ee}\}\right). \tag{6.6}$$

On the r.h.s., ϕ lives now only on the odd sides. In the ALPHA code, the first term on the r.h.s of (6.6) which denotes the determinant $\det\{\hat{Q}_A^2\}$ is again preconditioned with the Hasenbusch preconditioning [82, 83]. The following split for n pseudo-fermion fields is made

$$\begin{aligned}&\phi^\dagger\hat{Q}_A^{-2}\phi \to \\ &\qquad \phi_0^\dagger\left(\hat{Q}_A^2+\rho_0^2\right)^{-1}\phi_0 + \sum_{k=1}^{n-1}\phi_k^\dagger\left(\sigma_k^{-2}+\left[\hat{Q}_A^2+\rho_k^2\right]^{-1}\right)\phi_k\end{aligned} \tag{6.7}$$

where the real-valued parameters (σ_k, ρ_k) obey the relations

$$\sigma_k^2 = \rho_{k-1}^2 - \rho_k^2, \quad k = 1, \ldots, n-1, \tag{6.8}$$

$$\rho_{n-1}^2 = 0. \tag{6.9}$$

Using the properties (4.35), (4.36) and (4.37) of $\hat{Q}_S$ and $\hat{Q}_A$, the following relation can be derived

$$\hat{Q}_A^2 + \rho_0^2 = M_{oo}(\hat{Q}_S\hat{Q}_S^\dagger + \rho^2 M_{oo}^{-2})M_{oo}. \tag{6.10}$$

Now, the local clover determinants of the odd sites factor out

$$\det\{\hat{Q}_A^2+\rho_0^2\} = \det\{M_{oo}\}^2\det\{\hat{Q}_S\hat{Q}_S^\dagger + \rho^2 M_{oo}^{-2}\}. \tag{6.11}$$

So the action S is now composed of

$$S = S_{\mathrm{G}} + S_{\mathrm{pf}} + S_{\mathrm{det}} \tag{6.12}$$

with

$$S_{\mathrm{pf}} = \phi_0^\dagger\left(\hat{Q}_S\hat{Q}_S^\dagger + \rho_0^2 M_{oo}^{-2}\right)^{-1}\phi_0 + \sum_{k=1}^{n-1}\phi_k^\dagger\left(\sigma_k^{-2}+\left[\hat{Q}_A^2+\rho_k^2\right]^{-1}\right)\phi_k \tag{6.13}$$

$$S_{\mathrm{det}} = 2\cdot[\ln(\det\{M_{ee}\}) + \ln(\det\{M_{oo}\})]. \tag{6.14}$$

As required for symmetric even-odd preconditioning, both terms $\det\{M_{ee}\}$ and $\det\{M_{oo}\}$

are factored out in (6.14). Due to the decomposition

$$\hat{Q}_S\hat{Q}_S^\dagger + \rho_0^2 M_{oo}^{-2} = (\hat{Q}_S - i\rho M_{oo}^{-1})(\hat{Q}_S^\dagger + i\rho M_{oo}^{-1}), \tag{6.15}$$

the generation of the zeroth pseudo-fermion field ϕ_0 is performed by applying $\hat{Q}_S - i\rho M_{oo}^{-1}$ on a Gaussian random vector R

$$\phi_0 = (\hat{Q}_S - i\rho M_{oo}^{-1})R. \tag{6.16}$$

The factorization for the pseudo-fermion fields $\phi_{k\geq 1}$ in the split for the Hasenbusch preconditioning is slightly different

$$\frac{1}{\sigma^2} + \frac{1}{\hat{Q}_A^2 + \rho^2} = \frac{\hat{Q}_A^2 + \rho^2 + \sigma^2}{\sigma^2(\hat{Q}_A^2 + \rho^2)} \tag{6.17}$$

$$= \frac{\hat{Q}_A^2 + \mu^2}{\sigma^2(\hat{Q}_A^2 + \rho^2)}, \quad \mu^2 = \rho^2 + \sigma^2 \tag{6.18}$$

With (4.35), (4.36) and (4.37), the needed decomposition is obtained

$$\frac{1}{\sigma^2} + \frac{1}{\hat{Q}_A^2 + \rho^2} = \frac{1}{\sigma}\left[\hat{Q}_S - i\rho M_{oo}^{-1}\right]^{-1}\left[\hat{Q}_S - i\mu M_{oo}^{-1}\right] \times \left[\hat{Q}_S^\dagger + i\mu M_{oo}^{-1}\right]\left[\hat{Q}_S^\dagger + i\rho M_{oo}^{-1}\right]^{-1}\frac{1}{\sigma}. \tag{6.19}$$

The fields $\phi_{k\geq 1}$ are than generated according to

$$\phi_k = \sigma_k\left[\hat{Q}_S^\dagger + i\rho_k M_{oo}^{-1}\right]\left[\hat{Q}_S^\dagger + i\mu_k M_{oo}^{-1}\right]^{-1} R. \tag{6.20}$$

The implementation in the ALPHA code is made as follows. First

$$\psi = (\hat{Q}_S - i\mu_k M_{oo}^{-1})R \tag{6.21}$$

is built and the following equation is solved

$$(\hat{Q}_S - i\mu_k M_{oo}^{-1})(\hat{Q}_S^\dagger + i\mu_k M_{oo}^{-1})\phi_{\text{aux}} = \psi. \tag{6.22}$$

After obtaining ϕ_{aux}, the field ϕ_k is finally calculated by

$$\phi_k = \sigma_k(\hat{Q}_S^\dagger + i\rho_k M_{oo}^{-1})\phi_{\text{aux}}. \tag{6.23}$$

So, the generated pseudo-fermion fields are needed now for the calculation of the pseudo-fermion action (6.13). The first part of (6.13) is obtained by solving

$$(\hat{Q}_S - i\rho_0 M_{oo}^{-1})(\hat{Q}_S^\dagger + i\rho_0 M_{oo}^{-1})\xi_0 = \phi_0 \tag{6.24}$$

for ξ_0 where ϕ_0 is given by (6.16) and computing the scalar product $\phi_0^\dagger \xi_0$. For the remaining pseudo-fermion fields in the Hasenbusch preconditioning, the same strategy is applied. The gauge field dependent part $\phi_k^\dagger (\hat{Q}_A^2 + \rho_k^2)^{-1} \phi_k$ is calculated as the scalar product $\phi_k^\dagger \xi_k$ for given ϕ_k (equation (6.23)) where ξ_k is a solution of

$$(\hat{Q}_A^2 + \rho_k^2)\xi_k = \phi_k. \tag{6.25}$$

Actually, the implementation of the last line (6.25) is realized in three steps in the ALPHA code. In the decomposition

$$Q_A^2 + \rho_k^2 = \left[(\hat{Q}_S^\dagger + i\rho_k M_{oo}^{-1})M_{oo}\right]\left[M_{oo}(\hat{Q}_S - i\rho_k M_{oo}^{-1})\right] \tag{6.26}$$

the square brackets commute. This property is used to even-odd precondition the solver symmetrically (the second step below). The following steps are done:

1. $\tilde{\phi} = M_{oo}^{-1}\phi_k$
2. $(\hat{Q}_S - i\rho_0 M_{oo}^{-1})(\hat{Q}_S^\dagger + i\rho_0 M_{oo}^{-1})\tilde{\xi} = \tilde{\phi}$
3. $\xi_k = M_{oo}^{-1}\tilde{\xi}$

The understanding of the implementation of the pseudo-fermion action with the Hasenbusch preconditioning and the determinant action in the ALPHA code was crucial in our view for the extension of the code. Therefore we discussed it in detail.

The $\mathcal{O}(a)$ improvement term in the ALPHA code was included as discussed in [79]. A higher order leap frog integrator which was suggested by *Sexton and Weingarten* in [88] with a multiple time scale scheme was used for the integration of the equation of motion (for details see chapter 4).

6.2 Extension to arbitrary even numbers of flavors

A natural starting point for an extension of the ALPHA code is to consider the actions (6.13) and (6.14) and try to modify them in such a way that the inclusion of further pairs of flavors is easily possible. It should be kept in mind that we can only introduce pairs of flavors to guarantee the positivity of the Dirac matrix. For introducing odd numbers of flavors, we would need other algorithmic techniques as discussed in section 4.9. All our quarks will be mass-degenerated because we work in a massless scheme. In principle, it is also possible to give different pairs different masses using different values of the hopping parameter κ but for our purposes it is sufficient to have N_f (even) mass-degenerated flavors.

The pseudo-fermion representation of the fermion determinant for an even number of flavors can be written down in different ways. We want to discuss two possibilities. The first variant is to use only one pseudo-fermion field

$$\det\{QQ^\dagger\}^n = \int \mathscr{D}\phi^\dagger \mathscr{D}\phi \exp\left\{-\phi^\dagger (\{QQ^\dagger\}^n)^{-1}\phi\right\} \tag{6.27}$$

where $n = N_\mathrm{f}/2 = 1, 2, 3, \ldots$ and a second variant is to use multiple pseudo-fermion fields

$$\det\{QQ^\dagger\}^n = \prod_{i=1}^{n} \det\{QQ^\dagger\} = \int \mathscr{D}\phi^\dagger \mathscr{D}\phi \exp\left\{-\sum_{i=1}^{n} \phi_i^\dagger (QQ^\dagger)^{-1} \phi_i\right\}. \tag{6.28}$$

In principle, both descriptions are equivalent but a look on the fermion forces reveals that the second choice should be preferred in numerical simulations. In the first case, the fermion force is proportional to

$$F_\mathrm{f} \propto \phi^\dagger \delta\{(QQ^\dagger)^{-n}\}\phi = -\phi^\dagger \left[(QQ^\dagger)^{-n} \delta\{(QQ^\dagger)^n\}(QQ^\dagger)^{-n}\right] \phi, \tag{6.29}$$

where we used the following identity for the variation of the inverse of a matrix

$$\delta\{A^{-1}\} = -A^{-1}\delta\{A\}A^{-1}. \tag{6.30}$$

This formal-written expression for the force involves the inverse of $(QQ^\dagger)$ to the power n which corresponds to a condition number $[\mathrm{cond}(QQ^\dagger)]^n$ while for the second description the force is proportional to

$$F_\mathrm{f} \propto -\sum_{i=1}^{n} \phi_i^\dagger \left[(QQ^\dagger)^{-1} \delta\{(QQ^\dagger)\}(QQ^\dagger)^{-1}\right] \phi_i. \tag{6.31}$$

Only the inversion of $(QQ^\dagger)$ to the power one appears. The corresponding condition number $\mathrm{cond}(QQ^\dagger)$ is much smaller than in the first case. This simple consideration shows that the second variant should be preferred in numerical simulations what we also did. For the realization of this idea, we unplugged first the Hasenbusch preconditioning from the ALPHA code. In other words, we excluded the sum in (6.13) and set ρ_0 to zero in the remaining action so that S_pf consisted of

$$S_\mathrm{pf} = \phi^\dagger \left(\hat{Q}_S \hat{Q}_S^\dagger\right)^{-1} \phi. \tag{6.32}$$

Then, we introduced a new parameter N_f in our simulation and rewrote the pseudo-fermion action in the following way

$$S_\mathrm{pf} = \sum_{i=1}^{N_\mathrm{f}/2} \phi_i^\dagger \left(\hat{Q}_S \hat{Q}_S^\dagger\right)^{-1} \phi_i. \tag{6.33}$$

Each summand represents a two flavor pseudo-fermion action. By choosing the parameter N_f appropriately, we could control the number of flavors in our code. One advantage of such an implementation is that we do not need to compile the code again when we change the parameter N_f. It is just a parameter which is passed through to the simulation at the beginning.

Of course, the determinant contribution (6.14) had to be modified, too. The action in (6.14) denotes the determinant action for two flavors. Hence we introduced there a

factor of $N_\mathrm{f}/2$. Both parts of the action have now the form

$$S_\mathrm{pf} = \sum_{i=1}^{N_\mathrm{f}/2} \phi_i^\dagger \left(\hat{Q}_S \hat{Q}_S^\dagger\right)^{-1} \phi_i, \tag{6.34}$$

$$S_\mathrm{det} = \frac{N_\mathrm{f}}{2} \left\{2 \cdot [\ln(\det\{M_{ee}\}) + \ln(\det\{M_{oo}\})]\right\}. \tag{6.35}$$

By this changes, our code is able to simulate arbitrary even numbers of flavors.

7 Results

In this chapter, we want to present our results for the improvement coefficient $c_{\rm sw}$, the step scaling function and the running coupling of QCD. In the first section we will discuss briefly how we determined $c_{\rm sw}$ which is essential for $\mathcal{O}(a)$ improvement of Wilson quarks and quote a formula for $c_{\rm sw}$ with four flavors [138]. Then we will give a rough estimate for critical κ which will be obtained as a by-product of the $c_{\rm sw}$ data. In the remainder of this chapter, we will discuss how we extracted the step scaling function from the raw data and quote a value for the quantity $\ln(\Lambda L_{\rm max})$. Finally we will give the result for running coupling of QCD in Schrödinger functional scheme.

7.1 Determination of $c_{\rm sw}$

7.1.1 Introduction

The lattice regularization of QCD is a powerful tool to non-perturbatively study QCD in the low energy region. The numerical implementation involves however a finite lattice spacing a which has to be removed in the continuum limit. The rate of approaching the continuum limit will depend on the details of the lattice formulation. A systematic way to reduce the discretization effects order by order in a is the Symanzik improvement program (section 2.6) for on-shell quantities [38, 139]. In the case of Wilson fermions, Sheikoleslami and Wohlert [51] have shown that for reducing the lattice artifacts from $\mathcal{O}(a)$ to $\mathcal{O}(a^2)$ only one additional dimension five operator in the Lagrangian is needed. To achieve this acceleration of the continuum limit non-perturbatively the coefficient $c_{\rm sw}$ of the corresponding operator has to be determined in numerical simulations. In the quenched case [54], the ALPHA collaboration has found [122–124] that the non-perturbative result for $c_{\rm sw}$ deviates significantly from the one-loop perturbative value [51, 52]. Furthermore, the effect of two species of dynamical fermions on $c_{\rm sw}$ was also studied by the ALPHA collaboration and the difference to the quenched case was clearly visible [55]. The effect of a third flavor was studied by the CP-PACS and JLQCD collaborations [56] with the result that $c_{\rm sw}(g_0^2)$ is not very much affected by it and their result is very close to the two flavor values of the ALPHA collaboration which can be seen in Figure 7.4. Our aim is to calculate $c_{\rm sw}$ non-perturbatively for four flavors in the Schrödinger functional scheme.

7.1.2 Improvement condition

Our starting point for $\mathcal{O}(a)$ improved lattice QCD is the fermion action

$$S_{\mathrm{F}} = a^4 \sum_x \overline{\psi}(x) \left[D + m_0\right] \psi(x), \tag{7.1}$$

where a is the lattice spacing and m_0 is the bare quark mass. The matrix D is the Wilson-Dirac operator [21]

$$D = \frac{1}{2}\left[\left(\nabla_\mu^b + \nabla_\mu^f\right)\gamma_\mu - a\nabla_\mu^b\nabla_\mu^f\right] \tag{7.2}$$

with the lattice covariant forward and backward derivatives ∇_μ^f (2.27) and ∇_μ^b (2.28). The leading order lattice artifacts in on-shell quantities which are calculated with this action are linear in a. However, the leading order discretization effects may be canceled by adding the so-called Sheikoleslami Wohlert term to the action [51]

$$D_{\mathrm{improved}} = D + c_{\mathrm{sw}}\frac{ia}{4}\sigma_{\mu\nu}\mathcal{F}_{\mu\nu}. \tag{7.3}$$

The lattice field strength tensor $\mathcal{F}_{\mu\nu}$ is defined as in (2.48) and $\sigma_{\mu\nu} = \frac{i}{2}[\gamma_\mu, \gamma_\nu]$. The coefficient c_{sw} in (7.3) is a function of the bare coupling g_0 and if it is chosen properly, D_{improved} becomes the on-shell $\mathcal{O}(a)$ improved lattice Wilson-Dirac operator. For a complete cancellation of the $\mathcal{O}(a)$ effects[a] in correlation functions, the local composite fields that enter also have to be improved [130]. In our case, such composite fields are the isovector axial current $A_\mu^a(x)$ and the pseudo-scalar density $P^a(x)$. As already discussed in section 5.7, only the isovector axial current needs an improvement. The $\mathcal{O}(a)$ improvement requires the combination

$$(A_{\mathrm{I}})_\mu^a = A_\mu^a + a \cdot c_{\mathrm{A}}\frac{1}{2}(\partial_\mu^* + \partial_\mu)P^a \tag{7.4}$$

where A_μ^a and P^a are given by (5.59) and (5.60), ∂_μ, ∂_μ^* are the forward and backward difference operators and τ^a are Pauli matrices acting on one pair among the four degenerate flavors. The improvement coefficient c_{A} is known in perturbation theory [120] and from non-perturbative determinations for $N_{\mathrm{f}} = 0$ [54] and $N_{\mathrm{f}} = 2$ [131, 132] (see Table 5.2). As explained in section 5.7, we introduce the unrenormalized PCAC quark mass

$$m(x_0) = \frac{\frac{1}{2}(\partial_0^* + \partial_0)f_{\mathrm{A}}(x_0) + c_{\mathrm{A}}a\partial_0^*\partial_0 f_{\mathrm{P}}(x_0)}{2f_{\mathrm{P}}(x_0)} \tag{7.5}$$

where the correlation functions f_{A} and f_{P} contain A_μ^a and P^a and are given by (5.71). A second mass m' can be defined in the same way as (7.5) but with the primed correlation functions f'_{A} and f'_{P} eq. (5.72). The unprimed and primed correlation functions are

[a] This refers to the massless theory which we consider in connection with the Schrödinger functional renormalization scheme.

related to each other by a time reflection in the Schrödinger functional. Since the boundary conditions

$$U(x,k)|_{x_0=0} = \exp\{aC_k\}; \quad C_k = \frac{i}{6L}\mathrm{diag}(-\pi, 0, \pi) \tag{7.6}$$

$$U(x,k)|_{x_0=T} = \exp\{aC'_k\}; \quad C'_k = \frac{i}{6L}\mathrm{diag}(-5\pi, 2\pi, 3\pi) \tag{7.7}$$

are such that C_k and C'_k are not the same, f_{X} and f'_{X} also differ. Since with PCAC we have, however, inserted an 'operator identity', all $m(x_0), m'(y_0)$ differ only at the level of $\mathcal{O}(a^2)$ effects in the improved theory. We could hence for some choice, such as $x_0 = y_0 = \frac{T}{2}$, impose $m - m' = 0$ as one condition for the proper choice of c_{sw} and c_{A}. Because the coefficient c_{A} is a priori not known it is advantageous however to first eliminate this parameter and define a quark mass M independent of c_{A} which agrees with the quark mass m up to $\mathcal{O}(a^2)$ effects. For this purpose we name the partial contributions

$$r(x_0) = \frac{(\partial_0^* + \partial_0) f_{\mathrm{A}}(x_0)}{4 f_{\mathrm{P}}(x_0)} \tag{7.8}$$

$$s(x_0) = \frac{a\partial_0^*\partial_0 f_{\mathrm{P}}(x_0)}{2 f_{\mathrm{P}}(x_0)} \tag{7.9}$$

and rewrite the mass m as

$$m(x_0) = r(x_0) + c_{\mathrm{A}} s(x_0). \tag{7.10}$$

With an analogous definition for m', a quark mass M can than be written in the following way

$$M(x_0, y_0) = m(x_0) - s(x_0)\frac{m(y_0) - m'(y_0)}{s(y_0) - s'(y_0)} \tag{7.11}$$

$$= r(x_0) - s(x_0)\frac{r(y_0) - r'(y_0)}{s(y_0) - s'(y_0)}. \tag{7.12}$$

In this combination, which in the improved theory differs from m by $\mathcal{O}(a^2)$ only, c_{A} drops out. Now, we define $M'(x_0, y_0)$ analogously and could require that the difference

$$\Delta M\left(\frac{3}{4}T, \frac{1}{4}T\right) = M\left(\frac{3}{4}T, \frac{1}{4}T\right) - M'\left(\frac{3}{4}T, \frac{1}{4}T\right) \tag{7.13}$$

has to vanishes for our value of c_{sw}. The choice $(x_0, y_0) = (\frac{3}{4}T, \frac{1}{4}T)$ is one possible choice [54] for the argument of ΔM. For the quark mass M itself we choose $(x_0, y_0) = (\frac{1}{2}T, \frac{1}{4}T)$ [54]. In order to reproduce the tree level value of c_{sw} exactly for finite a, we finally impose the improvement condition

$$\Delta M = \Delta M^{(0)} \tag{7.14}$$

where $\Delta M^{(0)}$ is the tree level value of perturbation theory in the $\mathcal{O}(a)$ improved theory. For $L/a = 8$ one finds for example [54]

$$a\Delta M^{(0)}|_{M=0,c_{\rm sw}=1} = 0.000277. \tag{7.15}$$

As discussed in [106], improvement coefficients possess a unique perturbative expansion but non-perturbatively they are themselves ambiguous by cutoff terms and thus depend on the choice of the improvement conditions. Of course, for QCD these uncertainties amount to cutoff effects beyond the order that is improved, $\mathcal{O}(a^2)$ in the case at hand. In principle, one then has to determine improvement coefficients for one fixed set of conditions as functions of g_0 at constant physics, i. e. fixing all scale ratios except a that shrinks with g_0. For the Schrödinger functional this would in particular require constant L/r_0 as g_0 is lowered. For practical reasons we fix however L/a instead and refer the reader to sect. (I.2.4.1) of [106] for a detailed discussion. The replacement of zero by the small tree-level value on the right hand side of (7.15) guarantees that our definition has the correct limit for $g_0 \to 0$.

7.1.3 Simulations

As described in the last chapter, our simulations for $N_{\rm f} = 4$ are based on an adaptation of TAO codes — suitable for APE computers [135] — used earlier by the ALPHA collaboration for $N_{\rm f} = 2$ studies. To summarize it again, the code consist of an ordinary HMC algorithm [68] implemented with symmetric even-odd preconditioning [77, 78, 93] and the Sexton-Weingarten integration scheme [88]. Mass preconditioning [81, 82] was not enforced as we expect that the gain for the Schrödinger functional with the parameters envisaged here would not be so significant [140].

7.1.4 Simulation parameters and raw results

The simulations were performed in the Schrödinger functional scheme [122–124] with periodic boundary conditions for the spatial extension and Dirichlet boundary conditions in the temporal direction. This means the phase θ was here set to zero in all runs. The data were obtained on hypercubic Euclidean 16×8^3 lattices. The $\mathcal{O}(a)$ improvement of the Schrödinger functional requires additional improvement terms at the boundaries. However, since PCAC is an operator relation, these terms are irrelevant for a correct determination of $c_{\rm sw}$. Nevertheless, we have chosen them as follows. The pure gauge part of the action acquires a weight $w(p) = c_{\rm t}(g_0)$ of time-like plaquettes p attached to the boundary planes for which we have inserted the 2-loop value [109]

$$c_{\rm t}(g_0) = 1 + [-0.08900 + 0.0191410N_{\rm f}]g_0^2 + [-0.0294 + 0.002N_{\rm f} + 0N_{\rm f}^2]g_0^4\,, \tag{7.16}$$

and for the fermionic improvement coefficient $\tilde{c}_{\rm t}(g_0)$ [120] we took the 1-loop perturbative value [126]

$$\tilde{c}_{\rm t}(g_0) = 1 - 0.01795g_0^2\,. \tag{7.17}$$

In all our simulations the trajectory length was kept fixed to one. We chose the intervals in β similar to [55]. The mean acceptance rate was around 90% and we performed 4400 trajectories per value of β and $c_{\rm sw}$ on average. A large part of our computations ran on APEmille machines with 128 processors each. For some values of β and $c_{\rm sw}$ we also used apeNEXT crates with 256 processors. The summary Table of the measurements can be found in appendix B.

7.1.5 Numerical procedure for determining $c_{\rm sw}$

The numerical procedure for the determination of $c_{\rm sw}$ involves the following main steps

1. Compute ΔM and M for several κ at fixed g_0^2 (or β) and $c_{\rm sw}$. Then interpolate linearly in M to find ΔM at vanishing quark mass $M = 0$.

2. For fixed g_0^2, repeat step 1 for several values of $c_{\rm sw}$ and find $c_{\rm sw}^*$ which solves (7.14) by a linear fit in $c_{\rm sw}$.

3. Repeat the preceding steps for a sufficient range of g_0^2 and fit these data with an appropriate function to represent the smooth functional dependence of $c_{\rm sw}$ on g_0^2.

This procedure is computer time demanding because for each value of β and for each value of $c_{\rm sw}$, we would need several runs, at least three, for interpolating ΔM in M to $M = 0$. To save computer time, we modified this method slightly. As discussed in the determination of $c_{\rm sw}$ for $N_{\rm f} = 0, 2$ [54, 55], the weak dependence of ΔM on M holds also at $N_{\rm f} = 4$. For one set of parameters β and $c_{\rm sw}$, we checked the dependence explicitly (Figure 7.1). Since ΔM depends weakly on M, we contented ourselves with determining

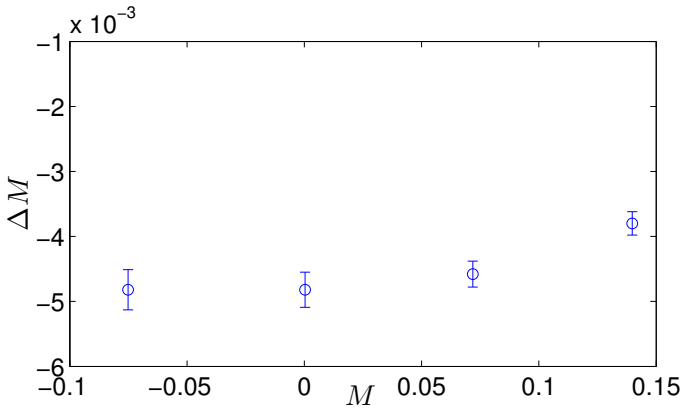

Figure 7.1: Mass dependence of ΔM at $\beta = 5.0$ and $c_{\rm sw} = 2.4$. The errors of M are smaller than the symbol sizes.

ΔM for some $|M| < 0.03$ [55] and used these values of ΔM as an approximation for ΔM at $M = 0$. A typical result is shown in Figure 7.2. We performed simulations from $\beta = 12$ to $\beta = 5.0$. For each β, we calculated the observables ΔM and M at least

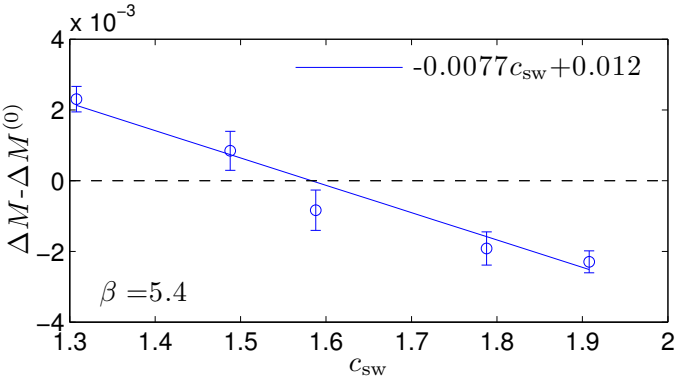

Figure 7.2: Determination of $c_{\rm sw}$ at $\beta = 5.4$. The desired value $c^*_{\rm sw}$ is located at the point where the fit curve (solid) passes through zero (dashed). A complete set of plots for all β can be found in appendix C.

for three different values of $c_{\rm sw}$ in such a way that the condition $|M| < 0.03$ held and that ΔM had a change of sign. The linear interpolation $\Delta M = s\ (c_{\rm sw} - c^*_{\rm sw}) + \Delta M^{(0)}$ yields the desired values $c^*_{\rm sw}$ shown in Table 7.1. We also tried to go below $\beta = 5.0$ but

β	$c^*_{\rm sw}$	β	$c^*_{\rm sw}$
12	1.1429(39)	6.0	1.463(19)
9.6	1.1895(62)	5.7	1.554(17)
7.4	1.2955(76)	5.4	1.583(25)
6.8	1.3375(94)	5.2	1.614(28)
6.3	1.389(12)	5.0	1.717(31)

Table 7.1: Results of the linear interpolation

at $\beta = 4.8$, we were not able to locate a significant sign change of ΔM in our data and therefore after some attempts, we decided to stop searching. The CP-PACS and JLQCD collaborations computed $c_{\rm sw}$ for $N_{\rm f} = 3$ in the Schrödinger functional setup of lattice QCD with the plaquette gauge action [56]. They found that the result for three flavors is very close to the two flavor result [55]. In addition, they calculated $c_{\rm sw}$ with four flavors for $\beta = 9.6$ and found $c^*_{\rm sw} = 1.1954(48)$ in good agreement with our $c^*_{\rm sw} = 1.1895(62)$.

After obtaining the proper values $c^*_{\rm sw}$ which satisfy the improvement condition (7.14), we want to represent and interpolate our data by a simple Padé formula, appropriate for the achieved precision, which also incorporates the known 1-loop perturbative result. The solution that we want to advocate here for $N_{\rm f} = 4$ is

$$c_{\rm sw}(g_0^2) = \frac{1 - 0.1372 g_0^2 - 0.1641 g_0^4 + 0.1679 g_0^6}{1 - 0.4031 g_0^2} \quad 0 \le g_0^2 \le 1.2. \tag{7.18}$$

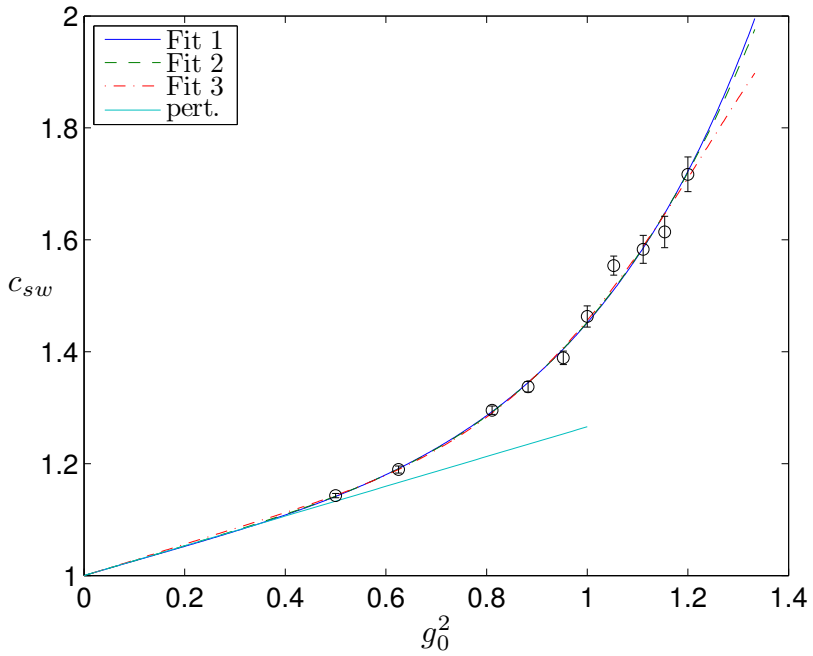

Figure 7.3: Comparison of different Padé-approximation formulae for our data.

This curve appears as `Fit1` in Figure 7.3. The two other lines `Fit2` and `Fit3` include one and two more powers in the numerator. The deviation of the different fit formulae in the range $g_0^2 \in [0, 1.2]$ ($\beta = [12.0, 5.0]$) is negligible and beyond $g_0^2 = 1.2$, `Fit1` and `Fit2` are almost the same down to $\beta = 4.5$ but `Fit3` deviates slightly. Our non-perturbatively determined formula (7.18) for $c_{\rm sw}$ with four flavors is valid down to $\beta = 5.0$ ($g_0^2 = 1.2$) but may perhaps be used to $\beta = 4.5$ within a small uncertainty. To conclude in Figure 7.4, we juxtapose our new data and fit formula at $N_{\rm f} = 4$ to those known for $N_{\rm f} = 0, 2, 3$.

7.2 An estimation of κ_c

As we already discussed in section 5.4, the PCAC mass has to be tuned to zero in the determination of the step scaling function. The position of the critical line where the current quark mass vanishes is a priori not known and κ has to be tuned explicitly to κ_c (critical κ). However considering the raw data for the determination of $c_{\rm sw}$, a rough estimate of κ_c can be given. In Table 7.2, we can see that the numerical values of M are rather small. Due to this, we will use the 1-loop formula to determine κ_c [55, 126]

$$M = Z_m m_q (1 + b \cdot m_q) \tag{7.19}$$

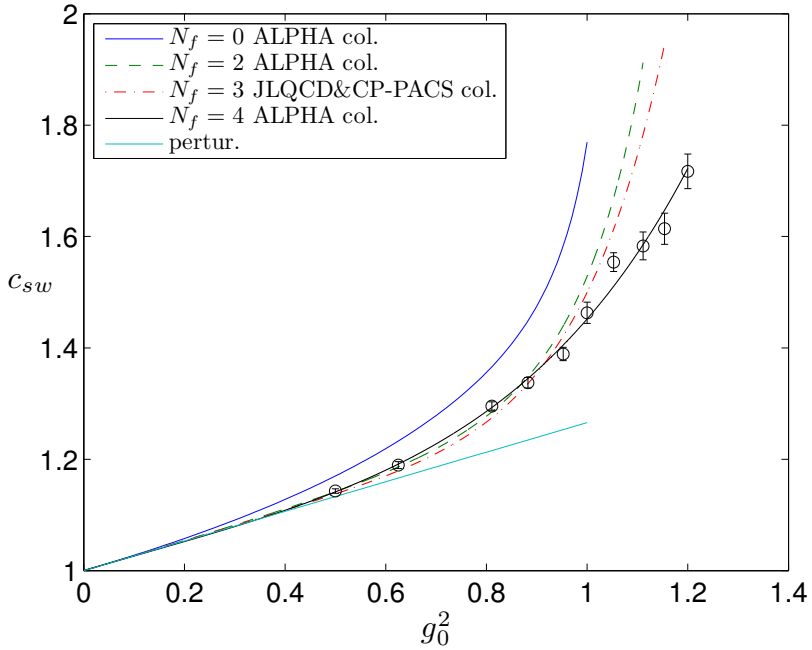

Figure 7.4: Summary plot of all known $c_{\mathrm{sw}}(g_0^2, N_{\mathrm{f}})$ for the plaquette gauge action.

where

$$m_q = \frac{1}{2\kappa} - \frac{1}{2\kappa_c} \tag{7.20}$$

$$Z_m = 1 + 0.0905 \cdot g_0^2 \tag{7.21}$$

$$b = -1/2 - 0.0962 \cdot g_0^2. \tag{7.22}$$

Equation (7.19) connects M with κ_c. Hence the statistical uncertainties of M can be transformed into uncertainties of κ_c. Since the values for M in Table 7.2 are rather small, we neglect the quadratic term m_q^2 in (7.19) and obtain the following expression for κ_c

$$\kappa_c = \frac{\kappa}{1 - 2\kappa \cdot \frac{M}{Z_m}}. \tag{7.23}$$

Now, we have to calculate κ_c for every value of M in Table 7.2 and fit the obtained values of κ_c for each β linearly with (7.24) to find the desired value κ_c^*

$$\kappa_c = \kappa_c^* + k(c_{\mathrm{sw}} - c_{\mathrm{sw}}^{\mathrm{impr}}). \tag{7.24}$$

$c_{\mathrm{sw}}^{\mathrm{impr}}$ in (7.24) is given by (7.18). The result of our analysis and the known formula for 1-loop [52, 120] perturbation theory, $N_{\mathrm{f}} = 2$ [55] and $N_{\mathrm{f}} = 3$ [56] are depicted in Figure

β	κ	M	β	κ	M
12	0.130280	0.000224(75)	5.7	0.140327	-0.0082(16)
12	0.129897	-0.001510(74)	5.7	0.138229	0.00034(63)
12	0.129449	-0.001371(82)	5.7	0.137008	0.00081(55)
9.6	0.131516	-0.00004(11)	5.7	0.135685	0.00564(63)
9.6	0.131164	0.00595(11)	5.7	0.133940	-0.00004(38)
9.6	0.131164	-0.00853(11)	5.4	0.141417	-0.00032(77)
7.4	0.134626	-0.00196(20)	5.4	0.139111	-0.00712(89)
7.4	0.133753	0.00072(20)	5.4	0.137815	-0.00762(70)
7.4	0.132989	0.00018(20)	5.4	0.135028	-0.00117(69)
7.4	0.132349	0.00027(20)	5.4	0.133775	-0.00854(39)
6.8	0.135638	0.00128(30)	5.2	0.143363	-0.0004(14)
6.8	0.135082	-0.00642(32)	5.2	0.140628	-0.00032(87)
6.8	0.134896	-0.00333(29)	5.2	0.139206	-0.00326(69)
6.8	0.133813	0.00320(29)	5.2	0.138147	0.00162(94)
6.8	0.133056	-0.00141(30)	5.2	0.136248	0.00030(91)
6.3	0.137098	-0.00129(38)	5.2	0.134556	0.00372(62)
6.3	0.136018	0.00142(36)	5.0	0.146056	0.0051(25)
6.3	0.135028	0.00140(36)	5.0	0.142554	0.0021(13)
6.3	0.134028	-0.00251(31)	5.0	0.138141	-0.0053(11)
6.0	0.138358	-0.00090(85)	5.0	0.136527	0.0009(11)
6.0	0.136669	0.00214(47)	5.0	0.135039	-0.00826(90)
6.0	0.134375	0.00677(43)	5.0	0.129603	0.00033(42)

Table 7.2: An extract of the table with the data for c_{sw}. The full table can be found in the appendix B.

7.5. Our interpolation formula can be summarized in

$$\kappa_c = 1/8 + \kappa_c^{(1)} g_0^2 + 0.000129 g_0^4 + 0.007470 g_0^6 - 0.007716 g_0^8 + 0.002748 g_0^{10} \qquad (7.25)$$

for $0 \leq g_0^2 \leq 1.2$. Here, $\kappa_c^{(1)}$ is the 1-loop value $\kappa_c^{(1)} = 0.008439857$ [120]. To conclude, all three non-perturbative lines of κ_c are very close to each other but we can see a small dependence on the number of flavors. In the considered range in Figure 7.5, the critical line is close to the 1-loop result. To emphasize, equation (7.24) is a rough estimate of the critical line and should only be used as a first guess for κ_c where the current quark mass vanishes.

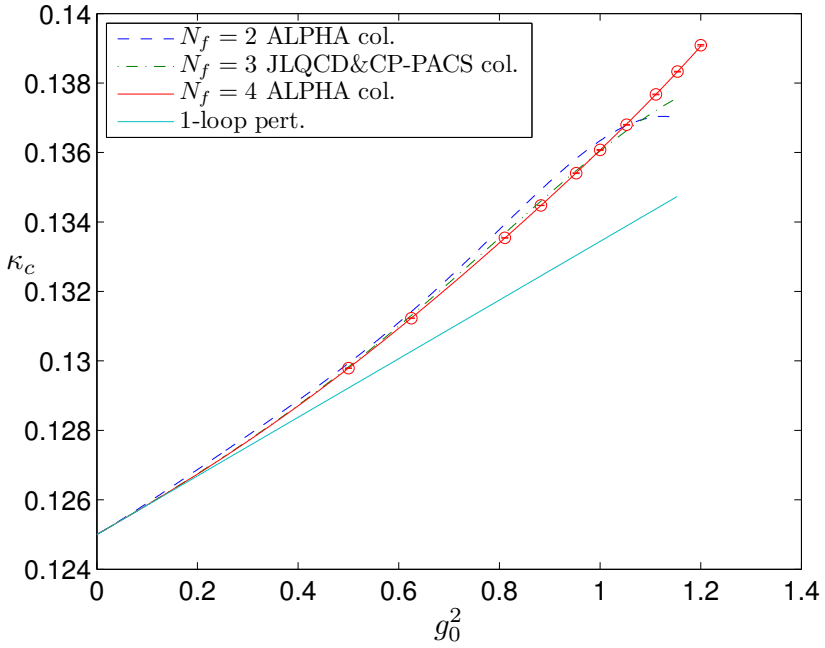

Figure 7.5: Estimations for κ_c: $N_\mathrm{f} = 2$ [55], $N_\mathrm{f} = 3$ [56], $N_\mathrm{f} = 4$ eq. (7.25) and 1-loop (lowest line) [52, 120] perturbation theory.

7.3 Determination of the step scaling function and the running coupling of QCD

7.3.1 Introduction

As we discussed in detail (chapter 1), QCD is believed to describe the strong interaction between quarks and gluons. The theory has six free mass parameters for the six quarks and one coupling parameter for the strength of interaction. As a peculiarity, all parameters of QCD run with the energy scale. This fact is expressed in the Callan-Symanzik β- and τ-functions (section 5.3). For example, in the *Review of Particle Physics* [6], the quark masses and the coupling are quoted at a particular scale in $\overline{\mathrm{MS}}$ scheme. In the following, we want to concentrate on the non-perturbative calculation of the coupling and refer to [114, 141] for the non-perturbative determination of the quark masses.

In the context of non-perturbative determination of the coupling, the step scaling function (section 5.4) plays a key role. When the step scaling function $\sigma(u)$ is known non-perturbatively, the running of the coupling can be computed easily. For this purpose, one solves the equation

$$u_i = \sigma(u_{i+1}), \quad i = 0, \ldots, n, \quad u_0 = u_\mathrm{max} = \bar{g}^2\left(L_\mathrm{max}\right), \tag{7.26}$$

where u_max is chosen such that the corresponding scale L_max is in the hadronic regime

of QCD, for some steps (in our case $n = 10$) recursively. Proceeding in this way the coupling can be obtained over a wide range of the energies. At a sufficiently large energy $\mu = 2^k/L_{\max}$ ($k \lesssim n$), the perturbation theory can be applied for determining the quantity $\Lambda L_{\max}$ using (5.13) with the β function truncated at 2-loop and 3-loop respectively. The physical value of $L_{\max}$ has not been determined yet. Therefore, we will show our result of running coupling as a function of μ/Λ.

The step scaling function [113, 142–145] and the running coupling [113, 146–148] have been examined for different numbers of flavors. In our calculation, we want to determine the step scaling function and the running coupling with four flavors of $\mathcal{O}(a)$ improved Wilson quarks in Schrödinger functional scheme and compare to the corresponding perturbative predictions.

7.3.2 Numerical computation and results

Simulation parameters and raw data

The simulations were performed in the Schrödinger functional scheme. The choice of the improvement coefficients $c_{\rm t}$, $\tilde{c}_{\rm t}$ were as in section 5.5. For the improvement coefficient $c_{\rm sw}$, we used our formula (7.18). As pointed out in [118], the choice of the fermion phase θ is made on the basis of practical considerations. It is observed that the additional gap to the mass in the spectrum of the Dirac operator which is caused by the Schrödinger functional boundary conditions can be extended additionally by varying θ. A maximum was obtained by $\theta \approx \pi/5$. In other words, the choice $\theta \approx \pi/5$ led to a significantly smaller condition number of the Dirac matrix. This result was also confirmed by [113] in the case of $N_{\rm f} = 2$ $\mathcal{O}(a)$ improved Wilson quarks. Hence we adopted this choice of θ, too. The matrices C_k and C'_k in (5.33) were chosen according to the boundary point 'A' of [112] and ν was set to zero [112]. The range of β for our simulations was limited by the validity range of $c_{\rm sw}$ with four flavors ($\beta \leq 5.0$) (7.18). Since our code allowed only an even number of lattice points in each direction and lattices beyond $L/a = 16$ are too time-consuming for our present resources, we chose lattices ($T = L$) $L/a = 4, 6, 8$. We picked a sufficient number of values of $\beta = 5.0, \ldots, 9.5$ to map out a range $\bar{g}^2(L) = 0.9, \ldots, 3.7$, $\bar{g}^2(2L) = 1.0, \ldots, 3.5$ adequately. We performed our simulations on 4-5 crates of the apeNEXT machine in DESY Zeuthen over a period of about a year. The raw data can be found in the appendix D. We used the 1-loop result for the improvement coefficient $c_{\rm A}$ (Table 5.2) in (5.73) and (5.74). As a first guess for the value of critical κ, we used (7.25) and with some tuning we could keep the quark mass small enough ($|m_1 L| \leq 0.005$) such that mass-effects in the step scaling function are negligible.

Analysis of data and results

The computation of the step scaling function on the lattice as described in section 5.4 requires $\bar{g}^2(L)$ to be fixed to certain values u while the resolution a/L is changed. Previously this was realized by tuning β for each pair $u, L/a$ [112, 113, 149]. Instead we here followed the more convenient proposal of [145] to pick a sufficient range and number of bare couplings for each considered L/a and interpolate the running coupling

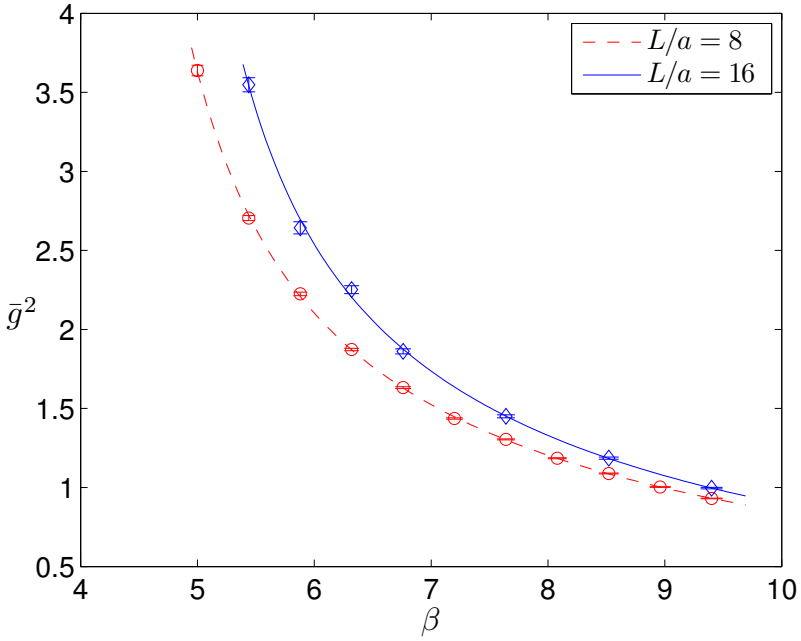

Figure 7.6: Data points for $L/a = 8$ and $L/a = 16$ and their interpolations. The parameter n in (7.28) is set to three. The hopping parameter κ was tuned only on the small lattices $L/a = 4, 6, 8$ such that the PCAC mass (5.74) vanished. The complete set of plots for all L/a and the associated tables of fit parameters can be found in appendix E.

$\bar{g}^2(\beta, L/a)$ with a smooth function of β. Afterward the function allows access to any value of $\bar{g}^2$ in the covered range. The authors of [145] argued that in perturbation theory the quantity $1/\bar{g}^2(\beta, L/a)$ takes the following form

$$\frac{1}{\bar{g}^2(\beta, L/a)} = \frac{1}{g_0^2}\left[1 + \mathcal{O}(g_0^2)\right] = \frac{\beta}{6}\left[1 + \mathcal{O}\left(1/\beta\right)\right] \tag{7.27}$$

and an approach motivated by this can be made[b]

$$\frac{1}{\bar{g}^2(\beta, L/a)} = \frac{\beta}{6}\left[1 + \sum_{m=0}^{n} c_{m,L/a}\left(\frac{6}{\beta}\right)^m\right]. \tag{7.28}$$

But they emphasize that this approach is based on empirical observation and does not mean that perturbation theory is valid in the non-perturbative regime. They reported also that different functional forms for modeling their data did not change the fit quality

[b]Note: Here, we write down explicitly the factor 1 in (7.28) on the r.h.s and do not absorb it into the coefficient $c_{0,L/a}$ in contrast to our notation in [150]. The values for the coefficients $c_{m,L/a}$ can be found in appendix E.

L/a	u	$\Sigma(u, a/L)$	$\Sigma^{(2)}(u, a/L)$	u	$\Sigma(u, a/L)$	$\Sigma^{(2)}(u, a/L)$
4	0.9300	0.9953(16)	0.9986(16)	1.4435	1.6084(34)	1.6079(34)
6		1.0004(29)	1.0035(29)		1.6266(63)	1.6328(63)
8		0.9945(50)	0.9966(50)		1.6318(80)	1.6370(81)
4	1.0000	1.0762(15)	1.0794(15)	1.6285	1.8441(50)	1.8394(49)
6		1.0827(31)	1.0862(31)		1.8677(83)	1.8750(83)
8		1.0789(40)	1.0813(40)		1.874(11)	1.880(11)
4	1.0813	1.1710(19)	1.1740(19)	1.8700	2.1685(77)	2.1551(76)
6		1.1794(41)	1.1834(41)		2.199(13)	2.208(13)
8		1.1778(47)	1.1807(48)		2.203(17)	2.212(17)
4	1.1787	1.2860(24)	1.2886(24)	2.2003	2.650(11)	2.617(11)
6		1.2968(50)	1.3014(50)		2.688(17)	2.698(17)
8		1.2977(61)	1.3011(61)		2.684(24)	2.697(24)
4	1.2972	1.4283(28)	1.4299(28)	2.6870	3.462(22)	3.378(21)
6		1.4423(56)	1.4476(57)		3.507(40)	3.517(40)
8		1.4455(72)	1.4497(72)		3.477(44)	3.496(44)

Table 7.3: Results for $\Sigma(u, a/L)$ and $\Sigma^{(2)}(u, a/L)$ for different lattices and couplings u.

significantly.

We adopted this method and calculated the coupling for different values of β and L/a. The tables of raw data can be found in the appendix D. Different forms and values n were checked and we verified that our results did not depend on the details of these interpolations. The coefficients $c_{m,L/a}$ were determined by a standard χ^2 fit. An example is shown in Figure 7.6 for a pair of lattice sizes, namely $L/a = 8$ and $L/a = 16$ (all details can be found in appendix E). Starting from the interpolations of our data, we obtained $\Sigma(u, a/L)$ in the following way. First we chose an initial coupling $u_{\text{in}} = 0.9$ which was around our lowest coupling in the simulations and used the interpolations to determine the corresponding values of β in the smaller lattices $L/a = 4, 6, 8$. In a second step, we took these β values and used the interpolations of data for the larger lattices $L/a = 8, 12, 16$ to determine the corresponding couplings. For the choice of couplings u starting from u_{in}, we took roughly a sequence which was given by the recursion (7.26). Our result for both step scaling functions $\Sigma(u, a/L)$ and the perturbatively corrected $\Sigma^{(2)}(u, a/L)$ are listed in Table 7.3. As one can see in Figure 7.7 which is a visualization of our data in Table 7.3, the cutoff effects seem to be very small except for $L/a = 4$. As a precaution against higher order cutoff effects, we thus excluded the data set of our coarsest lattice from our analysis leading to the continuum step scaling function. As one can see in Figure 7.7 by eye, the data for $L/a = 6, 8$ for each coupling u is compatible with a fit to a constant. Hence we looked at different fit strategies which were based on the constant fit. The first strategy was to fit the data for $L/a = 6, 8$ with a simple constant fit for each u. The result can be seen in Table 7.4. As mentioned before, we excluded our coarsest lattice to avoid the inclusion of cutoff effects into the results but there was still a danger of introducing systematic cutoff effects coming from $L/a = 6, 8$

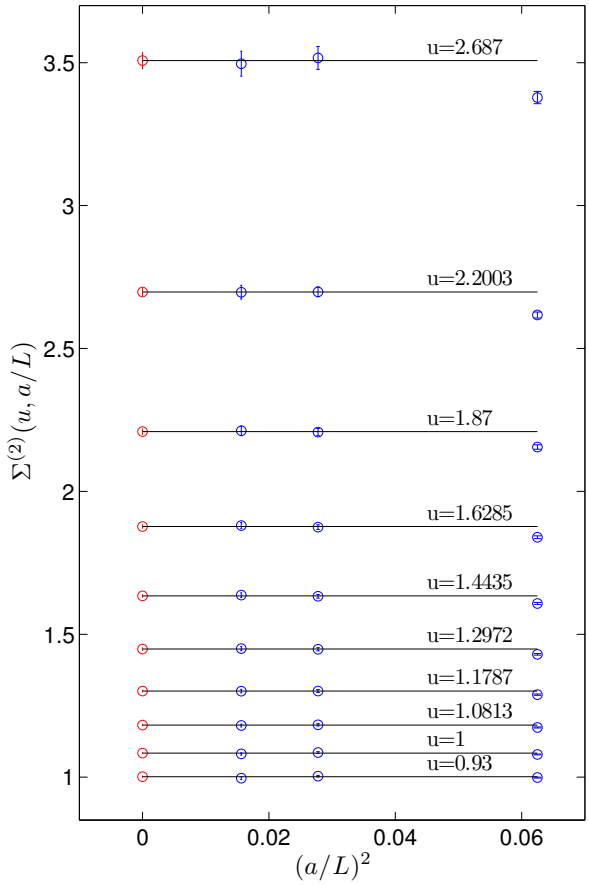

Figure 7.7: Continuum extrapolation of the step scaling function.

lattices. Hence, we performed a combined continuum extrapolation ("global fit") of all data sets for $L/a = 6, 8$ with the approach [113]

$$\Sigma^{(2)}(u, a/L) = \sigma(u) + \rho u^4 (a/L)^2 \tag{7.29}$$

which has a separate, independent parameter $\sigma(u)$ for each value u but a common parameter ρ. This two-parameter approach was used in the case of $N_\mathrm{f} = 2$ from the ALPHA collaboration for modeling the cutoff effects of their data sets. Application of such a fit to our data for $L/a = 6, 8$ resulted in a value for the parameter $\rho = 0.007(85)$ which is a good indication that cutoff effects are negligible. Therefore as a third procedure, we looked at only $L/a = 8$ data set and assumed that we already reached the continuum. All the results are recorded in Table 7.4. These different procedures were used to investigate the uncertainties of the continuum limit. In Figure 7.7, we depicted

u	$\sigma(u)$		
	constant fit	global fit	$L = 8$ data
0.9300	1.002(3)	1.002(3)	0.997(5)
1.0000	1.084(3)	1.084(3)	1.081(4)
1.0813	1.182(3)	1.182(4)	1.181(5)
1.1787	1.301(4)	1.301(5)	1.301(6)
1.2972	1.448(5)	1.448(7)	1.450(7)
1.4435	1.634(5)	1.634(10)	1.637(8)
1.6285	1.877(7)	1.877(16)	1.880(11)
1.8700	2.209(10)	2.207(27)	2.212(17)
2.2003	2.698(14)	2.694(49)	2.697(24)
2.6870	3.507(30)	3.50(104)	3.496(44)

Table 7.4: Results of different fit procedures (as described in the text) for the continuum extrapolation of the step scaling function.

the continuum extrapolation with the constant fit. However, as our final results we take just the $L/a = 8$ data. This is more conservative and we can count on the statistical errors dominating over residual cutoff effects. In particular these data agree with the $L/a = 6$ data and also using $\Sigma(u, a/L)$ instead of $\Sigma^{(2)}(u, a/L)$ has a negligible effect. Using a polynomial of degree five in u, we performed a constrained interpolation of the data in fourth column in Table 7.4. The coefficients up to u^3 were fixed by perturbation theory. Our result for the fit is

$$\sigma(u) = u + s_0 u^2 + s_1 u^3 + 0.0036\, u^4 - 0.0005\, u^5, \quad 0 \le u \le 2.7. \tag{7.30}$$

which is shown in Figure 7.8 (thick line). The perturbative step scaling functions are close to the one sigma range of the non-perturbative data points over the whole interval of the coupling u. Hence our interpolation is also close to the perturbation theory. In Figure 7.8, a peculiarity in the perturbation theory occurs. The 3-loop result lies below the 2-loop truncation of the β function and further away from the non-perturbative result. This is due to the fact that the 3-loop coefficient b_2 (equation (5.10)) in Schrödinger functional scheme changes its sign between $N_{\rm f} = 2$ and $N_{\rm f} = 3$ and it is rather small for $N_{\rm f} = 4$. It is hence not unlikely that the 4-loop term would move the perturbative curve closer again.

Using the parametrization (7.30) of the step scaling function, we calculated the combination $\ln(\Lambda L_{\rm max})$. We started from the highest coupling $u_{\rm max} = \bar{g}^2(L_{\rm max})$ which was covered by our non-perturbative step scaling function and solved the recursion step (7.26) numerically. In this way we obtained the couplings u_i which correspond to the energy scales $\mu = 2^i/L_{\rm max}$. With the help of (5.13) and using the truncated 3-loop β function, we computed the values for $\ln(\Lambda L_{\rm max})$ which are recorded in Table 7.5. From

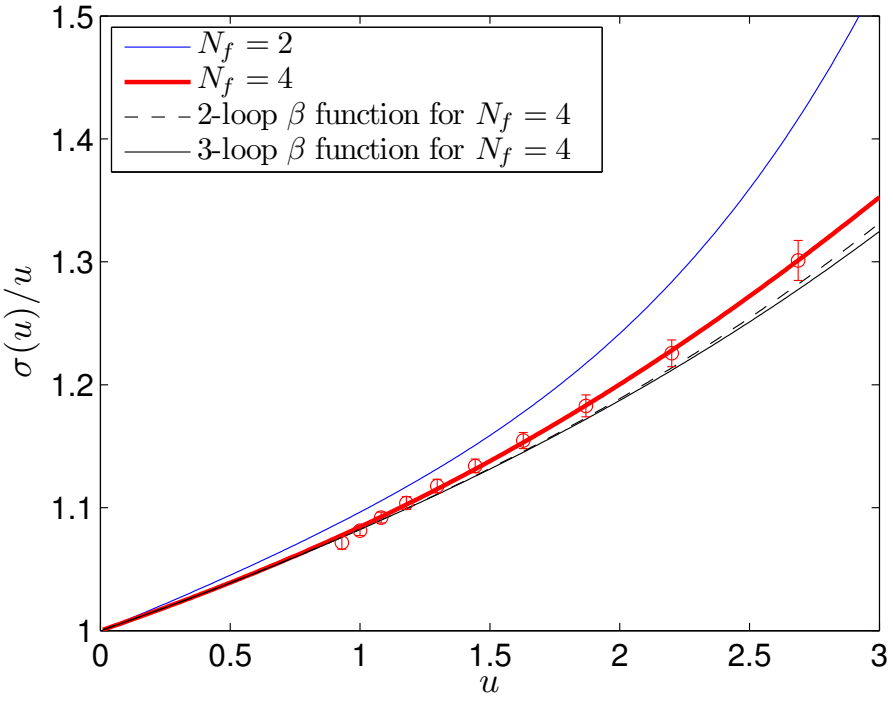

Figure 7.8: The step scaling function for $N_\mathrm{f} = 2, 4$ and the perturbative results. The thickest line is the fit of our data points. The upper solid line is the $N_\mathrm{f} = 2$ result and the lower lines show the perturbative results. It should be noticed that the perturbative result with the truncated 3-loop β function (black sold line) is below the 2-loop β function result (black dashed line).

the $L/a = 8$ results we quote

$$\ln(\Lambda L_\mathrm{max}) = -2.294(83) \quad \text{at } u_\mathrm{max} = 3.45 \tag{7.31}$$

as our final result. This determination of the Λ-parameter in units of L_max has a precision of $\approx 8\%$. It remains to gauge L_max in physical units through a large volume computation. Therefore we here show the running of the coupling in the Schrödinger functional scheme in units of Λ. Figure 7.9 displays α_SF computed from the sixth column of Table 7.5. We observe that upon the iterative application of the step scaling function the difference between the perturbative (using (7.31)) and the non-perturbative coupling is around a 3-sigma effect at the strongest coupling.

Error propagation

The uncertainties of the initial MC data which can be found in the appendix are statistically uncorrelated. For the purpose of propagating their errors, let us collect them in

	constant fit		global fit		$L = 8$ data	
i	u_i	$\ln(\Lambda L_{\max})$	u_i	$\ln(\Lambda L_{\max})$	u_i	$\ln(\Lambda L_{\max})$
0	3.45	−2.028	3.45	−2.028	3.45	−2.028
1	2.660(14)	−2.074(17)	2.666(46)	−2.066(56)	2.660(21)	−2.073(26)
2	2.173(13)	−2.117(24)	2.179(45)	−2.105(83)	2.173(20)	−2.116(37)
3	1.842(11)	−2.155(28)	1.847(37)	−2.141(97)	1.842(17)	−2.153(44)
4	1.6013(90)	−2.188(32)	1.606(30)	−2.17(10)	1.602(14)	−2.185(50)
5	1.4187(78)	−2.217(35)	1.422(25)	−2.20(11)	1.419(13)	−2.213(56)
6	1.2748(70)	−2.241(39)	1.278(20)	−2.23(11)	1.275(11)	−2.238(63)
7	1.1583(63)	−2.263(43)	1.161(17)	−2.25(12)	1.159(10)	−2.259(70)
8	1.0620(58)	−2.282(47)	1.064(15)	−2.27(12)	1.0626(95)	−2.278(76)
9	0.9809(53)	−2.299(50)	0.982(13)	−2.29(12)	0.9815(87)	−2.294(83)
10	0.9117(49)	−2.315(54)	0.913(11)	−2.30(12)	0.9122(81)	−2.309(89)

Table 7.5: Results for $\ln(\Lambda L_{\max})$ with different fit strategies (as described in the text).

a vector x with components x_i. The above fit function $\bar{g}^2(\beta, L/a)$ may then be regarded a function $f(x)$ of the initial data[c]. The error δf of f is simply given by

$$(\delta f)^2 = \sum_i \left(\frac{\partial f}{\partial x_i}\right)^2 (\delta x_i)^2 \,. \tag{7.32}$$

Since f is a relatively complicated function, it is convenient to avoid computing the derivatives $\partial f/\partial x_i$ analytically. The analytic derivative is approximated now with the symmetric derivative

$$\frac{\partial f}{\partial x_i} = \frac{f(x_1, \ldots, x_i + h, x_{i+1}, \ldots, x_n) - f(x_1, \ldots, x_i - h, x_{i+1}, \ldots, x_n)}{2h}. \tag{7.33}$$

A natural choice for the spacing h is e.g. the error of x_i ($h = \delta x_i$). Equation (7.32) becomes then

$$(\delta f)^2 = \sum_i \left(\frac{f(x_1, \ldots, x_i + \delta x_i, \ldots, x_n) - f(x_1, \ldots, x_i - \delta x_i, \ldots, x_n)}{2}\right)^2 . \tag{7.34}$$

This convenient method is applied for estimating the errors of all quantities derived from our data above. If desired also the correlation matrix of the errors of different observables can be obtained this way. As one can see in Figure 7.9, the highest coupling (the most right data point in Figure 7.9) has errorbars but in Table 7.5 there is no uncertainty quoted at this coupling. This is due to how the recursion relation (7.26) is solved. To calculate the errorbars of the highest coupling, we did the recursion two times. Once

[c] We neglect that in the way we determine the interpolation of $\bar{g}^2$ there is also a dependence on the uncertainties δx_i. In the fit we could also replace the errors δx_i by a smooth predefined function of β. The results would not change much.

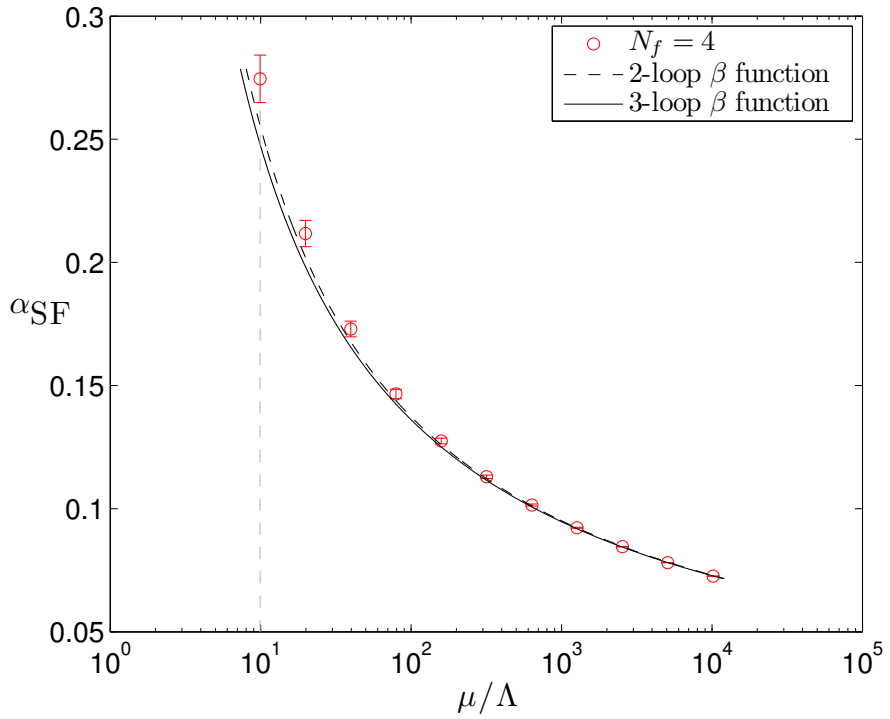

Figure 7.9: The running coupling in the Schrödinger functional scheme. The gray vertical dashed line is only for the guidance of the eyes to show what the perturbation theory predicts for α_{SF} at the lowest energy which we could reach.

forwards and once backwards. In forward direction, we first obtained the couplings u_i as quoted in Table 7.5. Then, we looked at the coupling u_k where our non-perturbative result goes into the perturbative results and regarded the errors of this coupling (we chose $i = 9$) as negligible. We started then the recursion backwards from this coupling and obtained the uncertainties which were shown in Figure 7.9. The uncertainties of Λ are also transformed and add to uncertainties of α_{SF} (Figure 7.9).

8 Summary and Outlook

In the first two chapters, we explained some aspects of the continuum QCD briefly and gave then an overview of the lattice formulation. After discussing numerical and algorithmic issues we gave a brief summary about the theoretical foundations on which this thesis is based. Then we discussed our idea of extending the ALPHA code with two flavors of $\mathcal{O}(a)$ improved Wilson quarks to four flavors of $\mathcal{O}(a)$ improved Wilson quarks. We presented then the results of our studies. The first part of our results concerned the determination of the improvement coefficient $c_{\rm sw}$ with four flavors (with plaquette gauge action). As one can see in equation (2.50) and Table 2.2, this coefficient was only known from perturbation theory up to 1-loop and non-perturbatively for $N_{\rm f} = 0, 2, 3$ [54–56]. Hence, it was essential to determine this coefficient for four flavors to $\mathcal{O}(a)$-improve the action. So, we have performed simulations for the calculation of the improvement coefficient $c_{\rm sw}$ for four flavors of Wilson fermions in the range of $\beta \geq 5.0$. A determination of $c_{\rm sw}$ beyond $\beta = 5.0$ was not possible because we could not show unambiguously that our improvement condition $\Delta M = 0$ (7.13) was fulfilled at $\beta = 4.8$. The errorbars of the raw data became too large and we were not able to determine the value for $c_{\rm sw}$ where ΔM vanishes. The raw data can be found in the appendix B. Then we gave a detailed description of how we determined $c_{\rm sw}$ from our raw data in section 7.1.5 and quoted

$$c_{\rm sw}(g_0^2) = \frac{1 - 0.1372 g_0^2 - 0.1641 g_0^4 + 0.1679 g_0^6}{1 - 0.4031 g_0^2}, \quad 0 \leq g_0^2 \leq 1.2.$$

as a suitable parametrization of our data (eq. (7.18)). We compared three simple-minded different Padé-approximation formulae for our data and could show that a small extrapolation of $c_{\rm sw}$ beyond $\beta = 5.0$ to $\beta = 4.5$ with the above formula may still be acceptable.

In the second part we gave an estimation of critical κ (abbreviated with κ_c) where the quark mass vanishes. This estimation was extracted from the raw data of the $c_{\rm sw}$ determination (Table 7.2). We quoted

$$\kappa_c = 1/8 + \kappa_c^{(1)} g_0^2 + 0.000129 g_0^4 + 0.007470 g_0^6 - 0.007716 g_0^8 + 0.002748 g_0^{10},$$
$$0 \leq g_0^2 \leq 1.2$$

where $\kappa_c^{(1)}$ is the 1-loop value $\kappa_c^{(1)} = 0.008439857$ [120] as our interpolation for κ_c. We emphasize that the above formula for κ_c was used as a first estimate in the simulations for the step scaling function and we tuned κ explicitly such that the PCAC mass vanishes. We compared then the non-perturbative estimations for κ_c with $N_{\rm f} = 2, 3, 4$ [55, 56] and the 1-loop perturbation theory [52, 120]. As one can see in Figure 7.5, the

non-perturbative results are never far from the 1-loop perturbative result but a small dependence on the number of flavors can be seen.

In the third part we used our determination of $c_{\rm sw}$ with our estimation of κ_c to determine the non-perturbative running of the Schrödinger functional coupling for $N_{\rm f} = 4$ massless flavors. For this purpose we computed first the step scaling function of the QCD coupling in the Schrödinger functional scheme with four massless flavors. As can be seen in Figure 7.7 and Table 7.3 the resulting cutoff effects were very small allowing for a continuum extrapolation. While the data are compatible with a constant for $L/a \geq 6$, we assumed this form only for $L/a \geq 8$; the smaller lattices thus only entered the analysis by demonstrating that cutoff effects were small. We emphasize that this statement refers to the present level of statistical errors. If in the future statistical errors are further reduced, larger L/a will be necessary at the same time. It will be very interesting to see also the efficiency of computations with different regularizations of the Schrödinger functional as well as the corresponding test of the universality of the continuum limit. Most notably there are chirally rotated boundary conditions for the quarks [151–153] and staggered quarks [154, 155] for which results are expected soon.

Our interpolation of the step scaling function based on our data resulted in

$$\sigma(u) = u + s_0 u^2 + s_1 u^3 + 0.0036\, u^4 - 0.0005\, u^5, \quad 0 \leq u \leq 2.7.$$

which is close to the perturbative results as shown in Figure 7.8. Using this parametrization we calculated the Λ parameter in units of $L_{\rm max}$ with $\approx 8\%$ precision and quoted

$$\ln(\Lambda L_{\rm max}) = -2.294(83) \quad \text{at } u_{\rm max} = 3.45$$

as our final result. Due to the undetermined technical scale $L_{\rm max}$ in physical units in our studies, we showed the running of the coupling in Schrödinger functional scheme in units of Λ (Figure 7.9). As one can see in Figure 7.9, we observed a small but significant deviation from 3-loop perturbation theory at the largest reached coupling. It is about 10% (three standard deviations) and the Schrödinger functional coupling has a value of $\alpha_{\rm SF} \approx 0.28$. For $N_{\rm f} = 2$ a similar effect was visible only for larger coupling [113][a]. These findings underline the necessity of going to weak coupling before applying renormalized perturbation theory in the continuum.

The present work has brought us a good step closer to the computation of the Λ-parameter in 4-flavor QCD, which may then be perturbatively connected to e.g. the 5-flavor $\overline{\rm MS}$ coupling at the Z-pole. However, the technically introduced scale $L_{\rm max}$ remains to be expressed in physical units through large volume 4-flavor simulations. Apart from the challenge of tuning more parameters, one needs to treat a massive charm quark at small enough lattice spacing. Presently this appears to be a considerable challenge due to a severe slowing down of lattice simulation algorithms at small lattice spacings [156, 157].

[a] For $\alpha_{\rm SF} \approx 0.45$ a similar deviation is visible but there are no non-perturbative data points in between $\alpha_{\rm SF} \approx 0.28$ and $\alpha_{\rm SF} \approx 0.45$ to see better where this sets in.

9 Publications

- Fatih Tekin, Rainer Sommer, and Ulli Wolff. Symanzik improvement of lattice QCD with four flavors of Wilson quarks. *Phys. Lett., B683:75*, 2010.
- Fatih Tekin, Rainer Sommer, and Ulli Wolff. The running coupling of QCD with four flavors. *Nucl. Phys., B840:114*, 2010
- Rainer Sommer, Fatih Tekin, Ulli Wolff. Running of the SF-coupling with four massless flavours. *PoS*, LAT2010, 2010.

Appendix A

Gell-Mann matrices

A representation of the $SU(3)$ generators is given by the eight Gell-Mann matrices, which are hermitian and traceless

$$\lambda^1 = \begin{pmatrix} 0 & 1 & 0 \\ 1 & 0 & 0 \\ 0 & 0 & 0 \end{pmatrix}, \quad \lambda^2 = \begin{pmatrix} 0 & -i & 0 \\ i & 0 & 0 \\ 0 & 0 & 0 \end{pmatrix}, \quad \lambda^3 = \begin{pmatrix} 1 & 0 & 0 \\ 0 & -1 & 0 \\ 0 & 0 & 0 \end{pmatrix},$$

$$\lambda^4 = \begin{pmatrix} 0 & 0 & 1 \\ 0 & 0 & 0 \\ 1 & 0 & 0 \end{pmatrix}, \quad \lambda^5 = \begin{pmatrix} 0 & 0 & -i \\ 0 & 0 & 0 \\ i & 0 & 0 \end{pmatrix}, \quad \lambda^6 = \begin{pmatrix} 0 & 0 & 0 \\ 0 & 0 & 1 \\ 0 & 1 & 0 \end{pmatrix}, \tag{1}$$

$$\lambda^7 = \begin{pmatrix} 0 & 0 & 0 \\ 0 & 0 & -i \\ 0 & i & 0 \end{pmatrix}, \quad \lambda^8 = \frac{1}{\sqrt{3}} \begin{pmatrix} 1 & 0 & 0 \\ 0 & 1 & 0 \\ 0 & 0 & -2 \end{pmatrix}.$$

They obey the following commutation relation

$$\left[\frac{\lambda^a}{2}, \frac{\lambda^b}{2}\right] = i \sum_{c=1}^{8} f^{abc} \frac{\lambda^c}{2}. \tag{2}$$

The structure constants f^{abc} are given by

$$\begin{aligned} &f^{123} = 1 \\ &f^{147} = -f^{156} = f^{246} = f^{257} = f^{345} = -f^{367} = \tfrac{1}{2} \\ &f^{458} = f^{678} = \tfrac{\sqrt{3}}{2}. \end{aligned} \tag{3}$$

These matrices have also the property

$$tr(\lambda^a \lambda^b) = 2\delta_{ab} \tag{4}$$

where δ_{ab} is the Kronecker δ.

The projection operator and γ matrices

The projection operator $P_\pm$ is given by

$$P_\pm = \frac{1}{2}(1 \pm \gamma_5) \tag{5}$$

and satisfies the following relations

$$P_\pm^2 = P_\pm, P_+P_- = 0. \tag{6}$$

γ_5 is defined by

$$\gamma_5 = i\gamma^0\gamma^1\gamma^2\gamma^3 \tag{7}$$

where γ_μ are represented in the *Weyl/chiral* and *Dirac* basis, respectively as follows

$$\begin{gathered}\text{Dirac basis}\\ \gamma^0 = \begin{pmatrix} 1_{2\times2} & 0 \\ 0 & -1_{2\times2} \end{pmatrix} \quad \gamma^i = \begin{pmatrix} 0 & \sigma^i \\ -\sigma^i & 0 \end{pmatrix} \quad \gamma^5 = \begin{pmatrix} 0 & 1_{2\times2} \\ 1_{2\times2} & 0 \end{pmatrix}\\ \text{Weyl basis}\\ \gamma^0 = \begin{pmatrix} 0 & 1_{2\times2} \\ 1_{2\times2} & 0 \end{pmatrix} \quad \gamma^i = \begin{pmatrix} 0 & \sigma^i \\ -\sigma^i & 0 \end{pmatrix} \quad \gamma^5 = \begin{pmatrix} -1_{2\times2} & 0 \\ 0 & 1_{2\times2} \end{pmatrix}\end{gathered} \tag{8}$$

The σ^i are the *Pauli* matrices

$$\sigma^1 = \begin{pmatrix} 0 & 1 \\ 1 & 0 \end{pmatrix} \quad \sigma^2 = \begin{pmatrix} 0 & -i \\ i & 0 \end{pmatrix} \quad \sigma^3 = \begin{pmatrix} 1 & 0 \\ 0 & -1 \end{pmatrix} \tag{9}$$

The anticommutation relation of the γ matrices is given by

$$\{\gamma^\mu, \gamma^\nu\} = 2g^{\mu\nu}1_{4\times4} \tag{10}$$

where $g^{\mu\nu}$ is the *Minkowski* metric $g^{\mu\nu} = \text{diag}(1,\text{-}1,\text{-}1,\text{-}1)$. The Pauli matrices obey the following relations

$$[\sigma_i, \sigma_j] = 2i\epsilon_{ijk}\sigma_k \tag{11}$$

$$\sigma_i\sigma_j = \delta_{ij} + i\epsilon_{ijk}\sigma_k \tag{12}$$

where ϵ_{ijk} is the *Levi-Civita tensor*

$$\epsilon_{ijk} = \begin{cases} +1, & \text{if } (i,j,k) \text{ is an even permutation of } (1,2,3) \\ -1, & \text{if } (i,j,k) \text{ is an odd permutation of } (1,2,3) \\ 0, & \text{if any two indices are the same} \end{cases} \tag{13}$$

Appendix B

Data for the determination of $c_{\mathbf{sw}}$

β	κ	c_{sw}	M	ΔM	$\delta\tau$	N_{meas}	accept.	ΔH
12	0.130280	1.028654	0.000224(75)	0.001735(89)	0.04	4800	84.1%	0.0783(41)
12	0.129897	1.128654	-0.001510(74)	0.000468(84)	0.04	4800	83.4%	0.0822(42)
12	0.129449	1.228654	-0.001371(82)	-0.000827(86)	0.04	4800	83.5%	0.0878(42)
9.6	0.131516	1.140488	-0.00004(11)	0.00077(12)	0.04	4800	82.7%	0.0995(44)
9.6	0.131164	1.170488	0.00595(11)	0.00053(11)	0.04	4800	82.6%	0.0924(45)
9.6	0.131164	1.250488	-0.00853(11)	-0.00040(12)	0.04	4800	82.6%	0.1033(45)
7.4	0.134626	1.163222	-0.00196(20)	0.00169(19)	0.04	4800	81.5%	0.1095(47)
7.4	0.133753	1.263222	0.00072(20)	0.00069(15)	0.04	4800	82.0%	0.1082(47)
7.4	0.132989	1.363222	0.00018(20)	-0.00036(16)	0.04	4800	81.3%	0.1166(49)
7.4	0.132349	1.443222	0.00027(20)	-0.00162(17)	0.04	4800	80.5%	0.1174(50)
6.8	0.135638	1.209613	0.00128(30)	0.00169(26)	0.04	4000	81.3%	0.1082(54)
6.8	0.135082	1.299613	-0.00642(32)	0.00033(26)	0.04	4000	80.7%	0.1173(54)
6.8	0.134896	1.309613	-0.00333(29)	0.00079(24)	0.04	4000	80.4%	0.1190(54)
6.8	0.133813	1.409613	0.00320(29)	-0.00000(24)	0.04	2960	80.7%	0.1123(63)
6.8	0.133056	1.509613	-0.00141(30)	-0.00204(22)	0.04	4000	79.8%	0.1266(55)
6.3	0.137098	1.239058	-0.00129(38)	0.00199(24)	0.02	4000	80.3%	0.1224(55)
6.3	0.136018	1.339058	0.00142(36)	0.00077(27)	0.02	4000	80.7%	0.1212(57)
6.3	0.135028	1.439058	0.00140(36)	-0.00075(27)	0.02	2960	92.9%	0.0173(24)
6.3	0.134028	1.550580	-0.00251(31)	-0.00115(24)	0.04	4800	79.5%	0.1341(54)
6.0	0.138358	1.250000	-0.00090(85)	0.00270(30)	0.02	6400	94.9%	0.0064(12)
6.0	0.136669	1.387912	0.00214(47)	0.00022(48)	0.02	2840	94.8%	0.0096(17)
6.0	0.134375	1.587912	0.00677(43)	-0.00123(34)	0.02	2840	94.7%	0.0105(18)
5.7	0.140327	1.250000	-0.0082(16)	0.00369(38)	0.02	6400	94.5%	0.0097(12)
5.7	0.138229	1.387912	0.00034(63)	0.00107(43)	0.02	3232	94.4%	0.0088(18)
5.7	0.137008	1.487912	0.00081(55)	0.00076(48)	0.02	3200	94.4%	0.0093(18)
5.7	0.135685	1.587912	0.00564(63)	-0.00032(37)	0.02	2840	94.8%	0.0111(20)
5.7	0.133940	1.754350	-0.00004(38)	-0.00156(28)	0.01	5360	98.5%	0.00097(37)
5.4	0.141417	1.307912	-0.00032(77)	0.00258(36)	0.02	6400	93.9%	0.0119(13)
5.4	0.139111	1.487912	-0.00712(89)	0.00112(55)	0.02	2960	93.9%	0.0140(20)
5.4	0.137815	1.587912	-0.00762(70)	-0.00056(57)	0.02	2960	93.8%	0.0126(21)
5.4	0.135028	1.787912	-0.00117(69)	-0.00164(47)	0.02	2960	93.6%	0.0150(21)
5.4	0.133775	1.907912	-0.00854(39)	-0.00202(31)	0.02	6400	93.6%	0.0128(14)

β	κ	c_{sw}	M	ΔM	$\delta\tau$	N_{meas}	accept.	ΔH
5.2	0.143363	1.307912	-0.0004(14)	0.00196(48)	0.02	5200	92.8%	0.0202(16)
5.2	0.140628	1.487912	-0.00032(87)	0.00076(42)	0.02	5360	93.3%	0.0155(16)
5.2	0.139206	1.587912	-0.00326(69)	0.00102(39)	0.02	5360	93.4%	0.0131(16)
5.2	0.138147	1.655891	0.00162(94)	0.00028(47)	0.02	2960	93.2%	0.0133(21)
5.2	0.136248	1.787912	0.00030(91)	-0.00084(65)	0.02	2960	93.3%	0.0122(23)
5.2	0.134556	1.907912	0.00372(62)	-0.00189(38)	0.02	4000	93.0%	0.0156(20)
5.0	0.146056	1.307912	0.0051(25)	0.00252(62)	0.01	6480	97.9%	0.00192(44)
5.0	0.142554	1.507912	0.0021(13)	0.00125(41)	0.01	8160	98.2%	0.00176(38)
5.0	0.138141	1.787912	-0.0053(11)	0.00102(68)	0.02	2960	92.2%	0.0161(26)
5.0	0.136527	1.885463	0.0009(11)	0.00004(55)	0.02	2960	92.9%	0.0173(24)
5.0	0.135039	2.000000	-0.00826(90)	-0.00070(59)	0.01	2960	98.2%	0.00028(65)
5.0	0.129603	2.400000	0.00033(42)	-0.00482(27)	0.01	7040	97.9%	0.00085(45)
4.8	0.158255	1.100000	-0.351(26)	-0.0012(22)	0.005	1072	99.1%	0.00140(47)
4.8	0.157000	1.300000	-0.526(45)	0.0026(25)	0.01	2400	96.6%	0.0149(79)
4.8	0.145928	1.500000	0.0083(54)	-0.0002(12)	0.01	3680	97.8%	0.00150(75)
4.8	0.142201	1.700000	-0.0022(31)	-0.0000(11)	0.01	2560	97.8%	0.00046(87)
4.8	0.138295	1.910000	0.0017(13)	0.00060(62)	0.01	5440	97.6%	0.00139(54)
4.8	0.137971	1.930000	0.0031(12)	-0.00054(48)	0.01	5440	97.7%	0.00192(54)
4.8	0.136844	2.000000	0.0008(11)	-0.00044(50)	0.01	5600	97.7%	0.00246(54)
4.8	0.135327	2.100000	-0.00492(87)	-0.00116(44)	0.01	6560	97.6%	0.00294(50)
4.8	0.132358	2.300000	-0.00550(72)	-0.00244(41)	0.01	5440	97.4%	0.00309(56)

Appendix C

The fits of the data in appendix B for the determination of c_{sw}. The improvement condition $\Delta M - \Delta M^{(0)} = 0$ is only fulfilled at the point where the solid line hits the dashed line. The numerical results of interpolation can be seen in table 7.1:

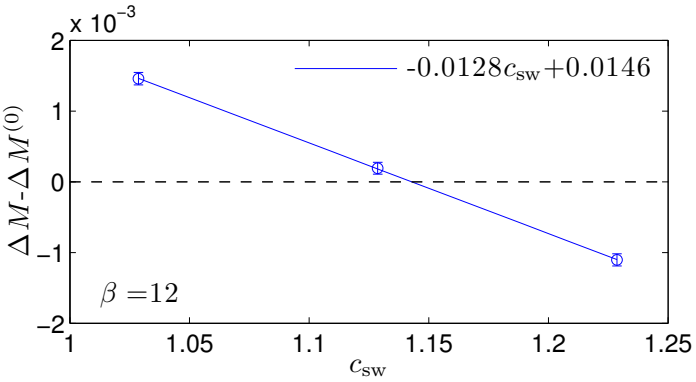

Figure 1: $\Delta M - \Delta M^{(0)}$ for $\beta = 12$

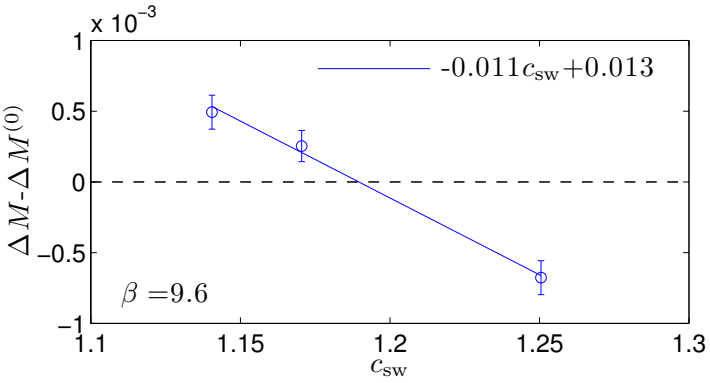

Figure 2: $\Delta M - \Delta M^{(0)}$ for $\beta = 9.6$

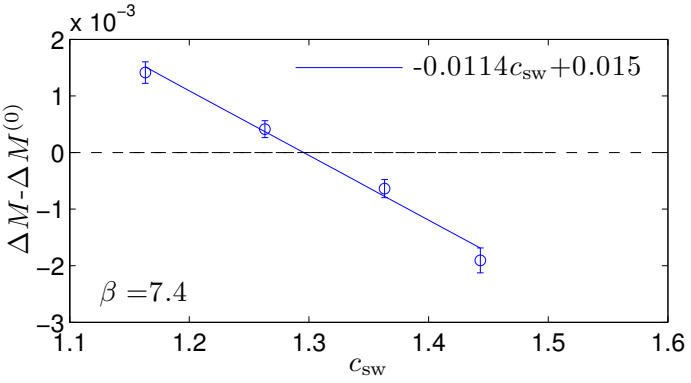

Figure 3: $\Delta M - \Delta M^{(0)}$ for $\beta = 7.4$

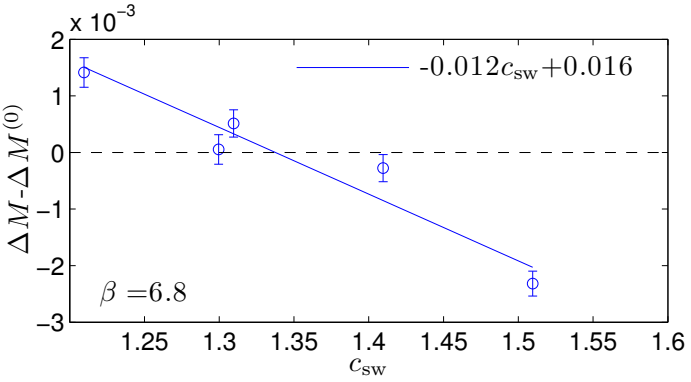

Figure 4: $\Delta M - \Delta M^{(0)}$ for $\beta = 6.8$

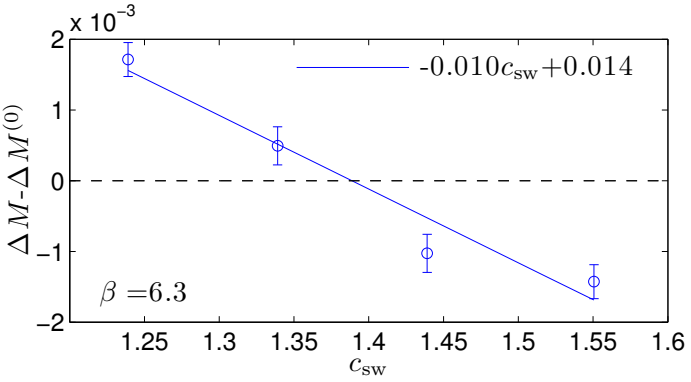

Figure 5: $\Delta M - \Delta M^{(0)}$ for $\beta = 6.3$

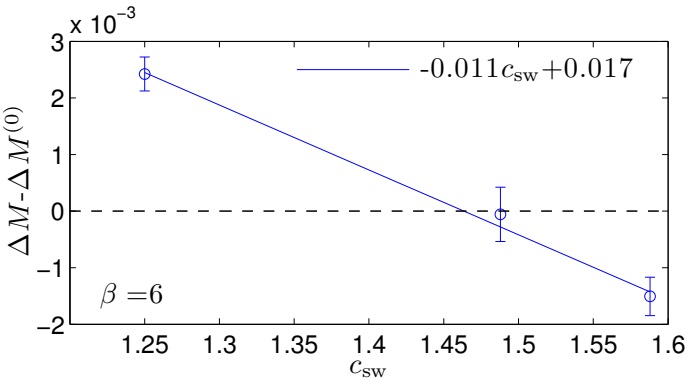

Figure 6: $\Delta M - \Delta M^{(0)}$ for $\beta = 6.0$

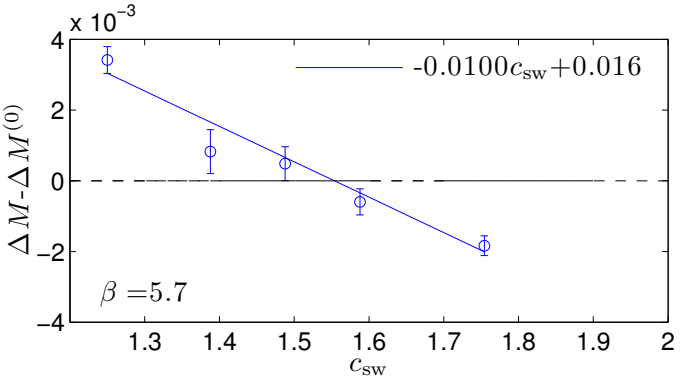

Figure 7: $\Delta M - \Delta M^{(0)}$ for $\beta = 5.7$

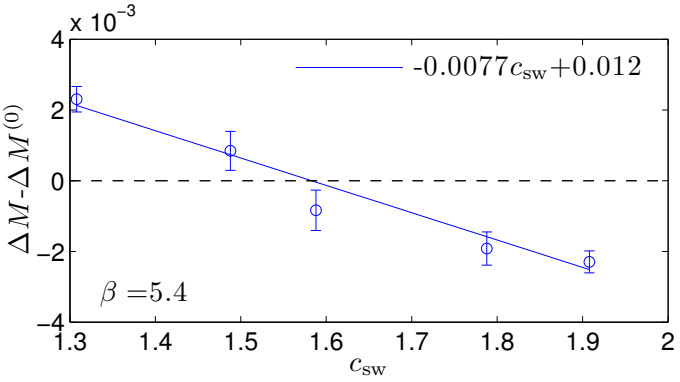

Figure 8: $\Delta M - \Delta M^{(0)}$ for $\beta = 5.4$

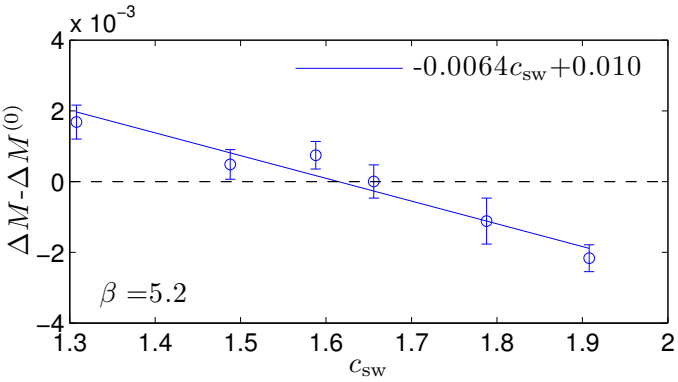

Figure 9: $\Delta M - \Delta M^{(0)}$ for $\beta = 5.2$

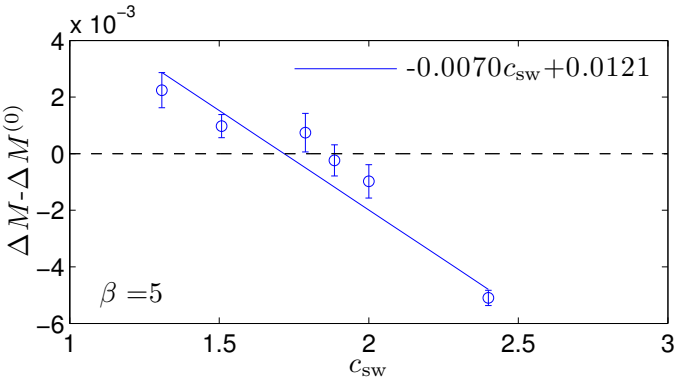

Figure 10: $\Delta M - \Delta M^{(0)}$ for $\beta = 5.0$

Appendix D

We here list the results of our MC simulations for the determination of the step scaling function. Each row refers to a separate simulation of about 50000 trajectories unless otherwise noted. Some of these simulations consist of independent replica (between 1 and 16). Measurements were taken after every trajectory for which we chose trajectory length $\tau = 1$.

		$L/a = 4$		$L/a = 8$	
β	κ	$\bar{g}^2$	am_1	$\bar{g}^2$	am_1
5.0	0.137975	2.913(10)	0.00033(42)	3.932(39)	0.03752(13)
5.3	0.137110	2.4700(76)	0.00040(34)	3.049(22)	0.02934(10)
5.6	0.136371	2.1505(49)	0.00042(29)	2.575(15)	0.024981(80)
6.2	0.135082	1.7300(31)	0.00162(24)	1.9853(91)	0.020192(61)
6.8	0.134053	1.4556(21)	0.00080(20)	1.6256(61)	0.016432(52)
7.4	0.133188	1.2609(13)	0.00032(18)	1.3844(42)	0.013977(47)
8.0	0.132455	1.1119(10)	0.00070(15)	1.2074(32)	0.012435(40)
8.6	0.131860	0.99575(77)	−0.00021(14)	1.0678(25)	0.010382(35)
9.2	0.131309	0.90315(54)	0.00094(11)	0.9662(20)	0.010176(33)

Table 1: The raw data for $L/a = 4$ and $L/a = 8$.

		$L/a = 6$		$L/a = 12$	
β	κ	$\bar{g}^2$	am_1	$\bar{g}^2$	am_1
5.25	0.138027	2.749(13)	−0.00005(16)	3.635(46)	0.000929(56)
5.55	0.137173	2.3507(92)	0.00110(13)	2.904(29)	0.000704(43)
5.85	0.136443	2.0865(71)	0.00053(11)	2.529(23)	−0.000031(37)
6.45	0.135190	1.6948(46)	−0.000294(94)	1.953(14)	−0.000922(31)
7.05	0.134123	1.4361(32)	0.000488(78)	1.6211(88)	−0.000227(25)
7.65	0.133261	1.2500(24)	0.000437(69)	-	-
8.25	0.132538	1.1025(18)	0.000435(62)	1.2051(50)	−0.000347(20)
8.85	0.131935	0.9908(14)	0.000154(57)	-	-
9.45	0.131411	0.8975(12)	0.000237(51)	0.9628(31)	−0.000547(16)

Table 2: The raw data for $L/a = 6$ and $L/a = 12$.

		$L/a = 8$		$L/a = 16$	
β	κ	$\bar{g}^2$	am_1	$\bar{g}^2$	am_1
5.0	0.138910	3.638(34)	0.00037(14)	-	-
5.44	0.137507	2.705(16)	0.000640(83)	3.548(45)	−0.000872(23)
5.88	0.136393	2.225(11)	0.000306(66)	2.643(38)	−0.001120(25)
6.32	0.135433	1.8728(77)	0.000288(57)	2.252(25)	−0.000875(22)
6.76	0.134597	1.6319(56)	0.000748(58)	1.861(16)	−0.000350(18)
7.2	0.133903	1.4364(42)	0.000041(44)	-	-
7.64	0.133275	1.3046(35)	0.000233(40)	1.4502(94)	−0.000666(15)
8.08	0.132736	1.1852(29)	0.000069(38)	-	-
8.52	0.132249	1.0886(24)	0.000328(36)	1.1860(67)	−0.000552(12)
8.96	0.131821	1.0034(20)	0.000368(33)	-	-
9.4	0.131442	0.9308(17)	0.000284(32)	0.9961(48)	−0.000504(11)

Table 3: The raw data for $L/a = 8$ and $L/a = 16$. The run $L/a = 16$, $\beta = 5.44$ has 98000 trajectories.

Appendix E

Here, we show the fits for all L/a of the data in appendix D. Details about the fits are given in section 7.3.2. The parameter n in (7.28) is set to three in all fits. The fit parameters and the covariance matrices can be found below.

$L/a = 4, 8$:

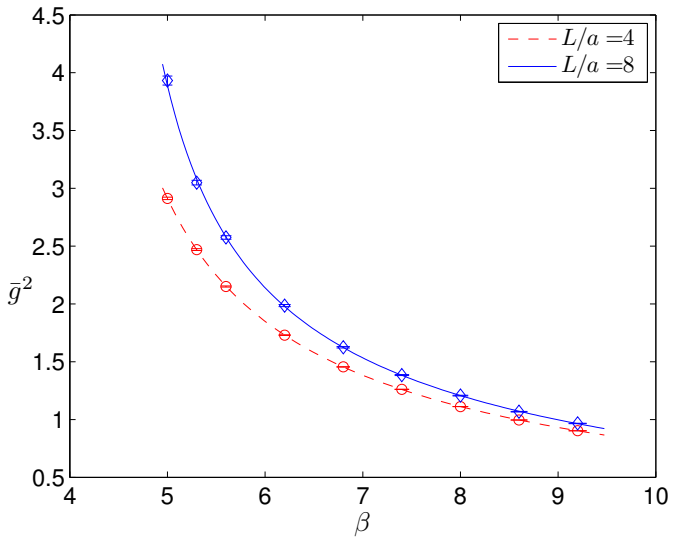

Figure 11: The raw data and the fits for $L/a = 4$ and $L/a = 8$.

L/a	$c_{0,L/a}$	$c_{1,L/a}$	$c_{2,L/a}$	$c_{3,L/a}$	χ^2/dof
4	0.083(49)	−0.71(17)	0.37(19)	−0.208(72)	0.35
8	0.19(12)	−1.21(42)	0.94(48)	−0.45(18)	1.21

Table 4: Fit parameters of $L/a = 4$ and $L/a = 8$.

$$\mathrm{cov}(L/a=4) = \begin{pmatrix} 0.0024 & -0.0082 & 0.0094 & -0.0035 \\ -0.0082 & 0.0289 & -0.0329 & 0.0122 \\ 0.0094 & -0.0329 & 0.0377 & -0.0140 \\ -0.0035 & 0.0122 & -0.0140 & 0.0052 \end{pmatrix} \tag{14}$$

$$\mathrm{cov}(L/a=8) = \begin{pmatrix} 0.0150 & -0.0518 & 0.0582 & -0.0213 \\ -0.0518 & 0.1791 & -0.2018 & 0.0741 \\ 0.0582 & -0.2018 & 0.2281 & -0.0840 \\ -0.0213 & 0.0741 & -0.0840 & 0.0310 \end{pmatrix} \tag{15}$$

$L/a = 6, 12$**:**

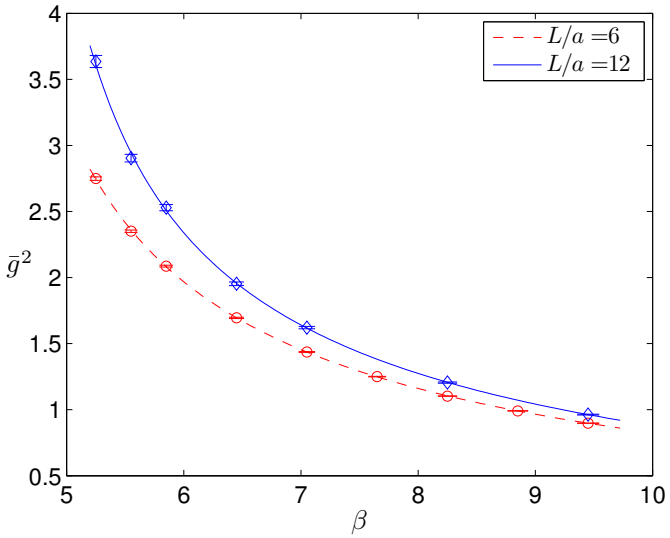

Figure 12: The raw data and the fits for $L/a = 6$ and $L/a = 12$.

L/a	$c_{0,L/a}$	$c_{1,L/a}$	$c_{2,L/a}$	$c_{3,L/a}$	χ^2/dof
6	0.158(92)	−1.01(33)	0.66(38)	−0.31(15)	0.53
12	0.26(23)	−1.48(81)	1.16(94)	−0.52(36)	0.72

Table 5: Fit parameters of $L/a = 6$ and $L/a = 12$.

$$\mathrm{cov}(L/a=6) = \begin{pmatrix} 0.0084 & -0.0300 & 0.0350 & -0.0133 \\ -0.0300 & 0.1075 & -0.1258 & 0.0480 \\ 0.0350 & -0.1258 & 0.1476 & -0.0565 \\ -0.0133 & 0.0480 & -0.0565 & 0.0217 \end{pmatrix} \tag{16}$$

$$\mathrm{cov}(L/a=12) = \begin{pmatrix} 0.0518 & -0.1843 & 0.2135 & -0.0807 \\ -0.1843 & 0.6577 & -0.7639 & 0.2893 \\ 0.2135 & -0.7639 & 0.8897 & -0.3378 \\ -0.0807 & 0.2893 & -0.3378 & 0.1285 \end{pmatrix} \tag{17}$$

$L/a = 8, 16$**:**

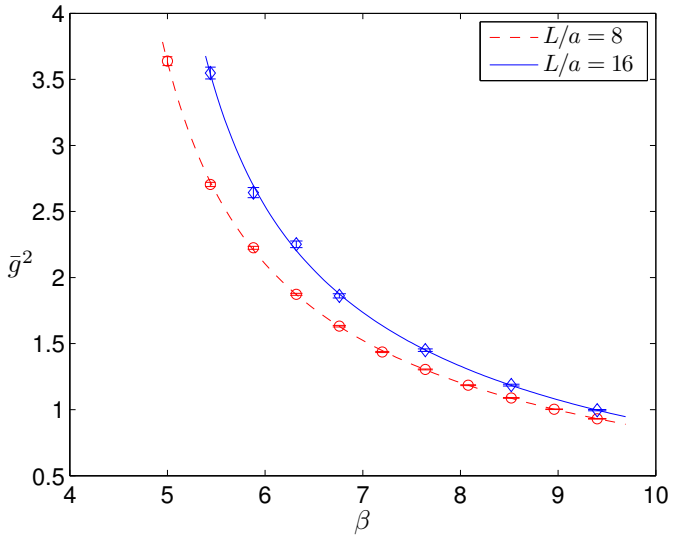

Figure 13: The raw data and the fits for $L/a = 8$ and $L/a = 16$.

L/a	$c_{0,L/a}$	$c_{1,L/a}$	$c_{2,L/a}$	$c_{3,L/a}$	χ^2/dof
8	0.180(95)	−1.14(33)	0.82(38)	−0.38(14)	1.29
16	0.43(35)	−2.05(1.27)	1.75(1.49)	−0.73(57)	1.32

Table 6: Fit parameters of $L/a = 8$ and $L/a = 16$.

$$\mathrm{cov}(L/a = 8) = \begin{pmatrix} 0.0091 & -0.0318 & 0.0362 & -0.0134 \\ -0.0318 & 0.1115 & -0.1273 & 0.0473 \\ 0.0362 & -0.1273 & 0.1459 & -0.0544 \\ -0.0134 & 0.0473 & -0.0544 & 0.0204 \end{pmatrix} \tag{18}$$

$$\mathrm{cov}(L/a = 16) = \begin{pmatrix} 0.1246 & -0.4464 & 0.5222 & -0.1997 \\ -0.4464 & 1.6027 & -1.8791 & 0.7200 \\ 0.5222 & -1.8791 & 2.2083 & -0.8480 \\ -0.1997 & 0.7200 & -0.8480 & 0.3263 \end{pmatrix} \tag{19}$$

Bibliography

[1] W.N. Cottingham and D.A. Greenwood. *An Introduction to the Standard Model of Particle Physics*. Cambrige University Press, 2st edition, 2007. ISBN 0-521-85249-8.

[2] R.K. Ellis, W.J. Stirling, and B.R. Webber. *QCD and Collider Physics*. Cambrige University Press, 1st edition, 1996. ISBN 0-521-58189-3.

[3] M.E. Peskin and D.V. Schroeder. *An Introduction to Quantum Field Theory*. Westview Press, 1st edition, 1995. ISBN 0-201-50397-2.

[4] S. Weinberg. *The Quantum Theory of Fields, Volume 1*. Cambrige University Press, 1st edition, 1995. ISBN 0-521-55001-7.

[5] S. Weinberg. *The Quantum Theory of Fields, Volume 2*. Cambrige University Press, 1st edition, 1996. ISBN 0-521-55002-5.

[6] C. Amsler et al. Review of Particle Physics. *Phys. Lett. B*, 667(1-5):1–6, 2008. ISSN 0370-2693.

[7] O. Bär and U. J. Wiese. Can one see the number of colors? *Nucl. Phys. B*, 609: 225–246, 2001.

[8] J. D. Bjorken. Asymptotic Sum Rules at Infinite Momentum. *Phys. Rev.*, 179(5): 1547–1553, Mar 1969.

[9] J. Goldstone. Field Theories with Superconductor Solutions. *Nuovo Cim.*, 19: 154–164, 1961.

[10] H. Leutwyler. On the foundations of chiral perturbation theory. *Ann. Phys.*, 235: 165–203, 1994.

[11] F. M. Flynn and N. Isgur. Heavy-quark symmetry: ideas and applications. *Journal of Physics G: Nuclear and Particle Physics*, 18(10):1627–1644, 1992.

[12] Matthias Neubert. Heavy quark symmetry. *Phys. Rept.*, 245:259–396, 1994.

[13] H. David Politzer. Reliable Perturbative Results for Strong Interactions? *Phys. Rev. Lett.*, 30(26):1346–1349, Jun 1973.

[14] David J. Gross and Frank Wilczek. Ultraviolet Behavior of Non-Abelian Gauge Theories. *Phys. Rev. Lett.*, 30(26):1343–1346, Jun 1973.

[15] David J. Gross and Frank Wilczek. Asymptotically Free Gauge Theories I. *Phys. Rev. D*, 8(10):3633–3652, Nov 1973.

[16] David J. Gross and Frank Wilczek. Asymptotically free gauge theories II. *Phys. Rev. D*, 9(4):980–993, Feb 1974.

[17] P. Z. Quintas, W. C. Leung, S. R. Mishra, F. Sciulli, C. Arroyo, K. T. Bachmann, R. E. Blair, C. Foudas, B. J. King, W. C. Lefmann, E. Oltman, S. A. Rabinowitz, W. G. Seligman, M. H. Shaevitz, F. S. Merritt, M. J. Oreglia, B. A Schumm, R. H. Bernstein, F. Borcherding, H. E. Fisk, M. J. Lamm, W. Marsh, K. W. B. Merritt, H. Schellman, D. D. Yovanovitch, A. Bodek, and H. S. Budd. Measurement of Λ_{QCD} from $\nu\mu$-Fe nonsinglet structure functions at the Fermilab Tevatron. *Phys. Rev. Lett.*, 71(9):1307–1310, Aug 1993.

[18] Siegfried Bethke. Summary of α_s measurements. *Nucl. Phys. Proc. Suppl.*, 39BC: 198, 1995.

[19] S. Bethke. Determination of the QCD coupling α_s. *Journal of Physics G: Nuclear and Particle Physics*, 26(7):R27–R66, 2000.

[20] Siegfried Bethke. α_s 2002. *Nucl. Phys. Proc. Suppl.*, 121:74–81, 2003.

[21] Kenneth G. Wilson. Confinement of quarks. *Phys. Rev. D*, 10(8):2445–2459, Oct 1974.

[22] M. Creutz. *Quarks, gluons and lattices*. Cambridge Univ. Pr., 1st edition, 1983. ISBN 0-521-31535-2.

[23] I. Montvay and G. Münster. *Quantum fields on a lattice*. Cambridge Univ. Pr., 1st edition, 1994. ISBN 0-521-40432-0.

[24] H. J. Rothe. *Lattice gauge theories*. World Scientific, 3st edition, 2005. ISBN 981-256-168-4.

[25] T. DeGrand and C. DeTar. *Lattice methods for quantum chromodynamics*. World Scientific, 1st edition, 2006. ISBN 981-256-727-5.

[26] J. Smit. *Introduction to Quantum Fields on a Lattice*. Cambridge Univ. Pr., 1st edition, 2002. ISBN 0-521-89051-9.

[27] John B. Kogut. The lattice gauge theory approach to quantum chromodynamics. *Rev. Mod. Phys.*, 55(3):775–836, Jul 1983.

[28] Colin Morningstar. The Monte Carlo method in quantum field theory. *arXiv:hep-lat/0702020*, 2007.

[29] Martin Lüscher. Lattice QCD: From quark confinement to asymptotic freedom. *Annales Henri Poincare*, 4:S197–S210, 2003.

[30] Rajan Gupta. Introduction to lattice QCD. *arXiv:hep-lat/9807028*, 1997.

[31] I. Montvay. Monte Carlo Methods in Quantum Field Theory. *arXiv:hep-lat/0705.4356*, 2007.

[32] Kurt Langfeld. Computational Methods in Quantum Field Theory. *arXiv:0711.3004*, 2007.

[33] R. P. Feynman. Space-Time Approach to Non-Relativistic Quantum Mechanics. *Rev. Mod. Phys.*, 20(2):367–387, Apr 1948.

[34] Colin J. Morningstar and Mike Peardon. Efficient glueball simulations on anisotropic lattices. *Phys. Rev. D*, 56(7):4043–4061, Oct 1997.

[35] K. Symanzik. Some Topics in quantum field theory. *Presented at 6th Int. Conf. on Mathematical Physics, Berlin, West Germany, Aug 11-21*, 1981.

[36] K. Symanzik. Continuum Limit and Improved Action in Lattice Theories. 1. Principles and ϕ^4 Theory. *Nucl. Phys. B*, 226:187, 1983.

[37] K. Symanzik. Continuum Limit and Improved Action in Lattice Theories. 2. O(N) Nonlinear Sigma Model in Perturbation Theory. *Nucl. Phys. B*, 226:205, 1983.

[38] M. Lüscher and P. Weisz. On-Shell Improved Lattice Gauge Theories. *Commun. Math. Phys.*, 97:59, 1985.

[39] H. B. Nielsen and M. Ninomiya. A no-go theorem for regularizing chiral fermions. *Phys. Lett. B*, 105(2-3):219 – 223, 1981. ISSN 0370-2693.

[40] R. Sommer. Introduction to lattice field theories. Private notes of the lecture given at the Humboldt Universität zu Berlin 2008, 2008-2009.

[41] John Kogut and Leonard Susskind. Hamiltonian formulation of Wilson's lattice gauge theories. *Phys. Rev. D*, 11(2):395–408, Jan 1975.

[42] Leonard Susskind. Lattice fermions. *Phys. Rev. D*, 16(10):3031–3039, Nov 1977.

[43] E. Marinari, G. Parisi, and C. Rebbi. Monte Carlo simulation of the massive Schwinger model. *Nucl. Phys. B*, 190(4):734 – 750, 1981. ISSN 0550-3213.

[44] B. Bunk, M. Della Morte, K. Jansen, and F. Knechtli. Locality with staggered fermions. *Nucl. Phys. B*, 697(1-2):343 – 362, 2004. ISSN 0550-3213.

[45] Roberto Frezzotti, Pietro Antonio Grassi, Stefan Sint, and Peter Weisz. A local formulation of lattice QCD without unphysical fermion zero modes. *Nucl. Phys. Proc. Suppl.*, 83:941–946, 2000.

[46] Roberto Frezzotti, Pietro Antonio Grassi, Stefan Sint, and Peter Weisz. Lattice QCD with a chirally twisted mass term. *JHEP*, 08:058, 2001.

[47] Paul H. Ginsparg and Kenneth G. Wilson. A remnant of chiral symmetry on the lattice. *Phys. Rev. D*, 25(10):2649–2657, May 1982.

[48] David B. Kaplan. A method for simulating chiral fermions on the lattice. *Phys. Lett. B*, 288(3-4):342 – 347, 1992. ISSN 0370-2693.

[49] P. Hasenfratz. Prospects for perfect actions. *Nucl. Phys. Proc. Suppl.*, 63:53–58, 1998.

[50] Herbert Neuberger. Exactly massless quarks on the lattice. *Phys. Lett. B*, 417 (1-2):141 – 144, 1998. ISSN 0370-2693.

[51] B. Sheikholeslami and R. Wohlert. Improved Continuum Limit Lattice Action for QCD with Wilson Fermions. *Nucl. Phys. B*, 259:572, 1985.

[52] R. Wohlert. Improved continuum limit lattice action for quarks. *DESY 87/069*, 1987.

[53] Martin Lüscher, Stefan Sint, Rainer Sommer, and Hartmut Wittig. Non-perturbative determination of the axial current normalization constant in O(a) improved lattice QCD. *Nucl. Phys. B*, 491:344–364, 1997.

[54] Martin Lüscher, Stefan Sint, Rainer Sommer, Peter Weisz, and Ulli Wolff. Non-perturbative O(a) improvement of lattice QCD. *Nucl. Phys. B*, 491:323–343, 1997.

[55] Karl Jansen and Rainer Sommer. O(a) improvement of lattice QCD with two flavors of Wilson quarks. *Nucl. Phys. B*, 530:185–203, 1998.

[56] N. Yamada et al. Non-perturbative O(a)-improvement of Wilson quark action in three-flavor QCD with plaquette gauge action. *Phys. Rev. D*, 71:054505, 2005.

[57] Martin Lüscher. Advanced lattice QCD. *Les Houches 1997, Probing the standard model of particle interactions, Pt. 2*, pages 229–280, 1998.

[58] A. D. Kennedy. Algorithms for dynamical fermions. *arXiv:hep-lat/0607038*, 2006.

[59] Ulli Wolff. Monte Carlo errors with less errors. *Comput. Phys. Commun.*, 156: 143–153, 2004.

[60] Nicholas Metropolis, Arianna W. Rosenbluth, Marshall N. Rosenbluth, Augusta H. Teller, and Edward Teller. Equation of State Calculations by Fast Computing Machines. *The Journal of Chemical Physics*, 21(6):1087–1092, 1953.

[61] Michael Creutz. Monte Carlo study of quantized SU(2) gauge theory. *Phys. Rev. D*, 21(8):2308–2315, Apr 1980.

[62] Nicola Cabibbo and Enzo Marinari. A new method for updating SU(N) matrices in computer simulations of gauge theories. *Phys. Lett. B*, 119(4-6):387 – 390, 1982.

[63] A. D. Kennedy and B. J. Pendleton. Improved heatbath method for Monte Carlo calculations in lattice gauge theories. *Phys. Lett. B*, 156(5-6):393 – 399, 1985.

[64] Simon Duane. Stochastic quantization versus the microcanonical ensemble: Getting the best of both worlds. *Nucl. Phys. B*, 257:652 – 662, 1985.

[65] Poul H. Damgaard and Helmuth Hüffel. Stochastic quantization. *Phys. Rept.*, 152 (5-6):227 – 398, 1987. ISSN 0370-1573.

[66] Michael Creutz. Global Monte Carlo algorithms for many-fermion systems. *Phys. Rev. D*, 38(4):1228–1238, Aug 1988.

[67] S. Duane and J. B. Kogut. The theory of hybrid stochastic algorithms. *Nucl. Phys. B*, 275(3):398 – 420, 1986.

[68] Simon Duane, A. D. Kennedy, Brian J. Pendleton, and Duncan Roweth. Hybrid Monte Carlo. *Phys. Lett. B*, 195(2):216 – 222, 1987.

[69] C. Gattringer and C. B. Lang. *Quantum Chromodynamics on the Lattice*. Springer-Verlag, 1nd edition, 2010. ISBN 978-3-642-01849-7.

[70] T. Kaneko et al. Light hadron spectrum in three-flavor QCD with O(a)-improved Wilson quark action. *Nucl. Phys. Proc. Suppl.*, 129:188–190, 2004.

[71] D. H. Weingarten and D. N. Petcher. Monte Carlo integration for lattice gauge theories with fermions. *Phys. Lett. B*, 99(4):333 – 338, 1981. ISSN 0370-2693.

[72] W. H. Press, S. A. Teukolsky, W. T. Vetterling, and B. P. Flannery. *Numerical Recipes in C*. Cambridge University Press, 2nd edition, 1994. ISBN 0-521-43108-5.

[73] M. R. Hestenes and E. Steifel. Methods of Conjugate Gradients for Solving Linear Systems. *Journal of Research of the National Bureau of Standards*, 49(6):409 – 436, 1952.

[74] Y. Saad. *Iterative Methods for Sparse Linear Systems*. SIAM, 2nd edition, 2003. ISBN 0-89871-534-2.

[75] H. A. van der Vorst. Bi-CGSTAB: A Fast and Smoothly Converging Variant of Bi-CG for the Solution of Nonsymmetric Linear Systems. *SIAM Journal on Scientific and Statistical Computing*, 13(2):631–644, 1992.

[76] M. Della Morte, M. Hasenbusch, R. Hoffmann, F. Knechtli, J. Rolf, R. Sommer, and I. Wetzorke. Documentation of the GHMC code. Internal notes about the ALPHA code, 2004.

[77] Rajan Gupta, Apoorva Patel, Clive F. Baillie, Gerald Guralnik, Gregory W. Kilcup, and Stephen R. Sharpe. QCD with dynamical Wilson fermions. *Phys. Rev. D*, 40(6):2072–2084, Sep 1989.

[78] Thomas A. Degrand and Pietro Rossi. Conditioning techniques for dynamical fermions. *Computer Physics Communications*, 60(2):211 – 214, 1990. ISSN 0010-4655.

[79] Karl Jansen and Chuan Liu. Implementation of Symanzik's improvement program for simulations of dynamical Wilson fermions in lattice QCD. *Comput. Phys. Commun.*, 99:221–234, 1997.

[80] S. Aoki, R. Burkhalter, M. Fukugita, S. Hashimoto, K-I. Ishikawa, N. Ishizuka, Y. Iwasaki, K. Kanaya, T. Kaneko, Y. Kuramashi, M. Okawa, T. Onogi, S. Tominaga, N. Tsutsui, A. Ukawa, N. Yamada, and T. Yoshié. Polynomial hybrid Monte Carlo algorithm for lattice QCD with an odd number of flavors. *Phys. Rev. D*, 65 (9):094507, Apr 2002.

[81] Martin Hasenbusch. Speeding up the Hybrid-Monte-Carlo algorithm for dynamical fermions. *Phys. Lett. B*, 519:177–182, 2001.

[82] M. Hasenbusch and K. Jansen. Speeding up lattice QCD simulations with clover-improved Wilson fermions. *Nucl. Phys. B*, 659:299–320, 2003.

[83] M. Hasenbusch and K. Jansen. Speeding up the Hybrid-Monte-Carlo algorithm for dynamical fermions. *Nucl. Phys. Proc. Suppl.*, 106:1076–1078, 2002.

[84] Martin Lüscher. Lattice QCD and the Schwarz alternating procedure. *JHEP*, 05: 052, 2003.

[85] Martin Lüscher. Schwarz-preconditioned HMC algorithm for two-flavour lattice QCD. *Comput. Phys. Commun.*, 165:199–220, 2005.

[86] Martin Lüscher. Local coherence and deflation of the low quark modes in lattice QCD. *JHEP*, 07:081, 2007.

[87] Martin Lüscher. Deflation acceleration of lattice QCD simulations. *JHEP*, 12:011, 2007.

[88] J. C. Sexton and D. H. Weingarten. Hamiltonian evolution for the hybrid Monte Carlo algorithm. *Nucl. Phys. B*, 380(3):665 – 677, 1992. ISSN 0550-3213.

[89] C. Urbach, K. Jansen, A. Shindler, and U. Wenger. HMC algorithm with multiple time scale integration and mass preconditioning. *Comput. Phys. Commun.*, 174: 87–98, 2006.

[90] Martin Lüscher. A New approach to the problem of dynamical quarks in numerical simulations of lattice QCD. *Nucl. Phys. B*, 418:637–648, 1994.

[91] Roberto Frezzotti and Karl Jansen. The PHMC algorithm for simulations of dynamical fermions. I: Description and properties. *Nucl. Phys. B*, 555:395–431, 1999.

[92] Roberto Frezzotti and Karl Jansen. The PHMC algorithm for simulations of dynamical fermions. II: Performance analysis. *Nucl. Phys. B*, 555:432–453, 1999.

[93] Oliver Witzel. *Non-Hermitian polynomial hybrid Monte Carlo*. PhD thesis, Humboldt-Universität zu Berlin, Mathematisch-Naturwissenschaftliche Fakultät I, 2008. `http://edoc.hu-berlin.de/docviews/abstract.php?id=29282` [Online: Stand 2010-06-22T16:32:19Z].

[94] M. A. Clark and A. D. Kennedy. The RHMC algorithm for 2 flavors of dynamical staggered fermions. *Nucl. Phys. Proc. Suppl.*, 129:850–852, 2004.

[95] M. A. Clark. The rational hybrid Monte Carlo algorithm. *PoS*, LAT2006:004, 2006.

[96] Andreas Frommer, Bertold Nockel, Stephan Güsken, Thomas Lippert, and Klaus Schilling. Many masses on one stroke: Economic computation of quark propagators. *Int. J. Mod. Phys.*, C6:627–638, 1995.

[97] M. A. Clark and A. D. Kennedy. Accelerating Dynamical-Fermion Computations Using the Rational Hybrid Monte Carlo Algorithm with Multiple Pseudofermion Fields. *Phys. Rev. Lett.*, 98(5):051601, 2007.

[98] Martin Lüscher. Solution of the Dirac equation in lattice QCD using a domain decomposition method. *Comput. Phys. Commun.*, 156:209–220, 2004.

[99] W. Pauli and F. Villars. On the Invariant Regularization in Relativistic Quantum Theory. *Rev. Mod. Phys.*, 21(3):434–444, Jul 1949.

[100] G. 't Hooft and M. Veltman. Regularization and renormalization of gauge fields. *Nucl. Phys. B*, 44(1):189 – 213, 1972. ISSN 0550-3213.

[101] G. 't Hooft. Dimensional regularization and the renormalization group. *Nucl. Phys. B*, 61:455 – 468, 1973. ISSN 0550-3213.

[102] William A. Bardeen, A. J. Buras, D. W. Duke, and T. Muta. Deep-inelastic scattering beyond the leading order in asymptotically free gauge theories. *Phys. Rev. D*, 18(11):3998–4017, Dec 1978.

[103] William Celmaster and Richard J. Gonsalves. Quantum-Chromodynamics Perturbation Expansions in a Coupling Constant Renormalized by Momentum-Space Subtraction. *Phys. Rev. Lett.*, 42(22):1435–1438, May 1979.

[104] David B. Kaplan. Effective field theories. *arXiv:nucl-th/9506035*, 1995.

[105] Stephan Hartmann. Effective Field Theories, Reductionism and Scientific Explanation. *Studies In History and Philosophy of Science Part B: Studies In History and Philosophy of Modern Physics*, 32(2):267, 2001. ISSN 1355-2198.

[106] Rainer Sommer. Non-perturbative QCD: Renormalization, O(a)-improvement and matching to heavy quark effective theory. *arXiv:hep-lat/0611020*, 2006.

[107] R. Sommer. A New way to set the energy scale in lattice gauge theories and its applications to the static force and α_s in SU(2) Yang-Mills theory. *Nucl. Phys. B*, 411:839–854, 1994.

[108] Martin Lüscher, Peter Weisz, and Ulli Wolff. A Numerical method to compute the running coupling in asymptotically free theories. *Nucl. Phys. B*, 359:221–243, 1991.

[109] Achim Bode, Peter Weisz, and Ulli Wolff. Two loop computation of the Schroedinger functional in lattice QCD. *Nucl. Phys. B*, 576:517–539, 2000. Erratum-ibid.B600:453,2001, Erratum-ibid.B608:481,2001.

[110] T. van Ritbergen, J. A. M. Vermaseren, and S. A. Larin. The four-loop β-function in quantum chromodynamics. *Phys. Lett. B*, 400(3-4):379 – 384, 1997. ISSN 0370-2693.

[111] K.G. Chetyrkin. Quark mass anomalous dimension to $O(\alpha_s^4)$. *Phys. Lett. B*, 404 (1-2):161 – 165, 1997. ISSN 0370-2693.

[112] Martin Lüscher, Rainer Sommer, Peter Weisz, and Ulli Wolff. A Precise determination of the running coupling in the SU(3) Yang-Mills theory. *Nucl. Phys. B*, 413:481–502, 1994.

[113] Michele Della Morte et al. Computation of the strong coupling in QCD with two dynamical flavours. *Nucl. Phys. B*, 713:378–406, 2005.

[114] Stefano Capitani, Martin Lüscher, Rainer Sommer, and Hartmut Wittig. Non-perturbative quark mass renormalization in quenched lattice QCD. *Nucl. Phys. B*, 544:669–698, 1999.

[115] Michele Della Morte et al. Non-perturbative quark mass renormalization in two-flavor QCD. *Nucl. Phys. B*, 729:117–134, 2005.

[116] F. Knechtli et al. Running quark mass in two flavor QCD. *Nucl. Phys. Proc. Suppl.*, 119:320–322, 2003.

[117] Bernd Gehrmann, Juri Rolf, Stefan Kurth, and Ulli Wolff. Schrödinger functional at negative flavour number. *Nucl. Phys. B*, 612:3–24, 2001.

[118] Stefan Sint and Rainer Sommer. The Running coupling from the QCD Schrödinger functional: A One loop analysis. *Nucl. Phys. B*, 465:71–98, 1996.

[119] Achim Bode et al. First results on the running coupling in QCD with two massless flavors. *Phys. Lett. B*, 515:49, 2001.

[120] M. Lüscher and P. Weisz. O(a) improvement of the axial current in lattice QCD to one-loop order of perturbation theory. *Nucl. Phys. B*, 479:429–458, 1996.

[121] Giulia de Divitiis et al. Universality and the approach to the continuum limit in lattice gauge theory. *Nucl. Phys. B*, 437:447, 1995.

[122] Martin Lüscher, Rajamani Narayanan, Peter Weisz, and Ulli Wolff. The Schrödinger functional: A Renormalizable probe for non-Abelian gauge theories. *Nucl. Phys. B*, 384:168–228, 1992.

[123] Stefan Sint. On the Schrödinger functional in QCD. *Nucl. Phys. B*, 421:135–158, 1994.

[124] Stefan Sint. One loop renormalization of the QCD Schrödinger functional. *Nucl. Phys. B*, 451:416–444, 1995.

[125] K. Symanzik. Schrödinger representation and Casimir effect in renormalizable quantum field theory. *Nucl. Phys. B*, 190(1):1 – 44, 1981. ISSN 0550-3213.

[126] Stefan Sint and Peter Weisz. Further results on O(a) improved lattice QCD to one-loop order of perturbation theory. *Nucl. Phys. B*, 502:251–268, 1997.

[127] M. Lüscher, R. Narayanan, R. Sommer, U. Wolff, and P. Weisz. Determination of the running coupling in the SU(2) Yang-Mills theory from first principles. *Nucl. Phys. Proc. Suppl.*, 30:139–148, 1993.

[128] Martin Lüscher, Rainer Sommer, Ulli Wolff, and Peter Weisz. Computation of the running coupling in the SU(2) Yang-Mills theory. *Nucl. Phys. B*, 389:247–264, 1993.

[129] Roland Hoffmann. *Chiral properties of dynamical Wilson fermions.* PhD thesis, Humboldt-Universität zu Berlin, Mathematisch-Naturwissenschaftliche Fakultät I, 2005. `http://edoc.hu-berlin.de/docviews/abstract.php?id=26277` [Online: Stand 2009-12-31T11:11:14Z].

[130] Martin Lüscher, Stefan Sint, Rainer Sommer, and Peter Weisz. Chiral symmetry and O(a) improvement in lattice QCD. *Nucl. Phys. B*, 478:365–400, 1996.

[131] Michele Della Morte, Roland Hoffmann, and Rainer Sommer. Non-perturbative improvement of the axial current for dynamical Wilson fermions. *JHEP*, 03:029, 2005.

[132] Michele Della Morte, Rainer Sommer, and Shinji Takeda. On cutoff effects in lattice QCD from short to long distances. *Phys. Lett. B*, 672:407–412, 2009.

[133] H. Meyer. Documentation to the multiple time-scale mutiple pseudo-fermion version of the $N_f = 2$ clover fermions in the Schrödinger functional simulation program. Internal notes about the ALPHA code, 2005.

[134] H. Meyer and O. Witzel. Symmetric Even-Odd-Preconditioning. Internal notes about the ALPHA code, 2006.

[135] R. Alfieri et al. Status of APE projects. *Nucl. Phys. Proc. Suppl.*, 94:846–853, 2001.

[136] R. Alfieri et al. apeNEXT: A multi-TFlops LQCD computing project. *arXiv:hep-lat/0102011*, 2001.

[137] F. Bodin et al. The apeNEXT project. *Nucl. Phys. Proc. Suppl.*, 106:173–176, 2002.

[138] Fatih Tekin, Rainer Sommer, and Ulli Wolff. Symanzik improvement of lattice QCD with four flavors of Wilson quarks. *Phys. Lett. B*, 683:75–79, 2010.

[139] M. Lüscher and P. Weisz. Computation of the Action for On-Shell Improved Lattice Gauge Theories at Weak Coupling. *Phys. Lett. B*, 158:250, 1985.

[140] Michele Della Morte et al. Simulating the Schrödinger functional with two pseudo-fermions. *Comput. Phys. Commun.*, 156:62–72, 2003.

[141] Jochen Heitger and Rainer Sommer. A strategy to compute the b-quark mass with non-perturbative accuracy. *Nucl. Phys. B - Proc. Suppl.*, 106-107:358 – 360, 2002. ISSN 0920-5632.

[142] S. Capitani et al. Non-perturbative quark mass renormalization. *Nucl. Phys. Proc. Suppl.*, 63:153–158, 1998.

[143] Bernd Gehrmann. The step scaling function of QCD at negative flavor number. *arXiv:hep-lat/0207016*, 2002.

[144] S. Takeda, S. Aoki, M. Fukugita, K-I. Ishikawa, N. Ishizuka, Y. Iwasaki, K. Kanaya, T. Kaneko, Y. Kuramashi, M. Okawa, Y. Taniguchi, A. Ukawa, and T. Yoshié. Scaling study of the step scaling function in SU(3) gauge theory with improved gauge actions. *Phys. Rev. D*, 70(7):074510, Oct 2004.

[145] Thomas Appelquist, George T. Fleming, and Ethan T. Neil. Lattice Study of Conformal Behavior in SU(3) Yang-Mills Theories. *Phys. Rev. D*, 79:076010, 2009.

[146] A. Spitz, H. Hoeber, N. Eicker, S. Güsken, Th. Lippert, K. Schilling, T. Struckmann, P. Ueberholz, and J. Viehoff. α_S from Υ spectroscopy with dynamical Wilson fermions. *Phys. Rev. D*, 60(7):074502, Sep 1999.

[147] C. Davies, A. Gray, M. Alford, E. Follana, J. Hein, P. Lepage, Q. Mason, M. Nobes, J. Shigemitsu, H. Trottier, and M. Wingate. The determination of α_s from lattice QCD with 2+1 flavors of dynamical quarks. *Nucl. Phys. B - Proc. Suppl.*, 119:595 – 597, 2003. ISSN 0920-5632. Proceedings of the XXth International Symposium on Lattice Field Theory.

[148] M. Göckeler et al. Determination of Lambda in quenched and full QCD: An update. *Nucl. Phys. Proc. Suppl.*, 140:228–230, 2005.

[149] Stefano Capitani, Martin Lüscher, Rainer Sommer, and Hartmut Wittig. Non-perturbative quark mass renormalization in quenched lattice QCD. *Nucl. Phys. B*, B544:669, 1999.

[150] Fatih Tekin, Rainer Sommer, and Ulli Wolff. The running coupling of QCD with four flavors. *Nuclear Physics B*, 840(1-2):114–128, 2010. ISSN 0550-3213.

[151] Stefan Sint. The Schrödinger functional with chirally rotated boundary conditions. *PoS*, LAT2005:235, 2006.

[152] Stefan Sint. Lattice QCD with a chiral twist. *arXiv:hep-lat/0702008*, 2007.

[153] Jenifer Gonzalez Lopez, Karl Jansen, Dru B. Renner, and Andrea Shindler. Chirally rotated Schrödinger functional: non-perturbative tuning in the quenched approximation. *PoS*, LAT2009:199, 2009.

[154] Urs M. Heller. The Schrödinger functional running coupling with staggered fermions. *Nucl.Phys. B*, 504:435, 1997.

[155] Paula Perez-Rubio and Stefan Sint. The SF running coupling with four flavours of staggered quarks. *PoS*, LAT2007:249, 2007.

[156] Luigi Del Debbio, Haralambos Panagopoulos, and Ettore Vicari. Theta dependence of SU(N) gauge theories. *JHEP*, 0208:044, 2002.

[157] Stefan Schaefer, Rainer Sommer, and Francesco Virotta. Investigating the critical slowing down of QCD simulations. *PoS*, LAT2009, 2009.

List of Figures

List of Tables

Selbständigkeitserklärung

Ich erkläre, dass ich die vorliegende Arbeit selbständig und nur unter Verwendung der angegebenen Literatur und Hilfsmittel angefertigt habe.

Berlin, den 9. Juli 2010 Fatih Tekin